This is to certify that the

dissertation entitled

Thermal Quench of Brittle Materials

presented by

Chin-Chen Chiu

has been accepted towards fulfillment
of the requirements for

Ph.D. degree in Materials Science

Eldon Case
Major professor

Date August 8, 1991

THERMAL QUENCH of BRITTLE MATERIALS

by

Chin-Chen Chiu

A DISSERTATION

Submitted to
Michigan State University
in Partial Fulfillment of the Requirements
for the Degree of

DOCTOR OF PHILOSOPHY

in

Materials Science

Department of Metallurgy, Mechanics, and Materials Science

1991

ABSTRACT

Thermal Quench of Brittle Materials

by

Chin-Chen Chiu

The objective of this dissertation was to study quench-induced mechanical property changes in brittle materials. In this study, commercial microscope glass slides (soda-lime glass) were quenched from above and below the glass's annealing temperature. The quenching media were water, motor oil, and air.

The experimental work includes single-quench thermal shock testing, cyclic thermal shock testing (fatigue), retained strength measurement, residual stress measurement, elastic modulus and internal friction measurement, heat flow analysis using Differential Scanning Calorimeter (DSC), and thermal expansion measurement by ThermoMechanical Analysis (TMA). In conjunction with the experimentation, the theoretical analyses include: (1) thermoelastic and thermoviscoelastic stress calculations infinite glass plates, (2) residual stress analysis, including its influence on dynamic elastic modulus, (3) statistical study of subcritical crack growth effect on thermal shock resistance, and (4) quench-induced strength degradation in glass plates.

Experimentally, there are significant differences in the effects of a thermal quench from above the annealing temperature when compared with thermal quenching from below the annealing

temperature. For example, the viscous flow occurring above annealing temperature can relieve transient thermal stresses and decrease the probability of thermal shock damage.

In addition to thermal quench of glass slides, a paper titled "Elastic modulus determination of coating layers as applied to layered composites" is included in the appendix of this dissertation. The appendix proposes two techniques, one based on the dynamic resonance method and the other based on the static loading method (four point bend), to measure the in-plane elastic modulus of SiC coating/graphite substrate composites.

ACKNOWLEDGEMENTS

I wish to express sincere appreciation to Dr. Eldon D. Case for his support, guidance, and willingness to share his time and knowledge throughout this research.

Special thanks to my colleagues, C. Y. Lee, W. J. Lee, and Y. M. Kim for their extra time and efforts during this research.

To my wife, shiow-ying, I thank for her support.

TABLE OF CONTENTS

LIST OF TABLES

LIST OF FIGURES

1. INTRODUCTION

Compared with metals, ceramics have good high-temperature properties, for example, chemical corrosion resistance, oxidation resistance, creep resistance, and mechanical strength. Thus, ceramic materials are promising candidates for use in severe thermal environments. However, ceramics are brittle and can be fractured by a thermomechanical loading. Consequently, thermal shock studies are basic to the characterization the reliability and performance of high-temperature structural ceramics.

Typical thermal shock of ceramics involves quenching of hot specimens into a water bath below the material's annealing temperature [1-3], by which tremendous heat flow occurs and severe thermal stresses develop in the quenched component. The thermal stresses may cause the pre-existing cracks in ceramic components to propagate, which degrades the fracture strength of the shocked components relative to that of the non-shocked components [4-6]. As a result, the thermal shock resistance can be specified by the critical quench temperature difference, ΔT_c, required for the fracture strength degradation.

In 1969, Hasselman proposed a famous model for the calculation of ΔT_c [7]. Hasselman also proposed that: (1) pre-existing cracks propagate when quenched above ΔT_c, (2) cracks are stable (do not grow) below ΔT_c, and (3) dynamic crack growth causes a discontinuous drop in the retained fracture strength at ΔT_c (Figure 1). From 1969 on, Hasselman's model became a basis for further study of the strength degradation of quenched brittle materials.

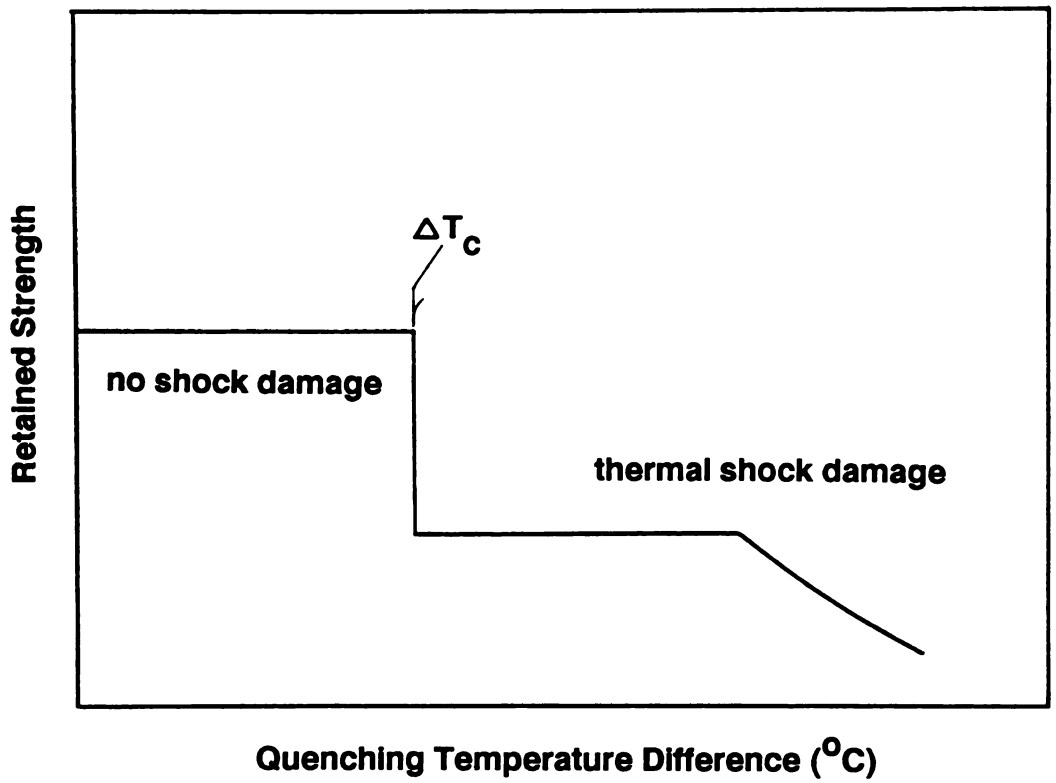

Figure 1. A plot of retained strength versus of quench temperature difference according to a strength degradation model proposed by Hasselman [7].

This is to certify that the

dissertation entitled

Thermal Quench of Brittle Materials

presented by

Chin-Chen Chiu

has been accepted towards fulfillment
of the requirements for

Ph.D. degree in Materials Science

Eldon Case
Major professor

Date August 8, 1991

THERMAL QUENCH of BRITTLE MATERIALS

by

Chin-Chen Chiu

A DISSERTATION

Submitted to
Michigan State University
in Partial Fulfillment of the Requirements
for the Degree of

DOCTOR OF PHILOSOPHY

in

Materials Science

Department of Metallurgy, Mechanics, and Materials Science

1991

ABSTRACT

Thermal Quench of Brittle Materials

by

Chin-Chen Chiu

The objective of this dissertation was to study quench-induced mechanical property changes in brittle materials. In this study, commercial microscope glass slides (soda-lime glass) were quenched from above and below the glass's annealing temperature. The quenching media were water, motor oil, and air.

The experimental work includes single-quench thermal shock testing, cyclic thermal shock testing (fatigue), retained strength measurement, residual stress measurement, elastic modulus and internal friction measurement, heat flow analysis using Differential Scanning Calorimeter (DSC), and thermal expansion measurement by ThermoMechanical Analysis (TMA). In conjunction with the experimentation, the theoretical analyses include: (1) thermoelastic and thermoviscoelastic stress calculations infinite glass plates, (2) residual stress analysis, including its influence on dynamic elastic modulus, (3) statistical study of subcritical crack growth effect on thermal shock resistance, and (4) quench-induced strength degradation in glass plates.

Experimentally, there are significant differences in the effects of a thermal quench from above the annealing temperature when compared with thermal quenching from below the annealing

temperature. For example, the viscous flow occurring above annealing temperature can relieve transient thermal stresses and decrease the probability of thermal shock damage.

In addition to thermal quench of glass slides, a paper titled "Elastic modulus determination of coating layers as applied to layered composites" is included in the appendix of this dissertation. The appendix proposes two techniques, one based on the dynamic resonance method and the other based on the static loading method (four point bend), to measure the in-plane elastic modulus of SiC coating/graphite substrate composites.

ACKNOWLEDGEMENTS

I wish to express sincere appreciation to Dr. Eldon D. Case for his support, guidance, and willingness to share his time and knowledge throughout this research.

Special thanks to my colleagues, C. Y. Lee, W. J. Lee, and Y. M. Kim for their extra time and efforts during this research.

To my wife, shiow-ying, I thank for her support.

TABLE OF CONTENTS

LIST OF TABLES

LIST OF FIGURES

1. INTRODUCTION

Compared with metals, ceramics have good high-temperature properties, for example, chemical corrosion resistance, oxidation resistance, creep resistance, and mechanical strength. Thus, ceramic materials are promising candidates for use in severe thermal environments. However, ceramics are brittle and can be fractured by a thermomechanical loading. Consequently, thermal shock studies are basic to the characterization the reliability and performance of high-temperature structural ceramics.

Typical thermal shock of ceramics involves quenching of hot specimens into a water bath below the material's annealing temperature [1-3], by which tremendous heat flow occurs and severe thermal stresses develop in the quenched component. The thermal stresses may cause the pre-existing cracks in ceramic components to propagate, which degrades the fracture strength of the shocked components relative to that of the non-shocked components [4-6]. As a result, the thermal shock resistance can be specified by the critical quench temperature difference, ΔT_c, required for the fracture strength degradation.

In 1969, Hasselman proposed a famous model for the calculation of ΔT_c [7]. Hasselman also proposed that: (1) pre-existing cracks propagate when quenched above ΔT_c, (2) cracks are stable (do not grow) below ΔT_c, and (3) dynamic crack growth causes a discontinuous drop in the retained fracture strength at ΔT_c (Figure 1). From 1969 on, Hasselman's model became a basis for further study of the strength degradation of quenched brittle materials.

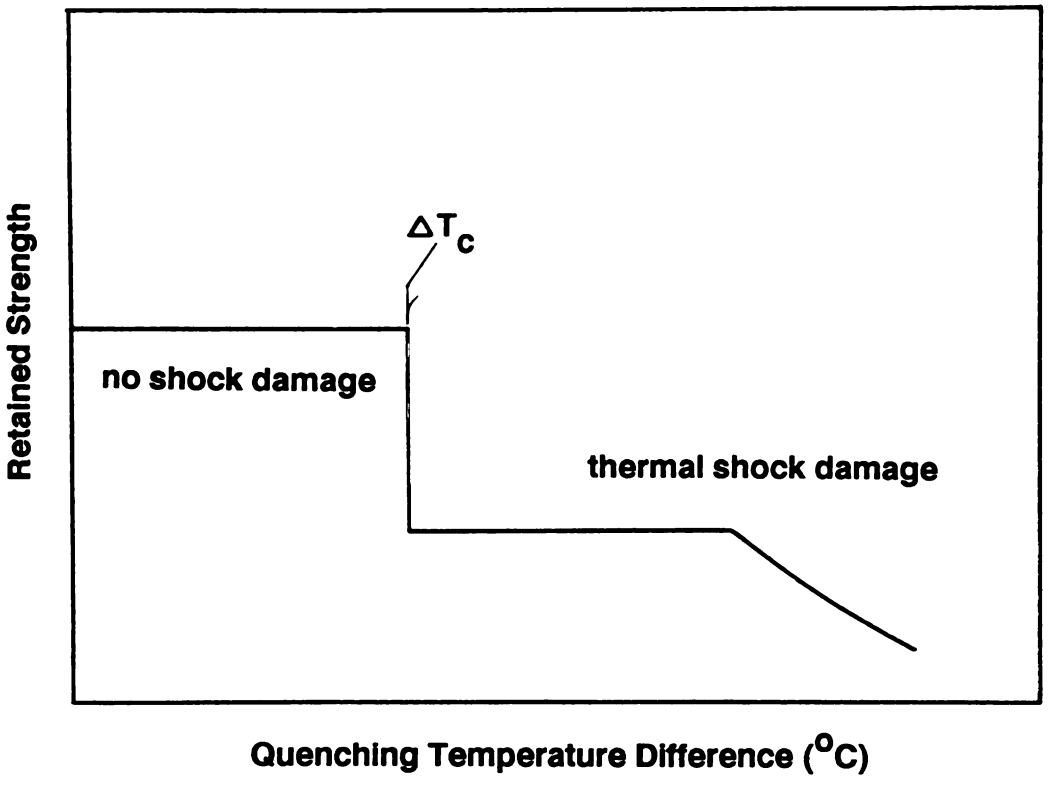

Figure 1. A plot of retained strength versus of quench temperature difference according to a strength degradation model proposed by Hasselman [7].

Hasselman's model is based on thermoelastic theory and fracture mechanics concepts (Griffith's failure criterion), which assumes that the quenched ceramics are linear elastic materials. The assumption of linear elasticity is reasonable for brittle ceramics quenched from below the annealing temperature. However, viscous flow occurs when some ceramics are heated to near their annealing temperature (for example, soda-lime silica glass or a glassy grain boundary phase in a polycrystalline ceramic [8-11]), and hence when viscous flow occurs, the materials behave as viscoelastic materials rather than purely elastic materials. Thus, for thermal quenching from above the annealing temperature, thermal stress calculations must include both thermoelastic theory and viscous flow effects.

Additionally, Hasselman's 1969 model neglected subcritical crack growth which may occur at $\Delta T < \Delta T_c$. In practice, ceramic components usually serve in thermal stress conditions corresponding to a temperature range of $\Delta T < \Delta T_c$. Thus, the effect of subcritical crack growth on thermal shock damage is of value for study.

The purpose of this dissertation is to investigate (1) the effect of thermal quench on brittle materials when quenched from above the annealing temperature and (2) the influence of subcritical crack growth ($\Delta T < \Delta T_c$) on thermal shock resistance. Commercial microscope glass slides (soda-lime glass) were tested in this study. The fracture strength, elastic modulus, and internal friction were used to experimentally monitor the quench-induced material property changes in the glass slides. In addition, the thermoviscoelastic theory, fracture mechanics, and statistics concept were used to theoretically analyze the thermal quench effect.

2. LITERATURE REVIEW

Thermal quench studies in ceramic materials can be divided into two areas. One area is the theoretical analysis of thermal quench-induced crack initiation and propagation. The other area is experimental observation and evaluation of the thermal shock damage in quenched components.

Before 1969, most theoretical researchers (such as Kingery) developed shock damage theory based on thermoelastic stress calculations and a maximum tensile stress failure criterion [12-14]. Thermal shock damage was assumed to initiate from the body's surface (or edge) where the maximum transient thermal stresses develop. Thermal quench damage occured when the transient stresses exceeded the material's strength. The critical quench temperature difference was calculated by [12-14]

$$\Delta T_c = \frac{S_f (1 - \nu)}{E \ F(B)} \tag{1}$$

where E, S_f, ν, and B are the elastic modulus, fracture strength, Poisson's ratio, and Biot's modulus, respectively. F(B) is a complicated function of Biot's modulus [12-14]. Equation (1) explains shock damage initiation. However, it does not predict the degree of crack propagation and strength degradation.

Few theoretical researchers developed shock damage models according to fracture mechanics. For example, Emery, et al. [15] calculated the quasistatic stress-intensity factor, K, of single edge crack using a Green's function method. Emery et al. [15]

assumed that the crack was small enough that the component compliance was not affected. K was then calculated according to the thermoelastic stress field existing in the absence of the crack. The quench-induced crack initiation and propagation was analyzed in terms of K. In contrast to Emery's study, Olesiak and Sneddon [16] and Kassir and Sih [17] calculated the thermal stress field taking into account the effect of pre-existing cracks. Olesiak et al. considered thermal stress is a secondary stress which could be weakened and redistributed by introducing a new crack (such as the stress for a fixed grips). Because of distinctive idea concerning the thermal stress field (Emery assumed that cracks did not weaken thermal stress field), Emery and Olesiak introduced different directions for the theoretical study of thermal shock damage.

Experimental studies of thermal shock damage usually accompanied the theoretical analysis. Based on statistical concepts, Manson proposed that quench-induced fracture is a complex stochastic process depending on the magnitude and spatial distribution of transient thermal stresses, as well as the size and spatial position of pre-existing flaws [18]. Manson indicated that the fracture probability of shocked components gradually increased with thermal stresses (ΔT). Manson was the first researcher to combine the maximum stress failure theory (equation (1)), statistics, and experiment in a thermal shock damage study.

In 1969, Hasselman presented a model to characterize the crack propagation and strength retention of quenched brittle materials [7]. Hasselman assumed that: (1) The quenched component contained pre-existing flaws in terms of Griffith microcracks. (2) The

quenched component was subjected to uniform thermal stress change (no stress gradient in the quenched component) during the thermal shock process. The maximum stresses, S, are

$$S = \alpha E \Delta T (1 - 2\nu) \qquad (2)$$

(3) The corresponding maximum thermal strain energy was calculated from equation (2). (4) The pre-existing cracks could release the strain energy by means of crack propagation. (5) When the strain energy release rate was greater than the fracture surface energy required to produce unit of new crack surface, the crack became unstable (Griffith's failure criterion). Hasselman proposed an equation for the calculation of ΔT_c and a map accounting for the strength degradation of brittle materials (see Figure (1)). Generally speaking, Hasselman's model was simple and qualitatively explained experimental results well [1-3]. Many experimental researchers considered Hasselman's model as a paradigm for further thermal shock damage study (from 1969 to 1983). For example, Coppola and Bradt [19] studied thermal shock damage in SiC according to Hasselman's model. Smith et al. [3] used Hasselman's model in their study of the thermal shock damage of alumina, indicating that the strength degradation and crack propagatin are functions of porosity. Seton and Dutta [20] proposed that the strength degradation of shocked alumina is a function of grain size.

However, Hasselman's model (see equation (2)) did not consider the effects of specimen size, heat transfer conditions, spatial distribution of thermal stress field (such as, transient tensile stress in component's surface and compressive stress in

interior [12-14]), etc. Some theoretists used fracture mechanics to model thermal shock damage [22-37]. For example, Emery and Kobayashi [21,22], Cheverton et al. [23], Evans and Charles [24], Nied [25,26], Ting and Jacobs [27], Noda et al. [28] evaluated K for a single crack with respect to different thermal stress conditions. Nasser [29,30] and Weiss et al. [31,32] investigated the influence of multiple cracks on K. Swain [33,34] studied the effect of R curve on the thermal shock damage. Those papers [21-34] involved the same stress field assumption as Emery [15]. On the other hand, Chell and Ewing [35], Tsai [36], and Singh et al. [37] calculated K assuming that cracks release and re-distribute the thermal stress filed (as Kassir did [16]).

In 1983, Lewis proposed that since the fracture strength of a group of unshocked specimens was characterized by a distribution, the retained strength of shocked specimens should exhibit a gradual decrease as ΔT increased (Figure (2)) [38]. Lewis presented experimental results to support his qualitative idea [39-41]. Later, Bradt et al. [42,43] also reported experimental data which agreed with Lewis' idea. As a result, some researchers gave attention to the statistical study on thermal shock damage [44-47].

All the papers [1-47] mentioned above are based on the assumption that: (1) quenched ceramics are linear elastic materials and the initial temperature of shocked components is below the annealing temperature, and (2) no subcritical crack growth occurs during the thermal shock process. In practice, thermal stress conditions for a ceramic component may include a broad quenching temperature range, such as thermal quenching from above the

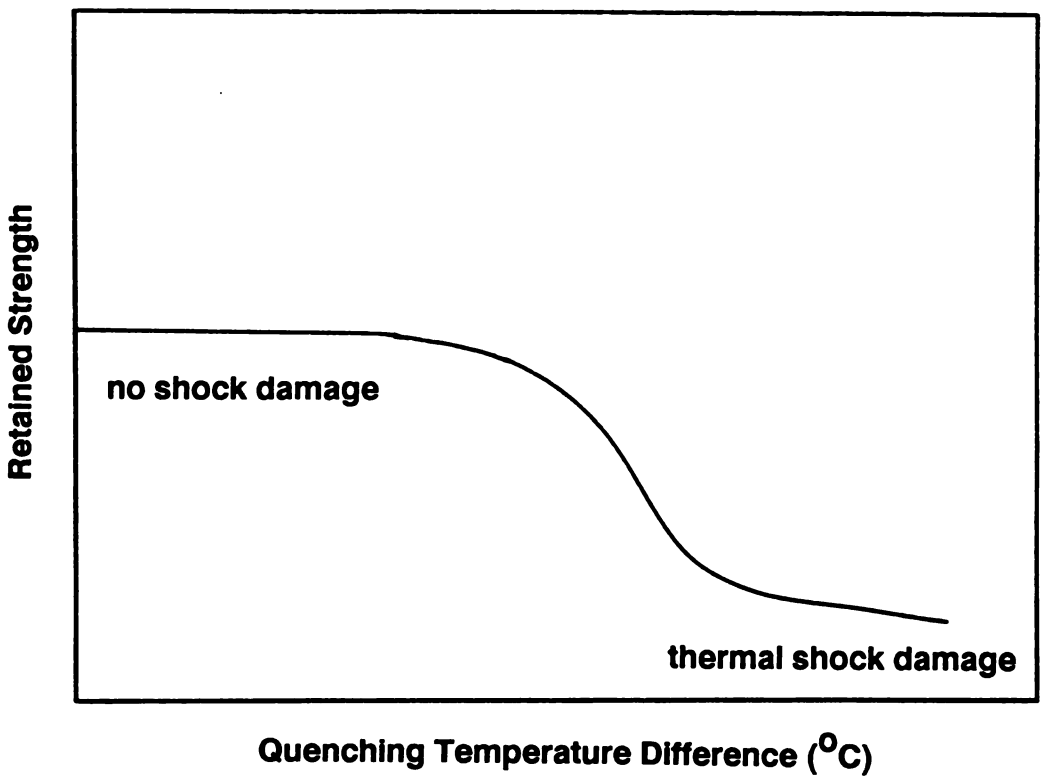

Figure 2. A plot of retained strength versus of quench temperature difference, a strength degradation model proposed by Lewis [38].

material's annealing temperature. For instance, tempered glass is strengthened by thermal quenching from above the annealing temperature [8]. Mai proposed that the retained strength behavior of WC did not follow either Figure 1 or Figure 2 [48]. For polycrystalline ceramics, Gebauer et al. [9,10], Ohira et al. [49], and Travitzky et al. [50], observed that quenching aluminosilicate specimens from about 1400 ^{o}C to room temperature silicone oil increased the retained fracture strength. Kirchner observed that quenching alumina components from above 1600 ^{o}C into a silicone oil bath more than doubled the average flexural strength of the components, compared to the as-received strength [11]. Kirchner proposed that this dramatic strength increase resulted from residual stresses induced by the quench from high temperature [11].

Badaliance, Krohn, and Hasselman proposed that pre-existing cracks could propagate in a single thermal quench below the critical quench temperature difference, ΔTc, and that subcritical crack growth had a significant effect on the thermal shock resistance of soda lime glass [51]. In contrast to Badaliance's results, Ashizuka, Easler, and Bradt presented experimental results indicating that subcritical crack growth effects were insignificant to the thermal shock resistance of borosilicate glass [52]. As will be discussed in the following sections, the difference between Badaliance's results and those of Ashizuka may be related more to their techniques for assessing subcritical growth rather than differences between the tested materials (soda lime glass and borosilicate glass).

3. EXPERIMENTAL PROCEDURES

Commercial glass microscope slides of 7.6 cm X 2.54 cm X 0.12 cm (Cat. No. 48300-036, VWR Scientific Inc., San Francisco, CA) were annealed in air in an electrical furnace at 650 ^{o}C for one-half hour. The specimens then were allowed to cool freely in the furnace. The slides were placed on an aluminosilicate refractory board to prevent viscous deformation during annealing.

The specimens' flexural fracture strength, linear thermal expansion rate, elastic modulus, and internal friction were measured after annealing. Flexural fracture strength was measured in a commercial testing machine with a crosshead speed of 0.1 cm per minute, using a three point bend test fixture with a span of 4.5 cm. The fracture strength, σ was calculated by

$$\sigma = \frac{3\ P\ L}{2\ B\ D^2} \qquad (3)$$

where P is bending load, L is the span between supports, B and D are the width and the thickness of slides.

Linear thermal expansion was measured by a ThermoMechanical Analyzer (TMA, DuPont 9900, DuPont Company, Wilmington, DE) at a heating rate of 5 ^{o}C/minute. Heat flow as a function of temperature was analyzed with a Differential Scanning Calorimeter (DSC, DuPont 9900) using a heating rate of 10 ^{o}C/minute and a nitrogen flow rate of 50 cc/minute.

Elastic moduli were measured by the standing wave resonance method and internal friction values were measured by the logarithmic

decrement technique. Both methods are described elsewhere [53-55].

The annealed slides were heated from room temperature in an electrical furnace. When the furnace temperature was stable for at least one-half hour, the aluminosilicate refractory board was quickly removed from the furnace for quenching. For the liquid bath quenching, the specimens were dumped into a distilled water bath or a motor oil bath (SAE 20W 50), where the initial temperature of both baths was 20 ^{o}C. For air quenching, the slides were quickly set on another cold aluminosilicate board, and again the specimens were allowed to cool freely in air. After the slides reached room temperature, the elastic modulus, internal friction, and retained fracture strength were measured. In addition to the room temperature measurements, the temperature dependence of the elastic modulus also was measured. In order to ensure a statistically reliable estimate of the fracture strength, at least 30 slides were fractured for each quench condition (that is, 30 or more slides were fractured for each quench temperature difference in each of the three quenching media used in this study).

Macro-residual stresses were qualitatively observed by a photoelasticity technique to determine the stress distribution. Residual stresses were measured quantitatively by placing thirty Vickers indentations with a 9.8 N load along the diagonals of both the annealed and quenched slides. The residual stresses on the slide surface were calculated using [56-58]

$$S_r = K_c \, [4 \, C_r / \pi]^{-1/2} \, [(C / C_r)^{3/2} - 1] \qquad (4)$$

2C and $2C_r$ are the crack lengths at a load of 9.8 N for the annealed

and quenched slides, respectively. K_c is the critical stress intensity factor, which is calculated from [59]

$$K_c = 0.016 \, (E/H)^{1/2} \left(\frac{P}{c^{3/2}}\right) \tag{5a}$$

where E is the elastic modulus of the specimen and P is the indentation load [59]. The hardness, H, was determined by

$$H = \frac{P}{2 \, a^2} \tag{5b}$$

where 2a represents the diagonal length of indentation impression [59].

In addition to single-quench testing, cyclic thermal shock (fatigue) was performed. An annealed slide was suspended in a specimen holder and translated back and forth between a water bath and the hot zone of an electric furnace (Figure 3). The slide was maintained in the furnace for 45 minutes and then suddenly dropped into the water bath. The distance from the hot zone of the furnace to the surface of the water bath was about 0.5 meters and the specimens traversed this distance in about 0.3 seconds. During each thermal shock, the specimen remained in the water bath for seven minutes. Eight minutes were required to slowly elevate the specimen and return it to the furnace's hot zone. After each slide was subjected to a pre-determined number of thermal shock cycles, the retained fracture strength of the shocked specimen was measured in three point bend. At least thirteen thermally fatigued glass slides were tested for each ΔT.

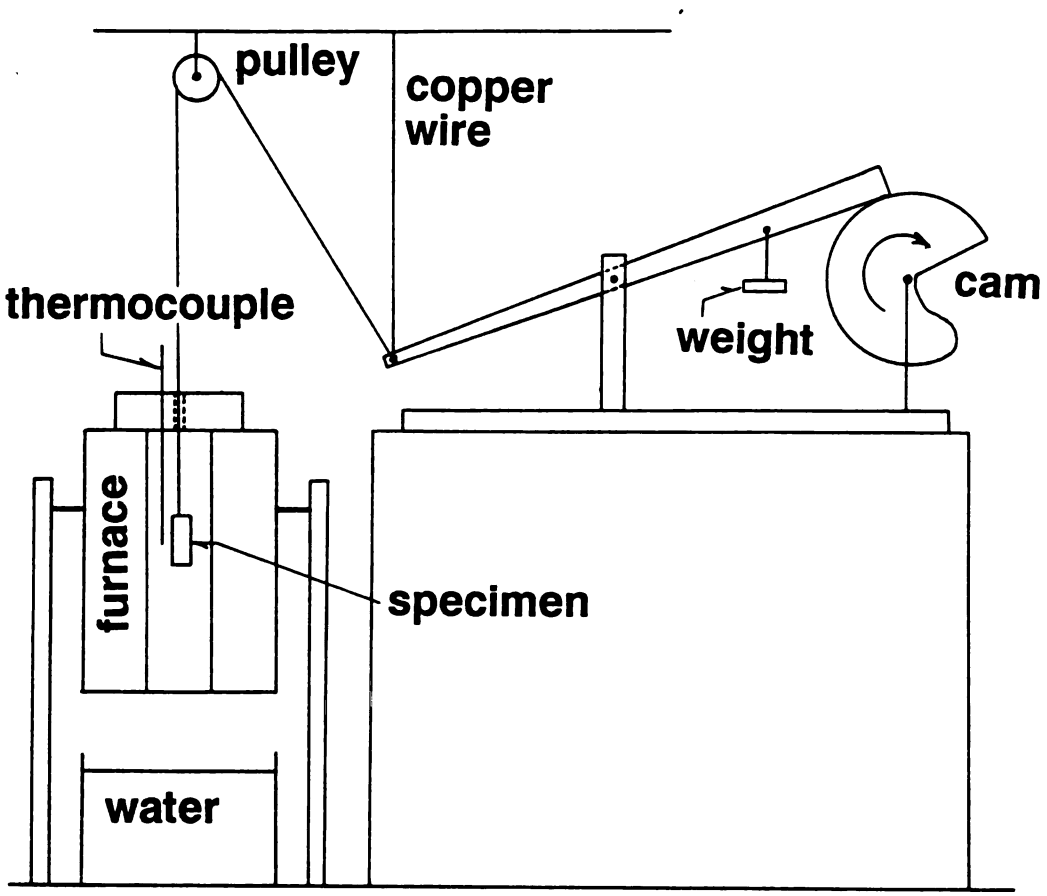

Figure 3. Schematic of the furnace and apparatus for thermal shock fatigue testing.

4. THEORETICAL ANALYSIS, EXPERIMENTAL RESULTS, AND DISCUSSION

(4.1). Thermoeastic and Thermoviscoelastic Stress Calculation and Residual Stresses Analysis

The section theoretically analyzes thermal shock damage and thermal residual stresses for glass plates quenched from above and from below the glass's annealing temperature, T_a. When the initial glass plate's temperature is below T_a, the transient thermal stresses are calculated using thermoelastic theory. When the initial temperature is above T_a, viscus flow is considered and the stresses are calculated using the thermoviscoelastic theory. Crack growth is assumed to occur if the magnitude of the transient tensile stress at the plate's surface or the residual stress in the plate's interior exceeds the fracture strength for the plate.

(4.1.1). Quench from below the annealing temperature

Nonuniform temperature distributions in an elastic heated body result in thermoelastic stresses. For this study's calculations of thermoelastic stresses in a glass plate quenched from below its annealing temperature, we assume the material properties and thermal transfer conditions (elastic modulus, thermal expansion, thermal conductivity, thermal diffusivity, and surface heat transfer coefficient) are independent of temperature. In addition, the initial glass plate temperature and quenching medium temperature are assumed to be constant.

Heat flow out of the plate occurs as a result of the thermal quench. Heat conduction takes place in the plate and heat

convection occurs in the quenching medium. The thickness of the plate is assumed to be small compared with its width and length. Thus, edge effects are neglected and the heat flow is one dimensional. The governing equation for the heat transfer is

$$\frac{1}{a}\frac{\partial T}{\partial t} = \frac{\partial^2 T(Z,t)}{\partial Z^2} \tag{6}$$

a = thermal diffusivity
Z = spatial coordinate in the direction normal to glass plate surfaces
t = time
T(Z,t) = temperature distribution in glass plate

The boundary and initial conditions are

$$\frac{\partial T}{\partial Z} = 0 \qquad \text{at } Z = 0 \tag{7a}$$

$$-K\frac{\partial T}{\partial Z} = h\,(T - T_o) \qquad \text{at } Z = \ell \text{ and } -\ell \tag{7b}$$

$$T = T_i \qquad \text{at } t = 0 \tag{7c}$$

T_o = quenching medium temperature
T_i = initial temperature of glass plate
h = surface heat transfer coefficient
K = thermal conductivity
ℓ = half thickness of glass plate. $Z = \ell$ and $Z = -\ell$ on the plate surfaces

Separation of variables gives the temperature gradient through the thickness of the plate (Z axis) as [60]

$$\Delta T_*(Z,t) = \Delta T \sum_{n=1}^{\infty} 2\left[\frac{\sin(\delta_n)\cos(\delta_n Z/\ell)}{\delta_n + \sin(\delta_n)\cos(\delta_n)}\right] \exp(-a\,(\delta_n/\ell)^2\, t) \tag{8a}$$

$$\delta_n \tan(\delta_n) = B \qquad n = 1, 2, 3, \ldots . \tag{8b}$$

$$T(Z,t) = T_o + \Delta T_*(Z,t) \tag{8c}$$

ΔT = quenching temperature difference between T_i and T_o
δ_n = the root of Equation (8b)

B = Biot's modulus [61], which is in turn given by

$$B = \frac{r\ h}{K} \tag{9}$$

where r is a characteristic dimension of the specimen. For the plate geometry considered here, r is equal to the plate's half thickness, ℓ [61]. Without considering surface traction, the thermoelastic stresses in an infinite plate are [62]

$$\sigma_{xx}(Z,t) = \sigma_{yy}(Z,t) = -\frac{\alpha E}{1-\nu}\left\{ -\Delta T_* + \frac{1}{2\ell}\int_{-\ell}^{\ell} \Delta T_*\, dZ + \frac{3Z}{2\ell^3}\int_{-\ell}^{\ell} \Delta T_*\, Z\, dZ \right\} \tag{10a}$$

$$\sigma_{zz} = \sigma_{xy} = \sigma_{xz} = \sigma_{yz} = 0 \tag{10b}$$

E = elastic modulus
ν = Poisson's ratio
α = thermal expansion
σ_{zz} = normal stress in the direction normal to plate surface
σ_{xx} and σ_{yy} = normal stress in the direction parallel to plate surface
σ_{xy}, σ_{xz}, and σ_{yz} = shear stress

Combining equations (8) and (10) gives

$$\sigma_{xx}(Z,t) = \sigma_{yy}(Z,t)$$

$$= 2 \frac{\alpha E \Delta T}{1 - \nu} \left\{ \sum_{n=1}^{\infty} \exp(-a (\delta_n/\ell)^2 t) \frac{\sin(\delta_n)}{\delta_n + \cos(\delta_n) \sin(\delta_n)} \right.$$

$$\left. \left(\frac{\sin(\delta_n)}{\delta_n} - \cos(\delta_n Z/\ell) \right) \right\} \qquad (8)$$

Equation 11 thus describes the thermoelastic stresses in an infinite glass plate of thickness 2ℓ quenched from below the annealing temperature.

(4.1.2). Quench from above the annealing temperature

When a glass plate is heated to near its annealing temperature, the viscosity of the glass decreases. At the annealing temperature, viscous flow is significant. For example, internal stress in glass is substantially relieved by viscous flow during a one hour heat treatment at the annealing temperature [63]. If a glass plate is quenched from above its annealing temperature, the transient thermal stresses are also influenced by viscous flow [64].

The mathematics of the thermal stresses in linear viscoelastic materials have been treated by several authors who account for the effect of viscous flow and stress relaxation [64-70]. Lee et al. unified the mathematical framework and presented a thermoviscoelastic theory for the thermal stresses and residual stresses that arise when a glass plate is quenched symmetrically from both surfaces [64]. Upon comparison with experimental results, Narayanaswamy et al. modified Lee's numerical calculation technique to bring the theoretical results into closer agreement with

experimental data [71]. Since Lee's theory can conveniently model the transient thermal stresses in a rapidly quenched glass plate, we use the formulations presented by Lee [64] and Narayanaswamy [71] in the present study.

Linear elastic materials have a constant elastic modulus so that materials subjected to a given strain do not experience stress relaxation. However, linear viscoelastic materials exhibit stress relaxation for an isothermal deformation, which is described by [65,72]

$$\sigma_{ij}(t) = \int_0^t G_{ijkl}(t - t') \frac{\partial \epsilon_{kl}(t')}{\partial t'} dt' \tag{12}$$

where σ_{ij}, ϵ_{kl}, $G_{ijkl}(t)$, and t are the stress tensor, strain tensor, relaxation modulus tensor, and time, respectively. For viscoelastic plates subjected to a thermal quench, Lee proposed that the transient thermal stresses may be calculated from [64]

$$\int_0^{\ell} \sigma_{xx}(Z,t)\, dZ = 0 \tag{13}$$

$$\sigma_{xx}(Z,t) = 3\int_0^t R(\xi(Z,t) - \xi(Z,t')) \frac{\partial}{\partial t'} \left[\epsilon(t') - \alpha T(Z,t') \right] dt' \tag{14}$$

where the reduced time, ξ, expresses the temperature and time dependence of the viscoelastic material properties. The parameter, ξ, is defined by [64,66,69]

$$\xi(Z,t) = \int_0^t \Phi[T(Z,t')]dt' \tag{15}$$

T(Z,t) is the temperature distribution in the quenched glass plate

(equation (8)). Lee indicated that the time shift factor $\Phi(T)$ for soda lime silica glass measured at a base temperature of 538 ^{o}C is [64]

$$\log_{10}[\Phi(T)] = 0.03861(T - 538) \tag{16}$$

$R(\xi)$ is an auxiliary modulus function associated with the relaxation modulus tensor, G, such that for a Maxwell solid $R(\xi)$ is given by [66,67]

$$R(\xi) = \frac{H(\xi)\, E_o}{3(1-\nu)} \exp(-\beta\, \xi/\tau_o) \tag{17a}$$

Normalizing $R(\xi)$ by the factor $(E_o/\, 3(1 - \nu)$ gives the unitless function $R(\bar{\xi})$, where

$$\bar{R}(\xi) = H(\xi) \exp(-\beta\, \xi/\tau_o) \tag{17b}$$

where

$$\beta = \frac{1 + \nu}{3\,(1 - \nu)} \tag{17c}$$

and $H(\xi)$ is the Heaviside unit step-function. E_o and τ_o are the instantaneous elastic modulus at t = 0 and the relaxation time, respectively. Batteh [73] approximated $\bar{R}$ directly from Narayanaswamy's data for soda lime silica glass [71] as

$$\bar{R}(\xi) = \exp(-\xi/700) \tag{18}$$

According to Narayanaswamy's modification [71], equation (14) is rewritten as

$$\sigma_{xx}(Z,t) = \sigma_{yy}(Z,t)$$

$$= -\frac{E_o}{1-\nu} \sum_{i=1}^{n} \left\{ \left(\frac{\epsilon(t_i) - \epsilon(t_{i-1}) - \alpha[T(Z,t_i) - T(Z,t_{i-1})]}{\xi(Z,t_i) - \xi(Z,t_{i-1})} \right) \right.$$

$$\left. \int_{\xi_{i-1}}^{\xi_i} \bar{R}(\xi - \xi')\, d\xi' \right\} \qquad (19)$$

Equations (13) and (19) constitute a set of nonlinear integral equations. To calculate the transient thermal stresses, we first numerically solve for $\xi(Z,t)$ by combining equations (8), (15), and (16). The integral of $\int R\, d\xi'$ in equation (19) is then calculated using equation (18). Finally, the transient stress $\sigma(Z,t)$ and strain $\epsilon(t)$ are calculated iteratively as a function of time t, using equations (13) and (19). The residual stresses are the steady-state values to which $\sigma(Z,t)$ converges if time becomes great enough, for example t = 50 seconds. The residual surface stresses correspond to the convergent values, $\sigma(\ell,t)$. Table 1 lists the required input values for the numerical analysis.

Table 1. Numerical values used in calculating the transient thermal stresses in microscope slide glass specimens. All values were measured in this research, unless otherwise indicated.

thermal expansion (α)	: $8 * 10^{-6}$	$^oC^{-1}$	[74,75]
elastic modulus (E)	: 70	GPa	
Poisson's ratio (ν)	: 0.25		[74,75]
half thickness of specimen (ℓ)	: 0.001	m	
thermal diffusivity (a)	: $4.8 * 10^{-7}$	$m^2\ s^{-1}$	[74,75]
Biot's modulus (B)	: 10		
quenching medium temperature (T_o)	: 20	^oC	
flexural fracture strength	: 101.4	MPa	

(4.1.3). Numerical calculation

For a glass plate quenched from below its annealing temperature, numerical modeling of the thermoelastic stresses shows that compressive stress arises internally in the plate and that tensile stresses develop on the plate's surface (Figure 4(a)). The maximum tensile stress always appears on the surface of the glass plate.

If a glass plate is quenched from above the annealing temperature, thermoviscoelastic stresses can induce viscous flow in the glass plate which in turn leads to complex stress fields and induces residual stresses in the plate (Figure 4(b) and Figure 5). The thermoelastic surface stresses versus time increase as ΔT increases (Figure 6(a)). The time evolution of the surface stresses that develop during quenching are keenly dependent on whether the plate is quenched from below or from above the annealing temperature. For quenching from below the annealing temperature, the thermoelastic stresses versus time increase monotonically as ΔT increases (Figure 6(a)). In contrast, for quenching form above the annealing temperature, the thermoviscoelastic stresses generally decrease as the temperature increases (Figure 6(b)).

Figure 7 illustrates the relationship between the ΔT and the maximum surface tensile stresses. For $\Delta T < 500\ ^{o}C$, the glass plate acts as an elastic material and the stresses follow the solid line. According to equation (11), the maximum surface tensile stresses increase linearly with increasing ΔT. For $\Delta T > 580\ ^{o}C$, viscous flow of the glass becomes significant, resulting in a decrease of the maximum surface tensile stresses as a function of increasing ΔT (the dashed line in Figure 7). Between $\Delta T=500\ ^{o}C$ and $\Delta T=580\ ^{o}C$, the two

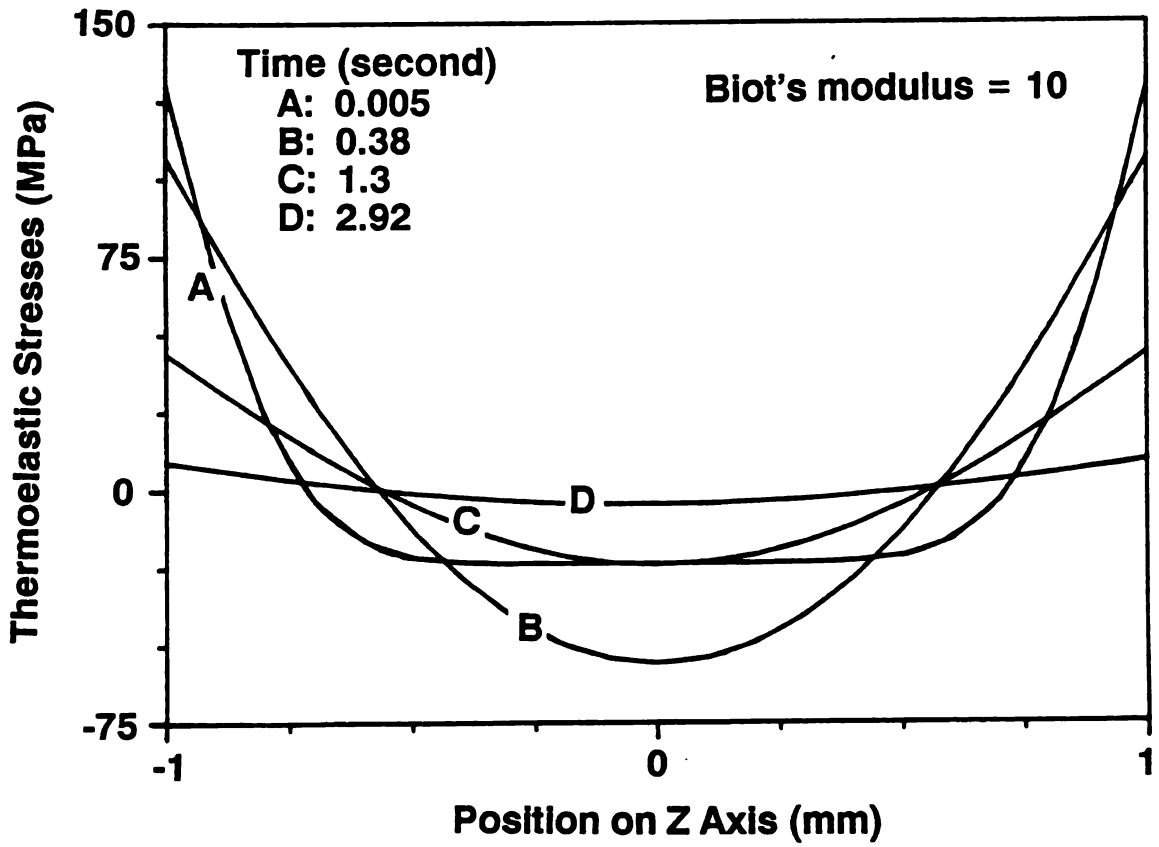

Figure 4(a). Transient thermal stresses in a quenched glass plate. Thermal quenching from below the annealing temperature, ΔT = 300 °C. The annealing temperature of the glass plate is taken as 580 °C and the quench medium temperature is assumed to be 25 °C.

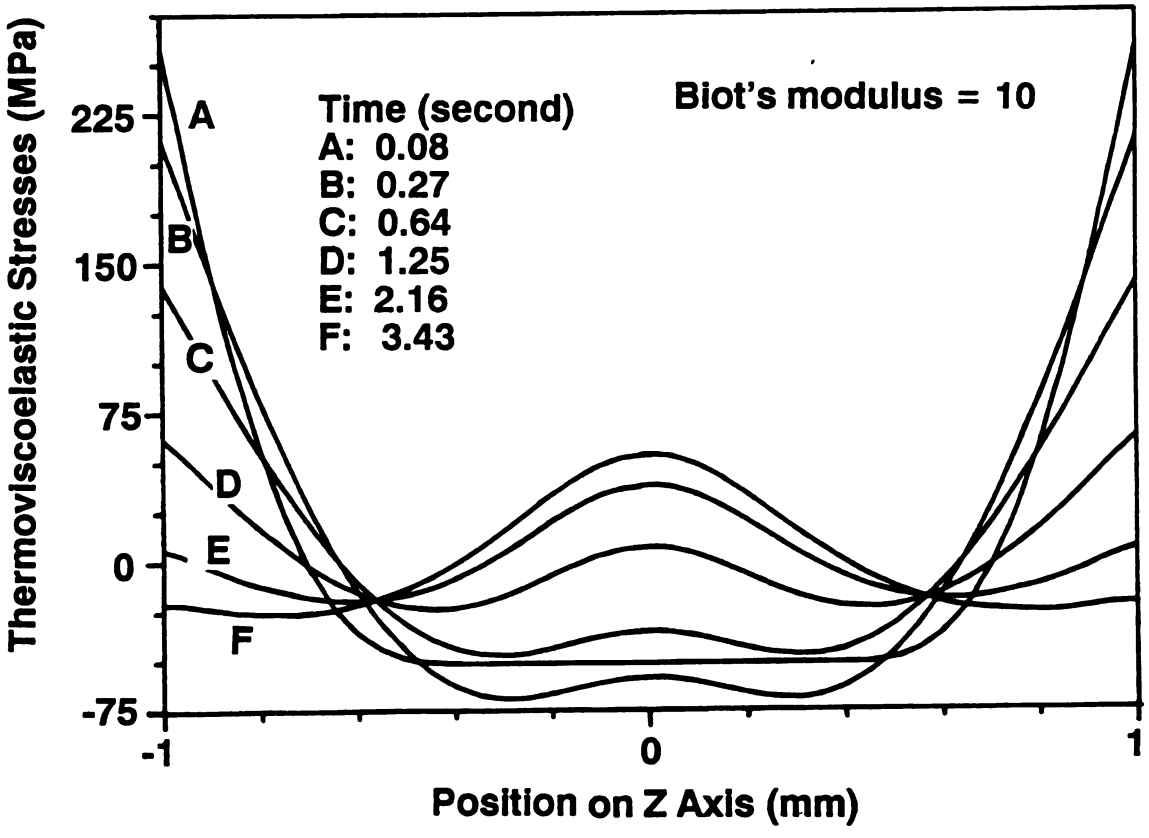

Figure 4(b). Transient thermal stresses in a quenched glass plate. Thermal quenching from above the annealing temperature, $\Delta T = 620\ ^{o}C$. The annealing temperature of the glass plate is taken as $580\ ^{o}C$ and the quench medium temperature is assumed to be $25\ ^{o}C$.

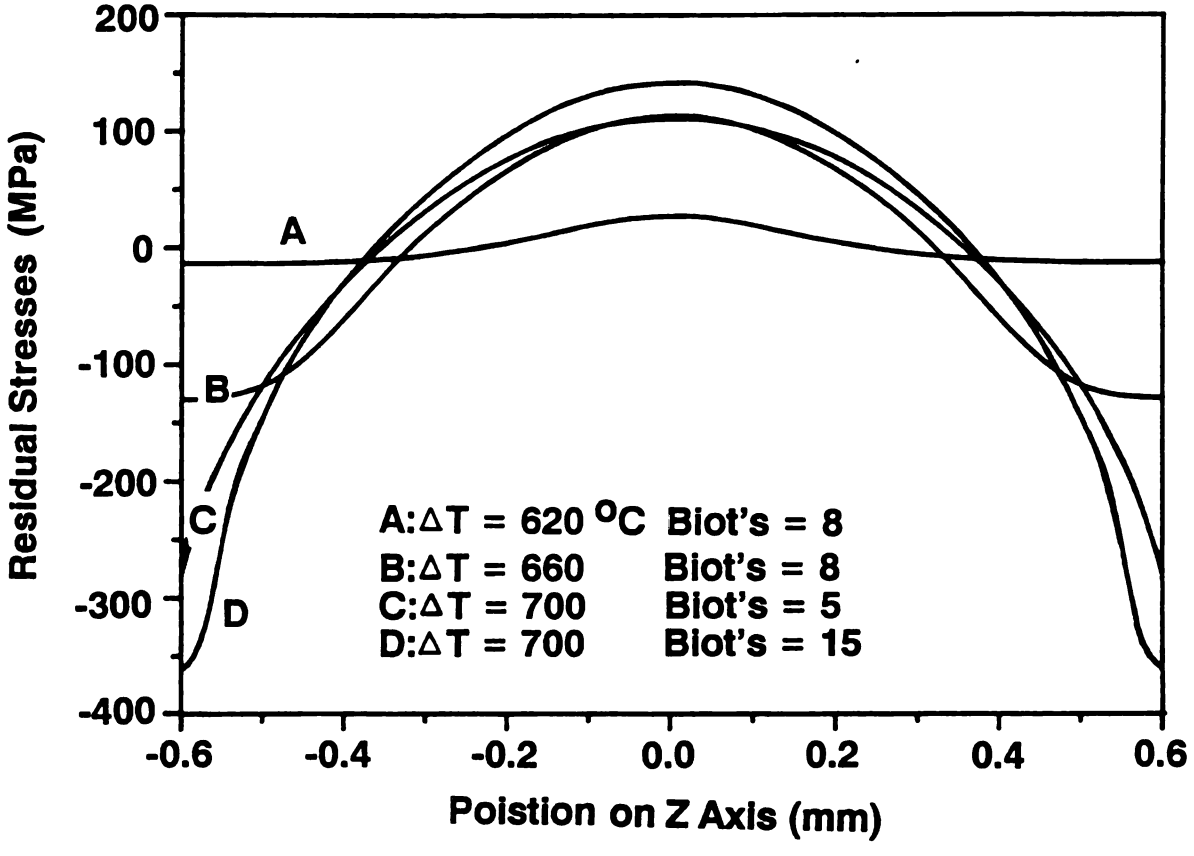

Figure 5. Residual stress profile in a glass plate quenched from above the annealing temperature. The annealing temperature of the glass plate is taken as 580 °C and the quench medium temperature is assumed to be 25 °C.

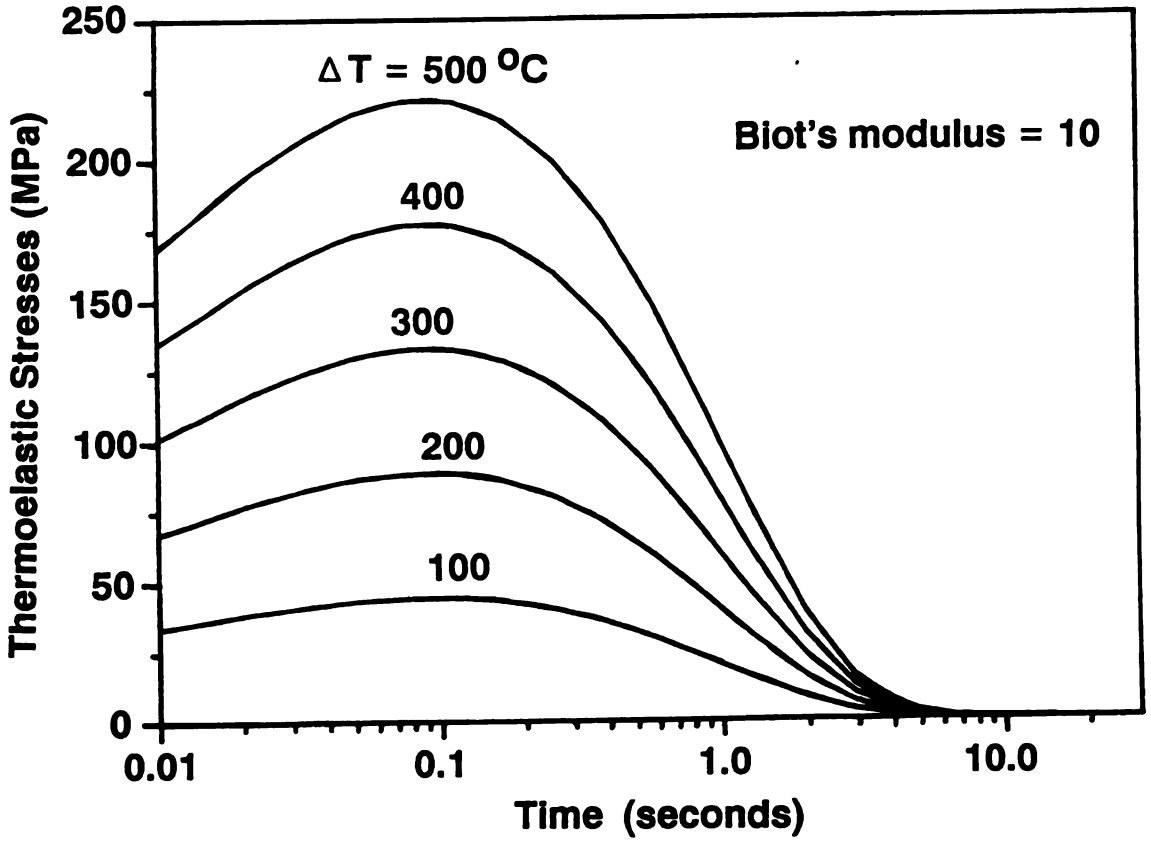

Figure 6(a). Influence of ΔT on surface thermoelastic stresses. The annealing temperature of the glass plate is taken as 580 °C and the quench medium temperature is assumed to be 25 °C. Therefore, each curve corresponds to a quench from below the annealing temperature.

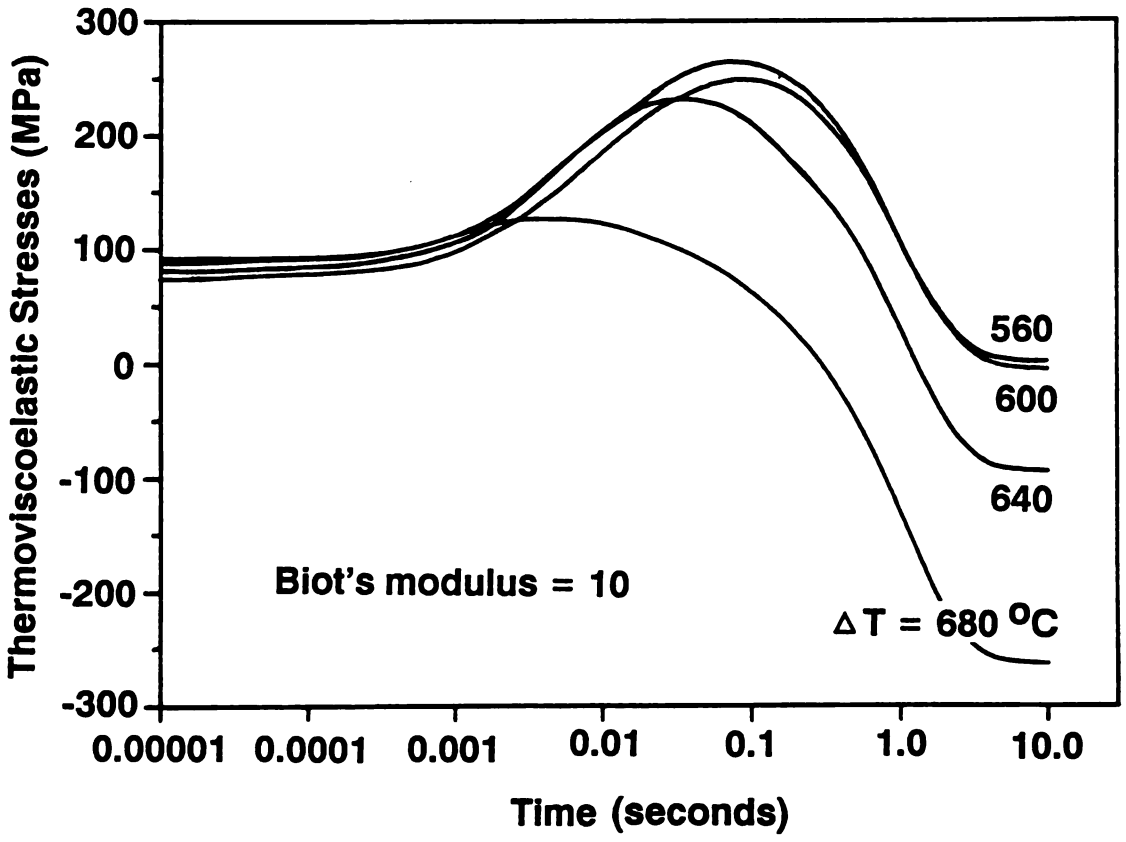

Figure 6(b). Influence of ΔT on surface thermoviscoelastic stresses. The annealing temperature of the glass plate is taken as 580 ^{o}C and the quench medium temperature is assumed to be 25 ^{o}C. Each curve corresponds to a quench from above the annealing temperature, thus thermoviscoelastic theory is required to calculate the transient stresses.

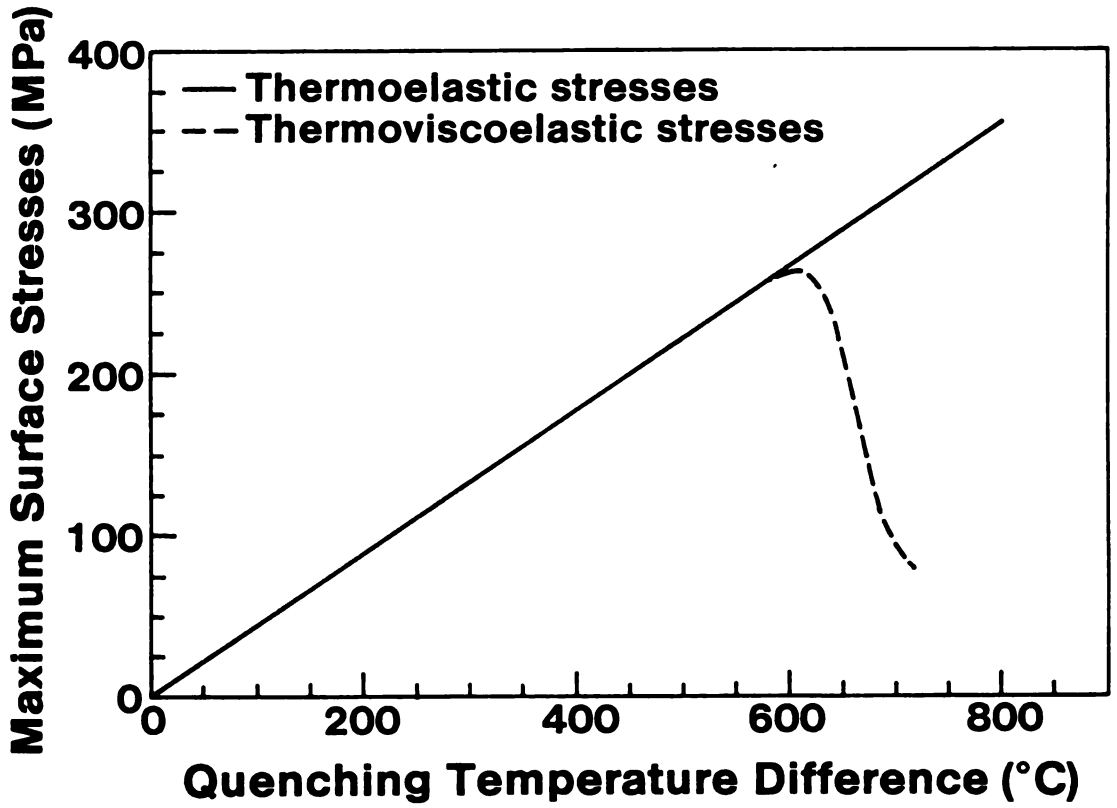

Figure 7. The maximum surface stresses versus ΔT in a quenched plate, as a function of the quench temperature difference ΔT. Note the divergence between the thermoelastic stress curve and the thermoviscoelastic stress curve that becomes evident for temperatures somewhat above the annealing temperature. Again, the temperature of the quenching medium is assumed to be 580 ^{o}C.

curves superimpose.

The thermal stresses illustrated in Figures 4, 6 and 7 are computed for a Biot's modulus equal to ten. However, Biot's modulus influences the magnitude of thermal stresses such that as Biot's modulus increases, the maximum value of the residual tensile stress increases in the plate's interior and the transient tensile stress on the plate's surface also increases (Figure 5, 8(a), and 8(b)). Thermal quench conditions for a given material system can be described in terms of the surface heat transfer coefficient, quench temperature difference, and the specimen dimension. However, Biot's modulus can replace both the surface heat transfer coefficient and specimen size variables such that thermal quench conditions can be simply expressed by two variables, Biot's modulus and quench temperature difference.

Thermal shock damage usually initiates at the regions of maximum transient tensile stress which occurs on the surface of quenched brittle components. Crack growth also may occur in the interior of tempered glass which develops sufficiently high residual stresses. To predict the thermal shock damage of glass plates quenched from above their annealing temperature, we assume that (1) during thermal quench, crack growth is dominated by the propagation of pre-existing surface cracks; (2) the surface layers in the initial cooling step approach elastic behavior; (3) the fracture strength is independent of temperature; and (4) after the thermal quench occurs, the residual tensile stress in the interior of the quenched glass plate may be large enough to propagate pre-existing flaws. Therefore, an appropriate shock damage criterion is that the

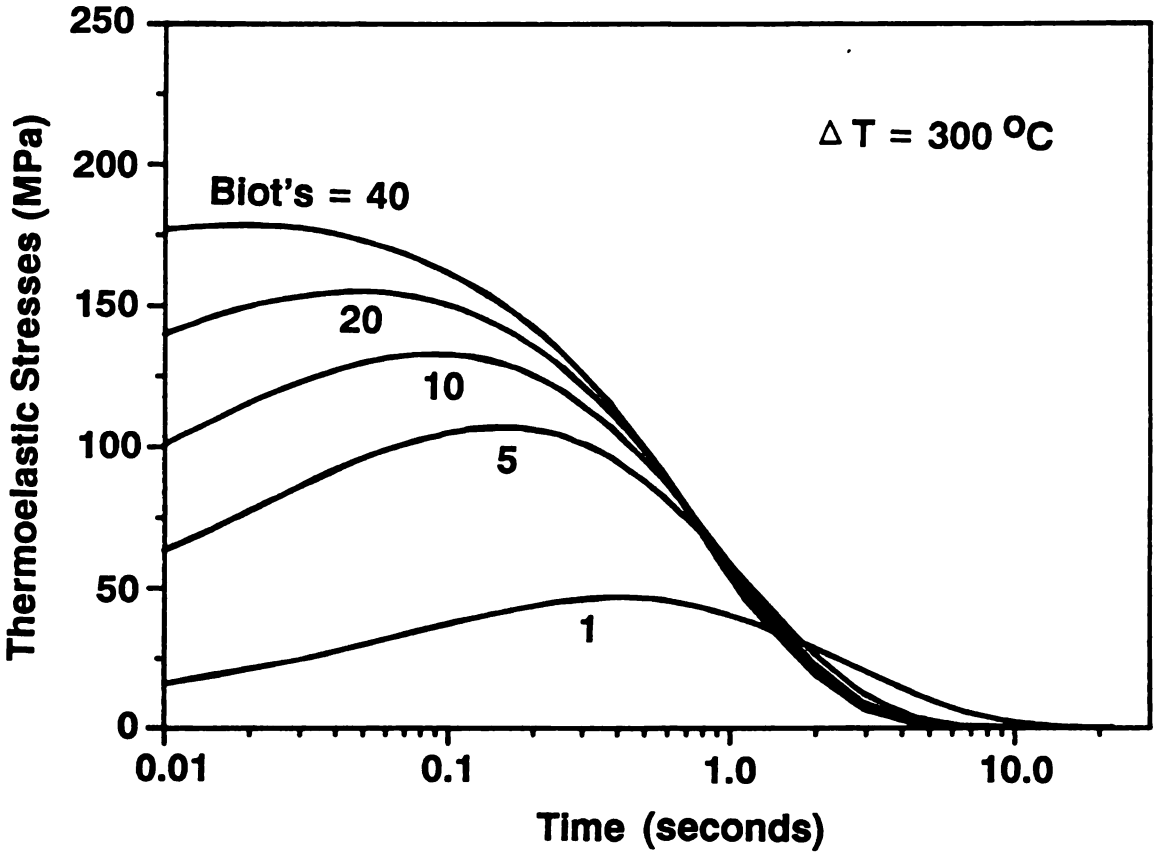

Figure 8(a). Influence of Biot's modulus on surface thermoelastic stresses, with ΔT = 300 °C. The annealing temperature of the glass plate is taken as 580 °C and the quench medium temperature is assumed to be 25 °C.

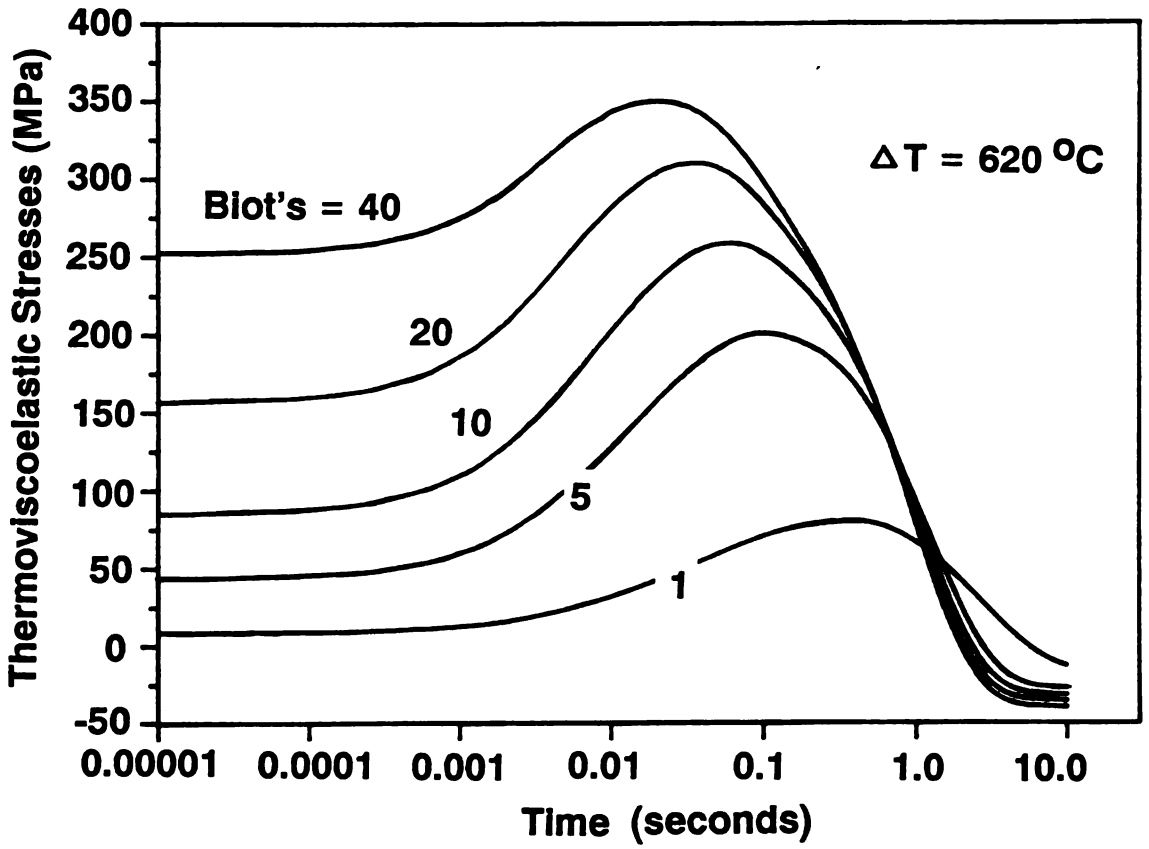

Figure 8(b). Influence of Biot's modulus on surface thermoviscoelastic stresses, with $\Delta T = 620^{o}C$. The annealing temperature of the glass plate is taken as 580 ^{o}C and the quench medium temperature is assumed to be 25 ^{o}C.

crack growth occurs if the magnitude of the transient surface stress or the residual interior tensile stress exceeds the fracture strength.

From the thermal stress calculations#, we can construct a thermal shock damage map consisting of three curves, curve A for the thermoelastic stresses and curves B and C for the thermoviscoelastic stresses (Figure 9). The thermal quench conditions in the map are characterized by Biot's modulus and the quench temperature difference. When the thermal quench conditions correspond to a point above curves A and B, the maximum surface tensile stresses exceed the fracture strength and cracks propagate. If the quench conditions correspond to a point above the curve C, crack growth is driven by the residual interior tensile stress. When the quench conditions correspond to a point below the curves, there is no shock damage. The effect of viscous flow upon the stresses becomes obvious near the annealing temperature, which is about 580 ^{o}C in this case (see Figure 7 and 9). Thus, residual thermal stresses develop in glass plates quenched from above about 600 ^{o}C.

For a thermal quench of a glass plate, three values of the critical quench temperature difference, ΔTc, may appear on the thermal shock damage map. The critical values of ΔTc may be calculated from the intersections of the three curves in the thermal shock damage map (Figure 9). For example, if the glass plate is quenched at B = 5, the critical quench temperature differences are ΔTc = 300 ^{o}C, ΔTc = 670 ^{o}C, and ΔTc = 780 ^{o}C. From the three

---

The curves in Figure 9 were evaluated using Computer programs No. 1 and No. 3. The curves correspond to the thermal stress conditions in which the maximum transient stress is 101.2 MPa.

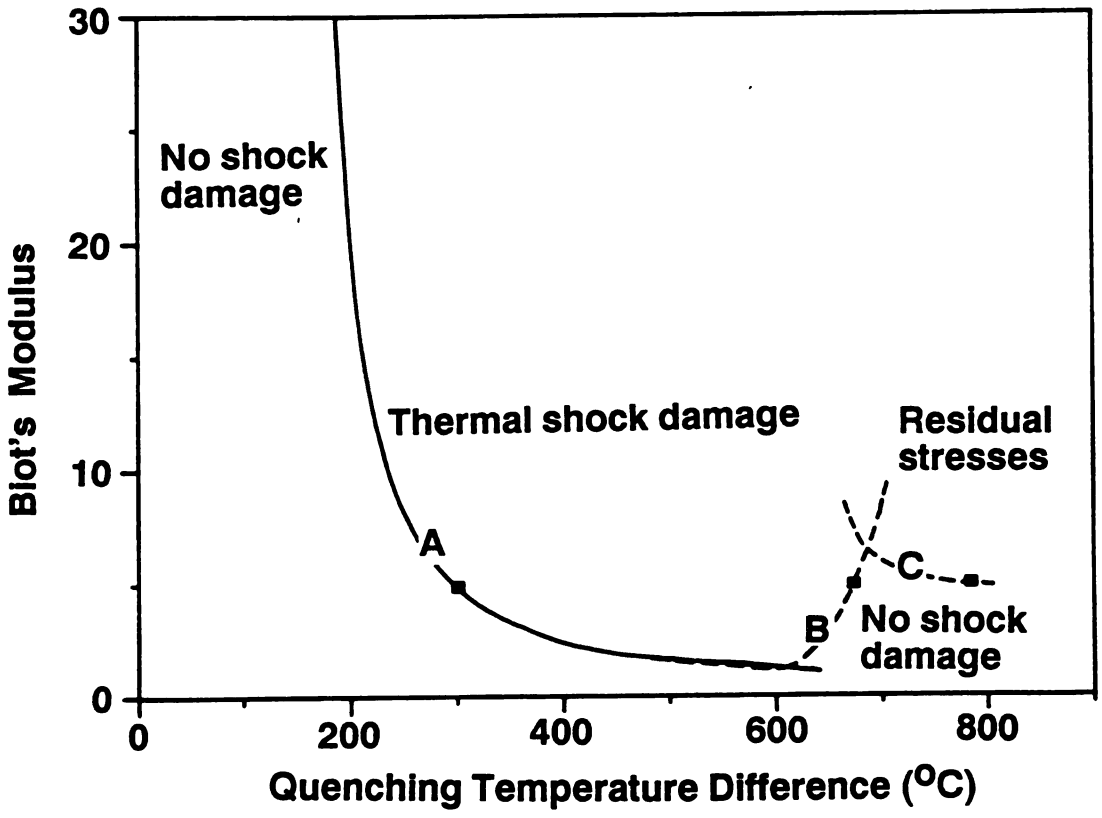

Figure 9. Thermal shock damage map for a glass plate. The annealing temperature of the glass plate is taken as 580 °C and the quench medium temperature is assumed to be 25 °C.

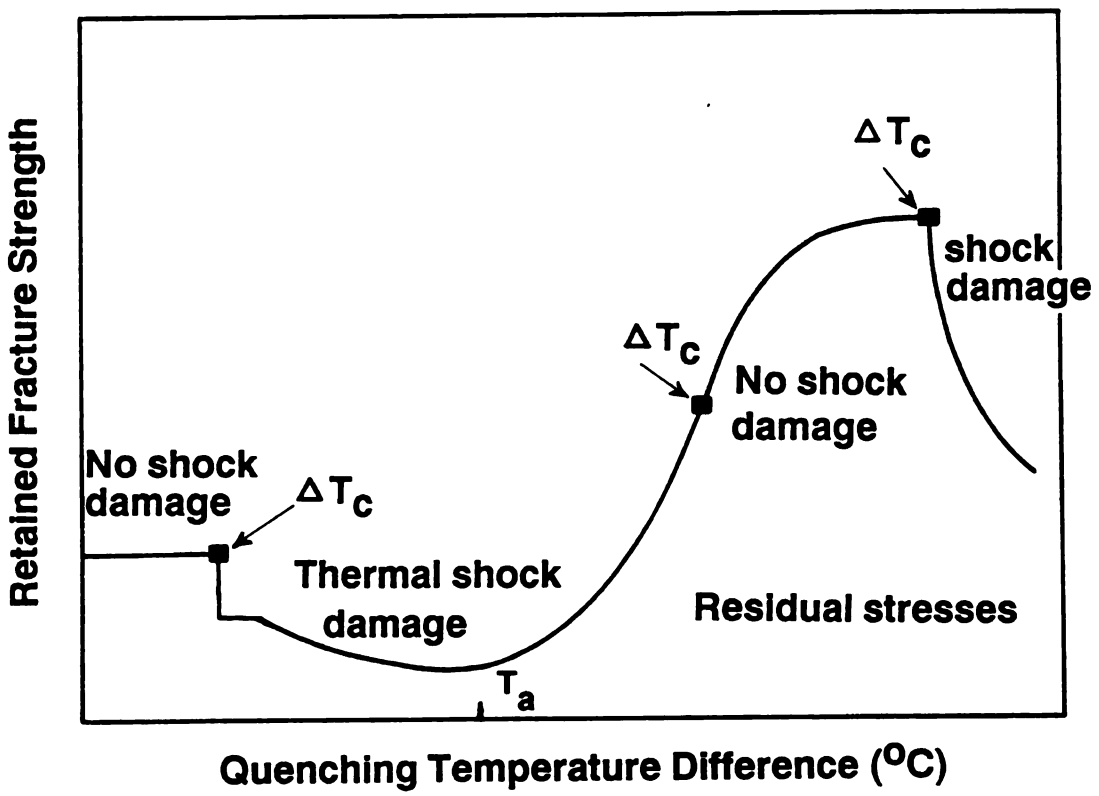

Figure 10. Schematic of a thermal shock induced strength degradation curve as inferred form the thermal shock damage map for a quenched glass plate. The T_a represents the ammealing temperature of glass plate, at which the minimum retained strength occurs.

critical values, we can qualitatively infer the shape of the thermal quench strength degradation curve (see Figure 10). Glass plates quenched from below $\Delta T = 300\ ^{o}C$ have no thermal shock damage and their fracture strength does not change. Above $\Delta T = 780\ ^{o}C$ as well as between $\Delta T = 300\ ^{o}C$ and $\Delta T = 670\ ^{o}C$, thermal shock damage reduces the retained fracture strength of the glass plate. When the initial specimen's temperature is near to the annealing temperature, T_a, the retained strength is minimized. Shock damage disappears for $670\ ^{o}C < \Delta T < 780\ ^{o}C$. The gradual increase and eventual saturation in retained fracture strength for $580\ ^{o}C < \Delta T < 780\ ^{o}C$ results from viscous flow of the glass. The viscous flow decreases the magnitude of thermal stresses, which in turn decreases the probability and the severity of the thermal shock damage. Thus, between $580\ ^{o}C$ and $780\ ^{o}C$ the glass plate can be tempered (strengthened) without thermal shock damage.

Figure 11 illustrates the relation among residual surface stresses, initial quenching temperature, and Biot's modulus. For thermal quench conditions corresponding to a given Biot's modulus, the residual surface stresses reach a saturation value with further increase of the initial glass temperature. Therefore, the residual-stress-induced increase in the retained fracture strength also saturates (Figure 11).

In this study, thermal shock damage was analyzed for glass plates. Physically meaningful changes in the input parameters (Table 1) for the numerical analysis only shifts the curves, without changing the essential characteristics of the thermal shock damage map. For example, in a plot of Biot's modulus versus the quenching

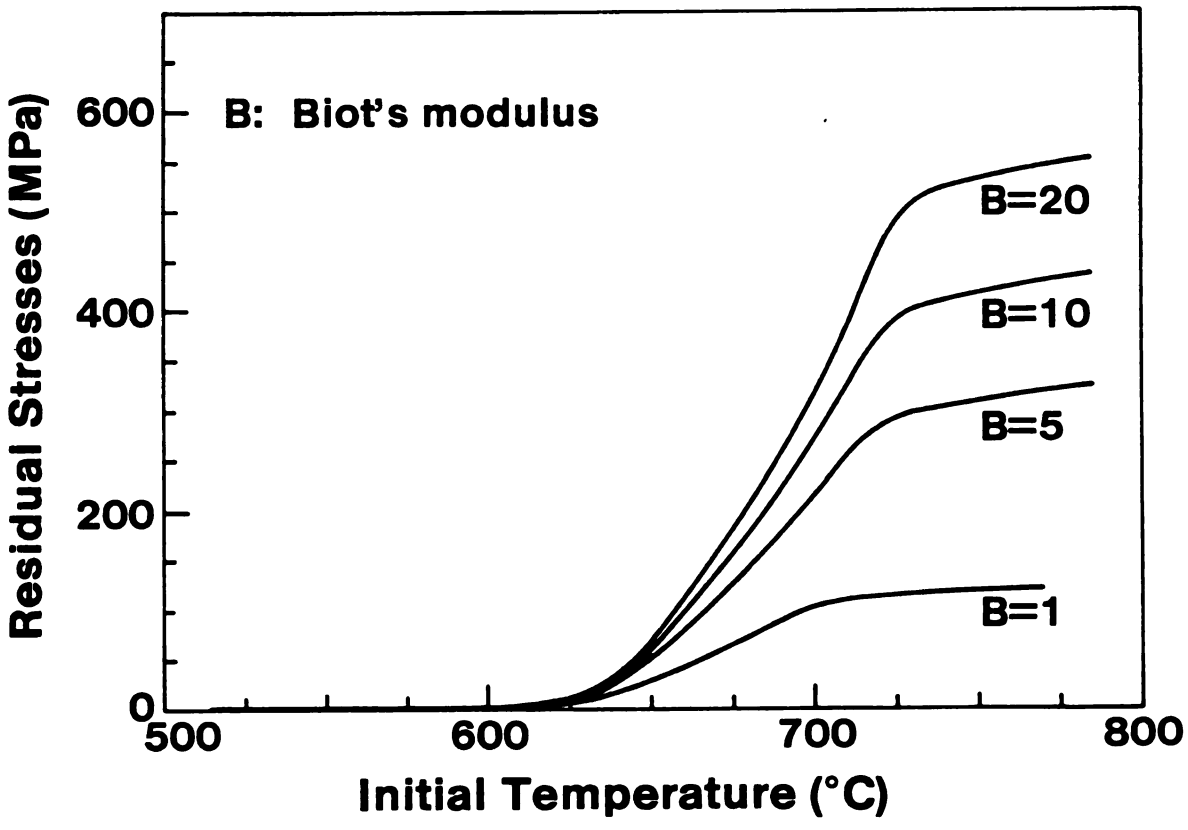

Figure 11. Relationship between residual surface stresses, initial glass temperature, and Biot's modulus for a quenched glass plate.

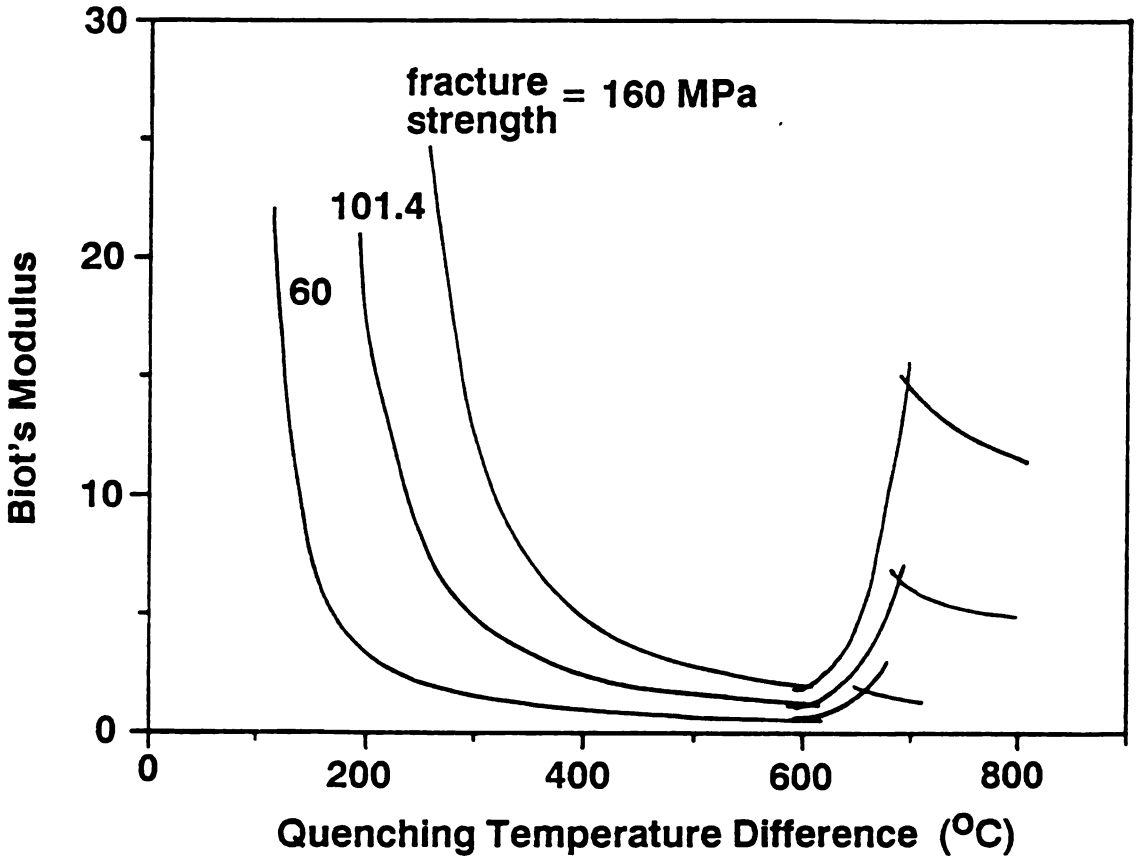

Figure 12. Shifts in the thermal shock damage map that result from assuming different flexural fracture strength values for the glass plate. The curves show that the numerical technique presented in this study is stable with respect to changes in the assumed fracture strength.

temperature difference, changing the fracture stress from the experimentally determined value of 101.4 MPa downward to 60 MPa or upward to 160 MPa systematically shifts the numerical results with respect to the quenching temperature difference, but the general shape of the curve is largely maintained (Figure 12). Variations in specimen thickness, surface heat transfer coefficient, and thermal conductivity are encompassed by B, the Biot modulus (equation (9)). Figure 12 is quite important with respect to the numerical modeling presented in this paper and the possibility of extending our analysis to other viscoelastic materials. Numerical techniques can be unstable, in that small changes in the input data may cause large swings in the results [76], but (at least with regard to changes in the fracture stress) the technique presented here seems to be stable.

Therefore, the map may apply also to those ceramic materials which are viscoelastic at high temperature. Gebauer et al. [9,10] and Ohira et al. [49] quenched aluminosilicate rods into an silicone oil bath over a range of different quench temperature differences and obtained a strength degradation curve similar to Figure 10. Mai [48] quenched TiC and WC in water bath at $\approx 20\ ^{o}C$ and also yielded a curve similar to Figure 10. Gebauer proposed that viscous flow in the glassy grain boundary phases might account for the observed strength changes. The analysis in the present study shows that the viscous flow of glass yields the same "shape" for the strength distribution curve as observed experimentally by Gebauer [9.10].

Although there are similarities between the behavior predicted in this study and the experimental results in the literature for polycrystalline ceramics quenched from high temperatures, additional

study is needed on the quench behavior of ceramics containing a significant glassy grain boundary phase.

(4.2) The Influence of Thermal Quench on Mechanical Properties

The experimental results on quenched microscope glass slides presented in this section will be compared with the theoretical analysis given in the previous section.

Thermal shock damage and residual stresses are typically evaluated via fracture strength. However, elastic modulus and internal friction also can be useful indicators of microcracks and microstructural change [77-83]. Thus, in this study, fracture strength, elastic modulus, and internal friction were used to monitor the effect of thermal quenching on glass slides. In addition, the annealing temperature of the glass was determined from linear thermal expansion measurements. Quench-induced residual stresses were evaluated using the Vickers indentation technique. The annealing-induced residual stress relaxation was detected from a heat flow analysis using Differential Scanning Calorimeter (DSC).

(4.2.1). Annealing temperature determination

The linear thermal expansion rate of the glass slides was nearly constant up to 510 ^{o}C, but increased sharply for the interval between about 550 ^{o}C and 600 ^{o}C (Figure 13). With further heating the expansion rate decreased as the viscous flow of the glass slides became significant. From Figure 13, the annealing temperature of the glass was around 580 ^{o}C [63].

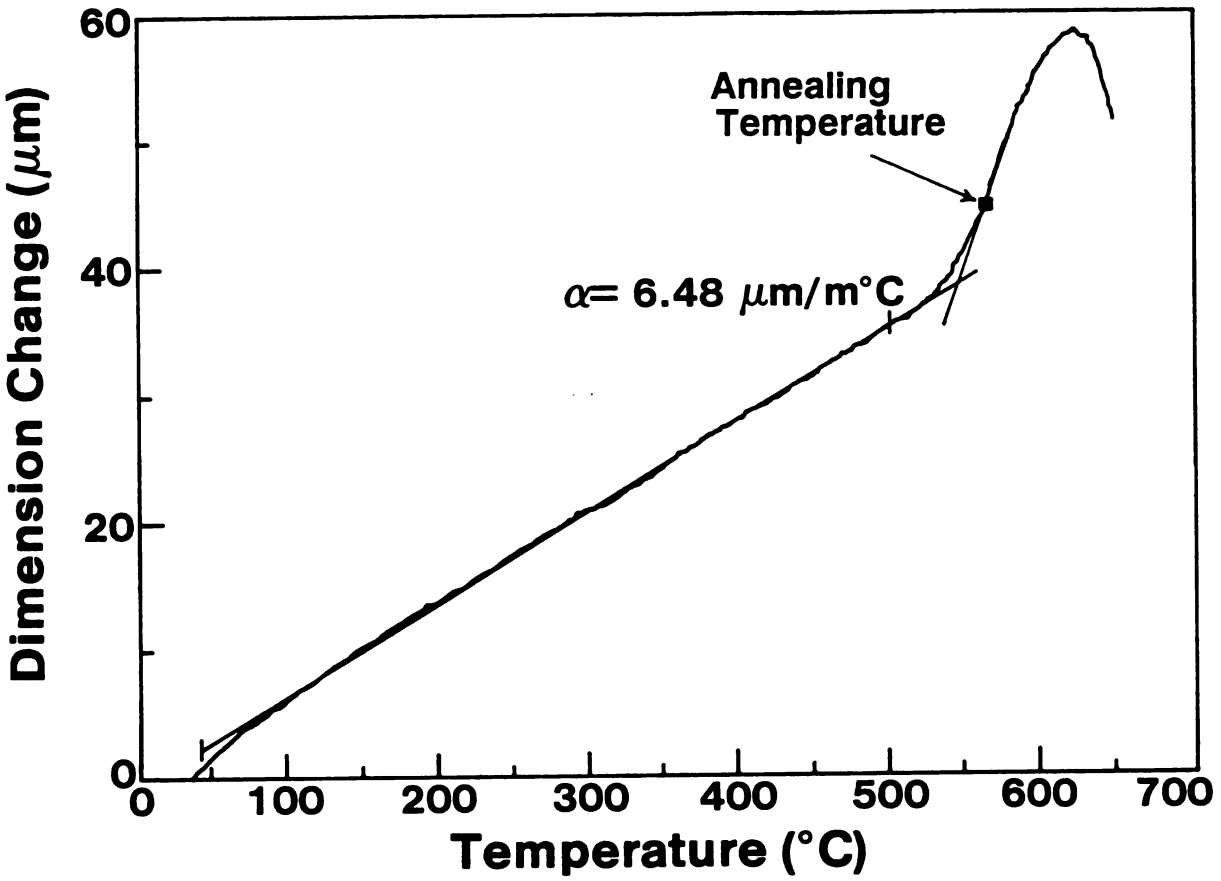

Figure 13. The dimensional change versus temperature for an annealed glass slide, as measured dilatometrically at a heating rate of 5 ^{o}C/minute. As indicated on the figure, from about 100 to 500 ^{o}C, a nearly constant coefficient of linear thermal expansion of 6.48 X 10^{-6}/^{o}C was measured.

(4.2.2). Fracture strength

In this study glass plates were quenched into three different media: water, oil, and air. The magnitude of the surface heat transfer coefficient, h, is such that h (water quench) > h (oil quench) > h (air quench) [61,84,85]. Thus, the Biot's modulus, B, is ranked as follows: B (water quench) > B (oil quench) > B (air quench), where B is defined as

$$B = \frac{r\ h}{K} . \qquad (9)$$

Typical thermal shock experiments involve quenching only from below the annealing temperature. In this study, we included thermal quenching from both above and below the annealing temperature. This wider range of temperatures is important since the observed retained fracture strength for specimens quenched from below the annealing temperature of 550 ^{o}C (for our specimens) can show very different trends from those specimens quenched from temperatures above the annealing temperature. In addition, the retained fracture strength behavior depends strongly on the quenching medium. For thermal quenching from below the glass annealing temperature, the retained fracture strength data indicate critical quench temperature differences of $\Delta Tc \approx 165$ ^{o}C and $\Delta Tc \approx 400$ ^{o}C for the water quench and the oil quench, respectively (Figure 14(a)). For air quenching from below the annealing temperature, the retained fracture strength does not change significantly, implying that thermal shock damage does not occur. These experimental results indicate that for thermal quenching from below the glass annealing temperature, a

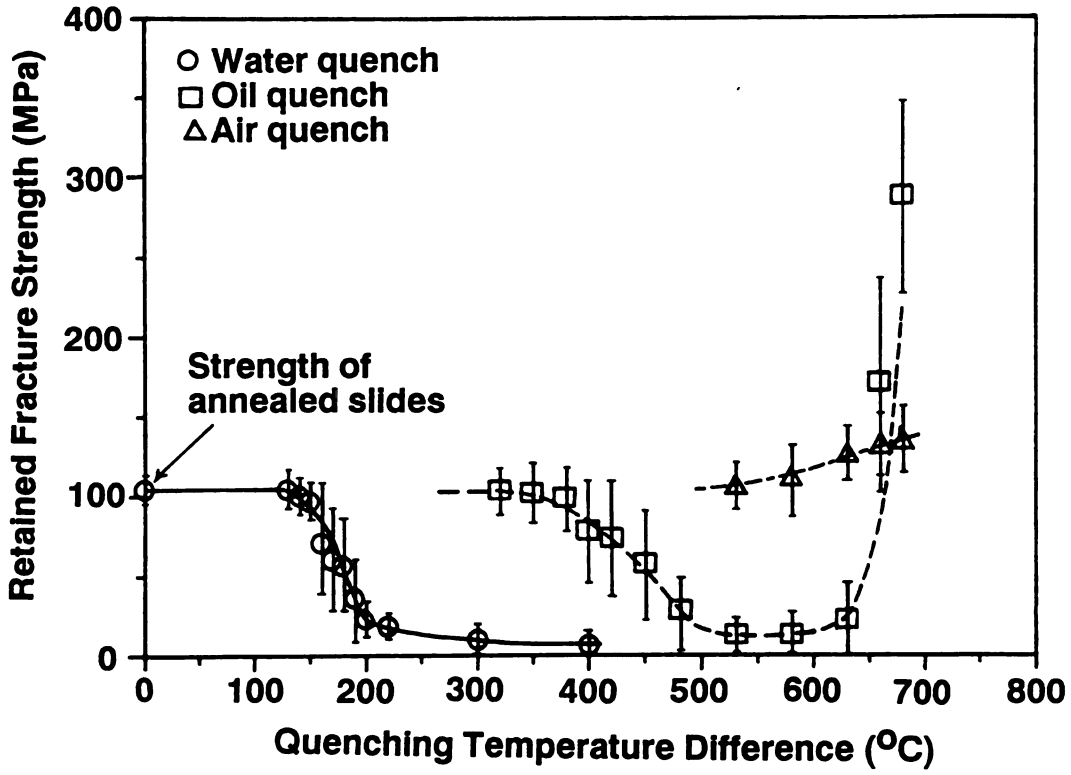

Figure 14(a). Retained fracture strength of glass slides thermally shocked by water quench, oil quench, and air quench as measured in three point bend.

greater Biot's modulus leads to a smaller ΔT_c, which agrees with the authors' previous theoretical analysis and with the thermal shock theories of other researchers, such as Kingery [61].

The retained fracture strength for quenching from above the annealing temperature is also a function of the quenching medium. Thermal quenching from above the annealing temperature in air results in a retained fracture strength which gradually increases with increasing ΔT. For the oil quench, the retained fracture strength decreases at $\Delta T \approx 400\ ^{o}C$ but increases for $\Delta T > 630\ ^{o}C$, where the increases in the retained fracture strength result from quench-induced residual stresses. Water quenching always resulted in a drop in residual strength between $\Delta T \approx 165\ ^{o}C$ and $\Delta T \approx 680\ ^{o}C$. In this study, a maximum ΔT of $680\ ^{o}C$ was not exceeded, since for $\Delta T > 680\ ^{o}C$, the specimens deformed macroscopically by viscous flow.

(4.2.3). Thermal quench induced residual stresses

Indentation measurements [56-58] on quenched glass slide specimens indicate that residual stresses arise in both the oil quench and the air quench for quenching from above the annealing temperature (Figure 14(b)). (Residual stress measurements were not attempted on specimens quenched into water from above the annealing temperature, since these specimens cracked extensively.) The oil quench corresponds to a greater Biot's modulus than the air quench, thus the oil quench induces higher residual stresses than the air quench. Although the experimentally determined residual stresses rise very rapidly with increasing ΔT (Figure 14(b)), a numerical

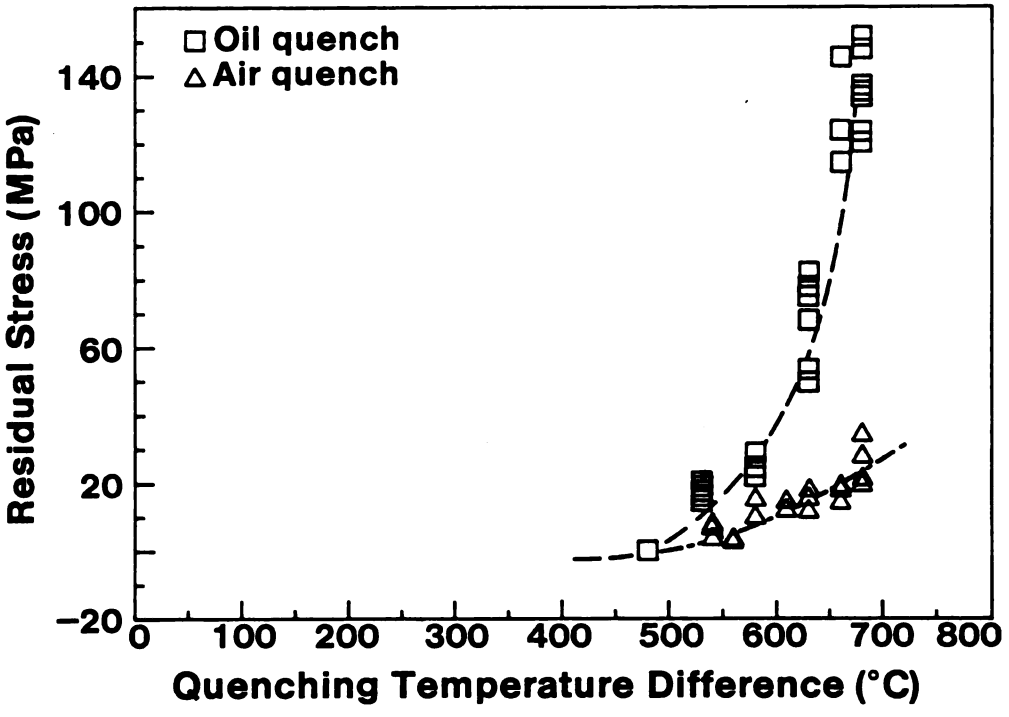

Figure 14(b). Residual stresses in quenched glass slides determined by Vicker's indentation.

analysis by the authors predicts that as ΔT continues to rise (for quenching from above the annealing temperature), the residual stress values will level off and saturate with further increases in ΔT. Viscous deformation of the specimens prevented us from determining whether or not a saturation in residual stress does occur for $\Delta T > 680\ ^{o}C$.

(4.2.4). Effect of thermal quenching on elastic modulus and internal friction

Measurements of elastic modulus and internal friction are nondestructive and reflect the total accumulation of microstructural damage. Figures 15 and 16 illustrate the relationship between elastic modulus, internal friction, and ΔT. As was the case for retained fracture strength, the water quench and oil quench curves change at $\Delta T \approx 165\ ^{o}C$ and $\Delta T \approx 400\ ^{o}C$, respectively, indicating that thermal shock damage decreases the elastic modulus and increases the internal friction. For water quench, surface cracks became visible at $\Delta T > 165\ ^{o}C$, with more and more cracks accumulating as ΔT increased (Figure 16). Elastic modulus and internal friction continuously vary with increasing ΔT, reflecting an accumulation of cracks. However, the retained strength curves in Figure 14(a) are nearly constant despite the accumulation of surface cracks. Analysis of the retained strength behavior in this case (water quench, $\Delta T > 165\ ^{o}C$) is very complicated, since the accumulating cracks eventually form a network of cracks. One simple interpretation of the near constancy in the retained fracture strength is that the critical flaw size does not increase. However, classical fracture mechanics models of isolated,

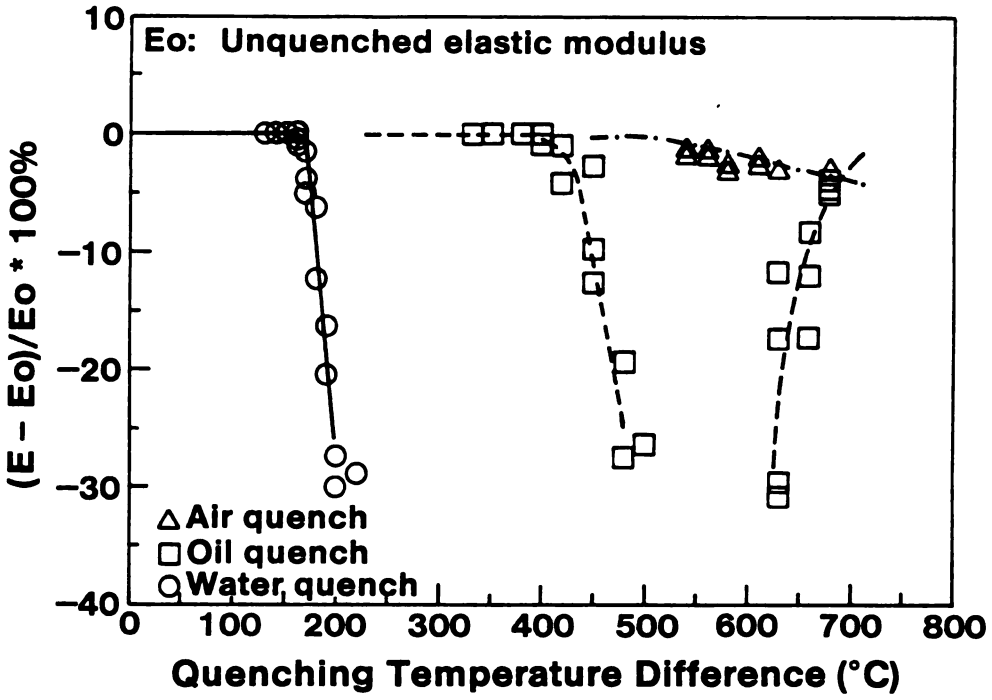

Figure 15. Relative decrease in elastic modulus as a function of the thermal quench of glass slides.

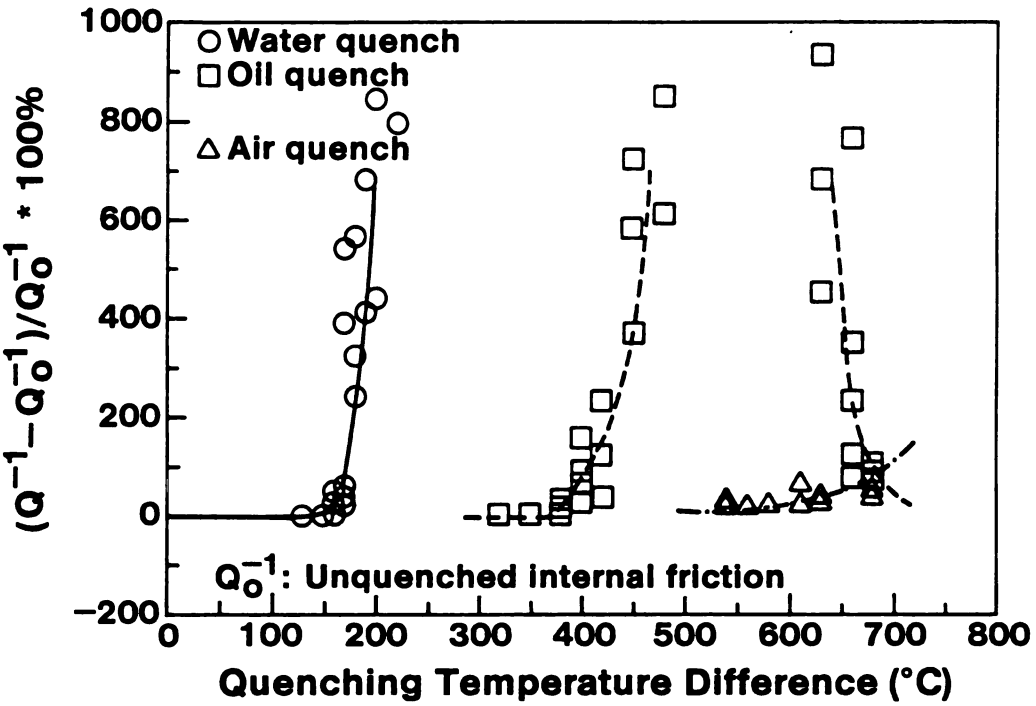

Figure 16. Relative increase in internal friction Q_o^{-1} as a function of the thermal quench of glass slides.

non-interacting cracks in a brittle specimen are likely not adequate for the web-like crack field that develops at high ΔT in the water quench (Figure 17).

The elastic modulus and internal friction are essentially constant for air-quenched specimens (Figures 15 and 16) quenched from below the annealing temperature. Above the annealing temperature, the elastic modulus and internal friction gradually change, and this change may be associated with quench-induced residual stresses (see Appendix A). The elastic modulus (internal friction) for oil-quenched specimen first decreases (increases) as ΔT increases from $\Delta T = 400\ ^{o}C$ to $\Delta T = 500\ ^{o}C$, which is due to the increasing degree of thermal shock damage. When $500\ ^{o}c < \Delta t < 630\ ^{o}c$, the shock damage becomes great enough. Thus, the elastic modulus (internal friction) of shocked specimen is difficult to measure and the experimental data are absent between $500\ ^{o}C < \Delta T < 630\ ^{o}C$. When $\Delta T > 630\ ^{o}C$, viscous flow results in the decrease in the transient thermal stress. The degree of the shock damage decreases and the the experimental data appear in Figures 15 and 16 again.

Changes in elastic modulus and internal friction as a function of static strain or as a function of thermal quenching have been reported for inorganic and polymer glasses. Mallinder et al. indicated that the elastic modulus of soda glass fiber was a function of static strain, $E = E_o(1-5.11\epsilon)$, where $E_o = 72.5$ GPa [79]. The strain, ϵ, was induced via an external tensile load acting on both ends of a fiber about 0.02 mm in diameter. Vega et al. [80] pointed out that thermal quenching into several media caused residual stresses and

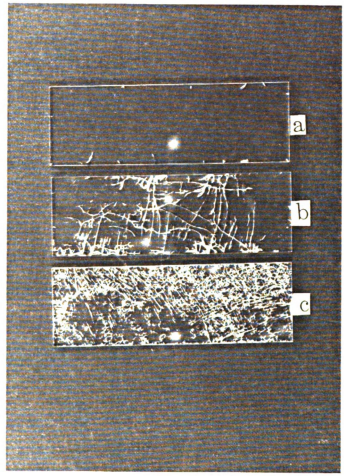

Figure 17. Surface cracks of glass slides quenched into a water bath. Figures a, b, and c correspond to ΔT = 180 ^{o}C, ΔT=230 ^{o}C, and ΔT=400 ^{o}C, respectively.

decreased the elastic modulus of polymer glass (see Table 2). Pavlushkin et al. [81] observed that the elastic modulus of an industrially tempered glass was lower by about 3 percent than that of annealed glass*. Room temperature vibrational pendulum measurements in chilled glasses gave an internal friction that was about 40 percent greater than the internal friction of annealed glass [82,83].

However, thermal history can affect the specific volume (the reciprocal density), viscosity, and other physical properties of a glass [70,86]. While thermal quenching does induce residual stress in the glass slides, it is unclear what role (if any) changes in physical properties such as specific volume (that also accompany the thermal quench) play in the observed simultaneous decrease in elastic modulus and increase in internal friction.**

As indicated by equation (4), the quenched-in residual surface stresses in the glass slides were determined as a function of C/C_r, using the Vickers indentation technique [56-58], where 2C is the indentation crack length for an annealed specimen and 2Cr is the indentation crack length for a residually stressed specimen (indented at a load identical to that used for the annealed slide). Thus, in this study the ratio of C/C_r is used as an index of the severity of

---

* Quench temperature and quench media were not specified by Pavlushkin et al. [81], Fitzgerald [82], and Day et al. [83].

** Thermal quenching results in compressive residual stresses in the specimen's surface. However, the residual stresses do not affect the observed hardness.

Table 2. Elastic Modulus as a Function of the Quench Medium Temperature of Quenched Polymer Glass Reported by Vega et al. [80].

quenching rate	Media Temp. (^{o}C)	Modulus (GPa)
slow cool^{+}	30	1.7
water quench	30	1.5
slow cool	70	1.5
water quench^{++}	70	0.95
nitrogen quench	70	1.0

+ slow cool = 0.01 ^{o}C/s.
++ water quench = 160 ^{o}C/s.

thermal quench conditions and residual stresses. The experimentally determined values of residual stress, S_r, ranged from $S_r = 0$ to $S_r = 160$ MPa (Figure 18). In this study, it was found that the elastic modulus and internal friction changes as a function of quench-induced residual stresses can be expressed as an empirical function of C/C_r (Figure 18) such that

$$\frac{E - E_o}{E_o} * 100\% = - 4.35 [1 - (C/C_r)^{-9}] \quad (20a)$$

$$\frac{Q^{-1} - Q_o^{-1}}{Q_o^{-1}} * 100\% = 100 [1 - (C/C_r)^{-3}] \quad (20b)$$

where E and Q^{-1} represent the elastic modulus and the internal friction of the quenched glass slides. E_o and Q_o^{-1} are elastic

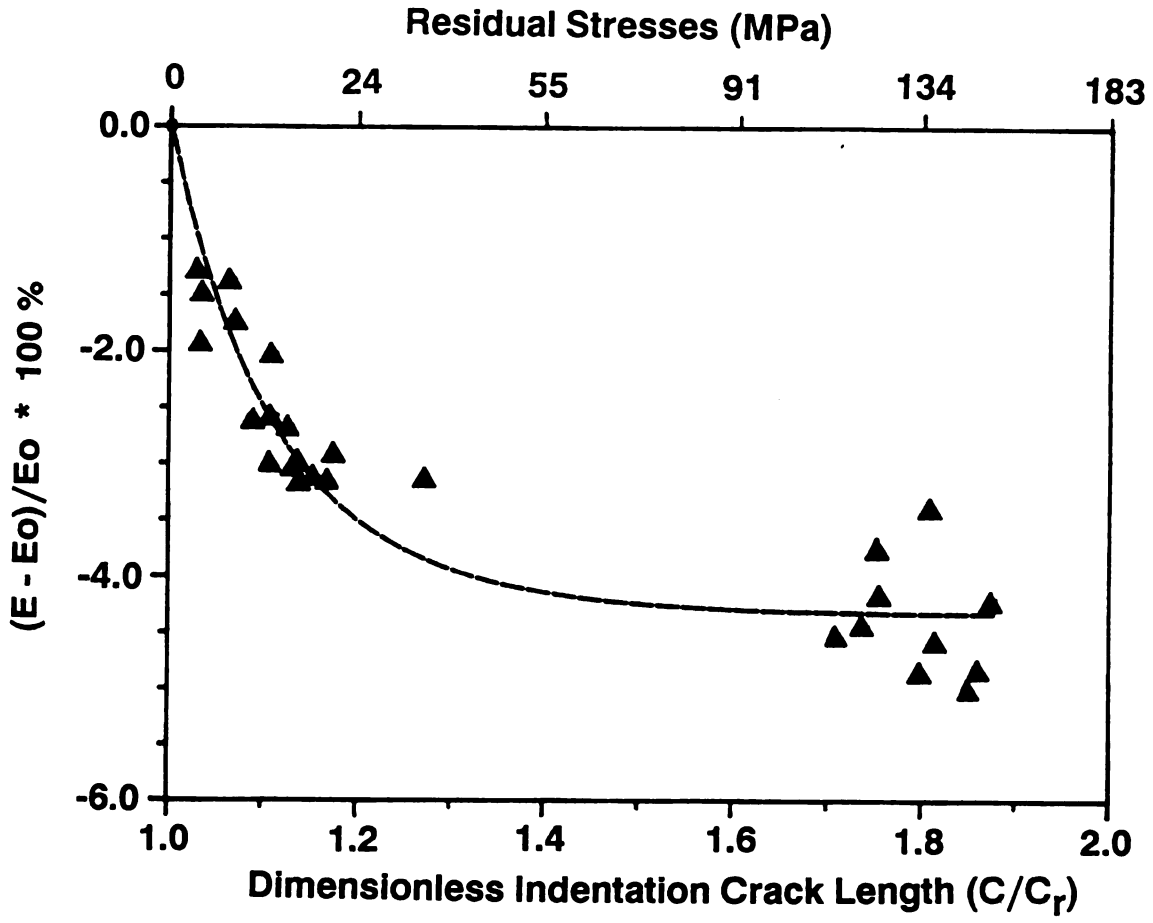

Figure 18(a). Elastic modulus versus thermal quench conditions. The ratio of C/C_r is used as an index of the severity of thermal quench conditions and residual stresses.

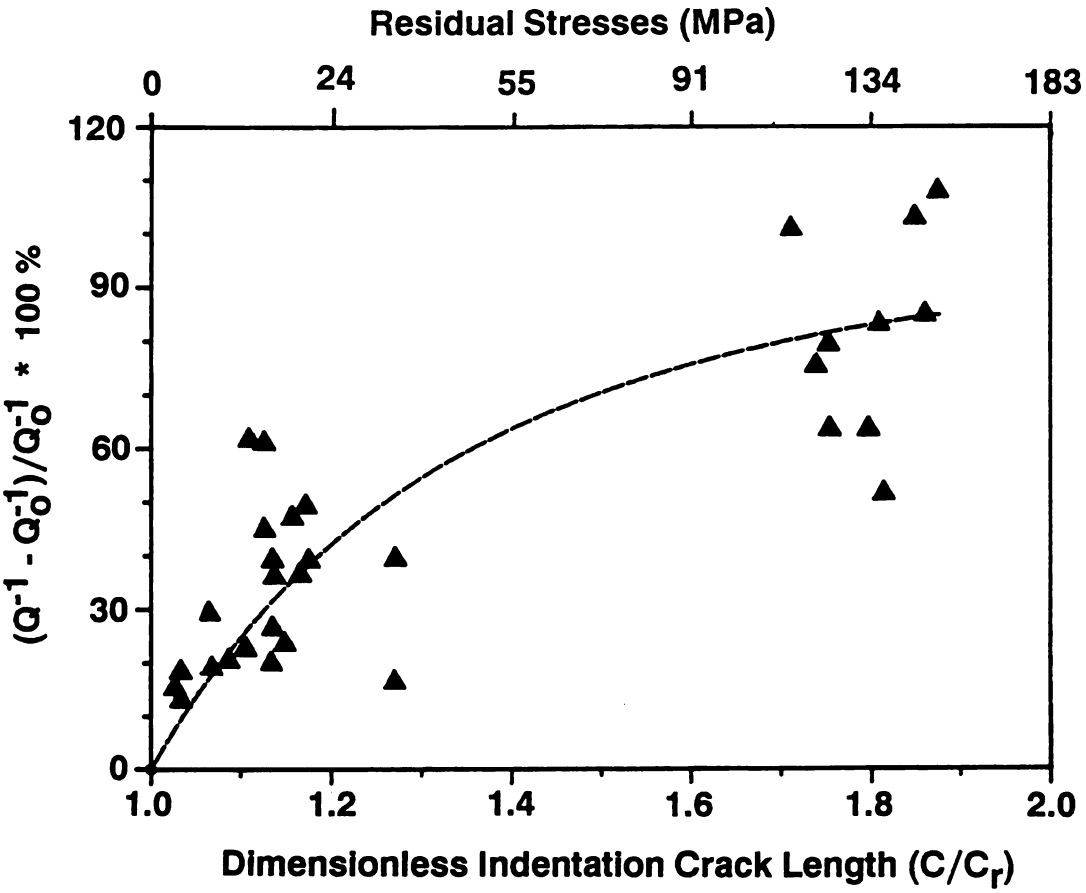

Figure 18(b). Internal friction versus thermal quench conditions. The ratio of C/C_r is used as an index of the severity of thermal quench conditions and residual stresses.

modulus and internal friction of the annealed slides. Since the shock damage-free specimens with the residual stresses of from 100 MPa to 40 MPa could not be produced by either motor oil quench (SAE 20W 50) or by air quench (cooling in air), the data in Figure 18 forms two clusters (Appendix B).

(4.2.5). Relaxation of the quench-induced residual stresses

Evidence of the relaxation of quench-induced residual stresses can be obtained via both elasticity and calorimetric measurements. While the elastic modulus of an annealed glass slide decreases with temperature, the modulus versus temperature curve for an annealed glass slide is identical upon heating and cooling. The solid line in Figure 19 shows the reversibility of the elastic modulus for an annealed glass slide heated and cooled at a rate of one degree Celsius per minute. In contrast, a slide having a quenched-in residual stress does not show reversibility in the elastic modulus for the first heating and cooling cycle. For example, when the annealed glass slide in figure 8 was quenched into an oil medium at a quench temperature difference of $\Delta T = 680\ ^{o}C$, a residual surface stress of 140 MPa was induced in the slide, as measured by the Vickers indentation technique [56-58]. After quenching, room temperature elasticity measurements on the residually stressed slide showed a lower elastic modulus than the same slide had in its annealed state (Figure 19). When the residually stressed slide was heated from room temperature to approximately 300 ^{o}C (again at a rate of approximately 1 ^{o}C/minute), the modulus curve of the quenched slide remained below and approximately parallel to the

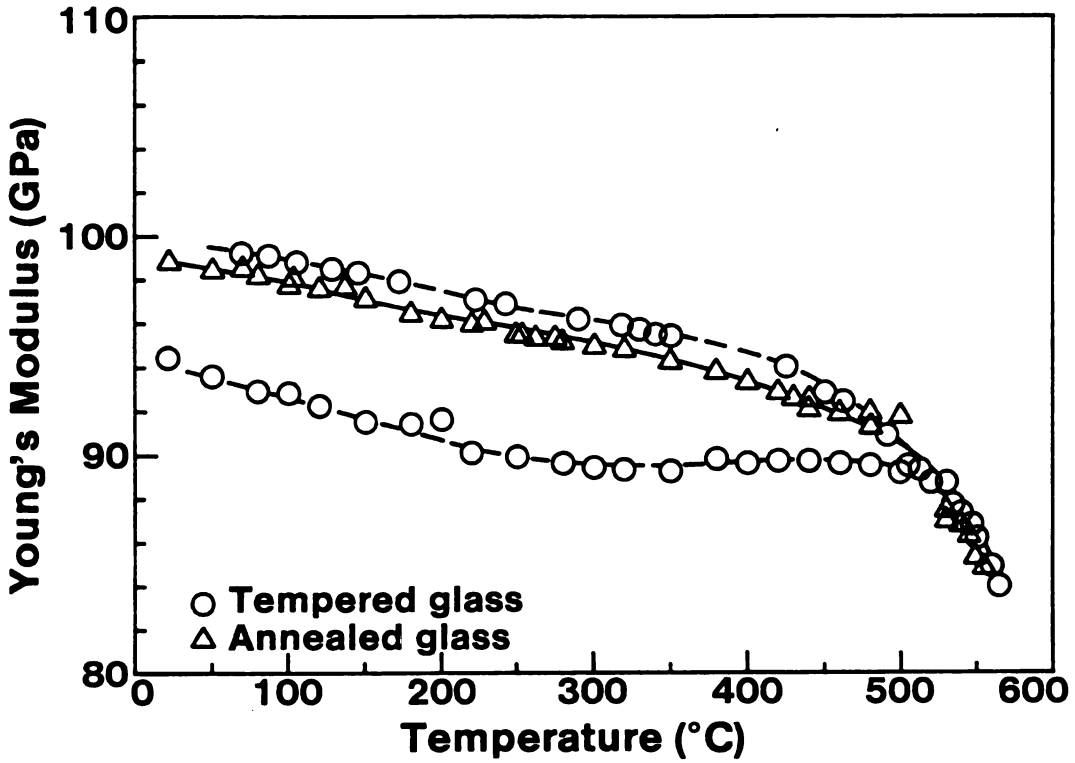

Figure 19. The Young's modulus versus temperature for the annealed state (solid line) and the residually stressed state of a glass slide.

curve for the annealed state of the slide. Upon heating from 300 °C to a maximum test temperature of 600 °C, the modulus for the residually stressed state of the slide approached the modulus for the annealed state of the slide (Figure 19). Upon cooling, the modulus of the residually stressed state was slightly below and parallel to the modulus for the initial annealed state. Thus the heating and cooling curves for the residually stressed state form an open loop (the dashed curves in Figure 19).

It should be noted that when the heating and cooling cycle was repeated for a second temperature cycle from room temperature to 600 °C and back to room temperature (not shown in Figure 19), the modulus versus temperature curve was reversible. Thus, the relatively high state of residual stress (140 MPa) apparently did affect the elastic modulus, but (as would be expected) the thermal cycling of the specimen from room temperature to 600 °C and back to room temperature at a rate of 1 °C/minute released the residual stresses to the extent that the modulus was reversible upon subsequent thermal cycling at the same heating and cooling rate. Appendix A discusses a model for the experimentally observed change in elastic modulus due to the residual stress state.

Thermodynamically, residual stresses can be regarded as an unstable state, such that when a residually stressed glass plate is heated, the residual stresses are released. The release of the stored elastic strain energy associated with the residual stresses can be examined calorimetrically. Figure 20 illustrates a Differential Scanning Calorimetric (DSC) analysis of the heat flow as a function of temperature for the annealed and the residually

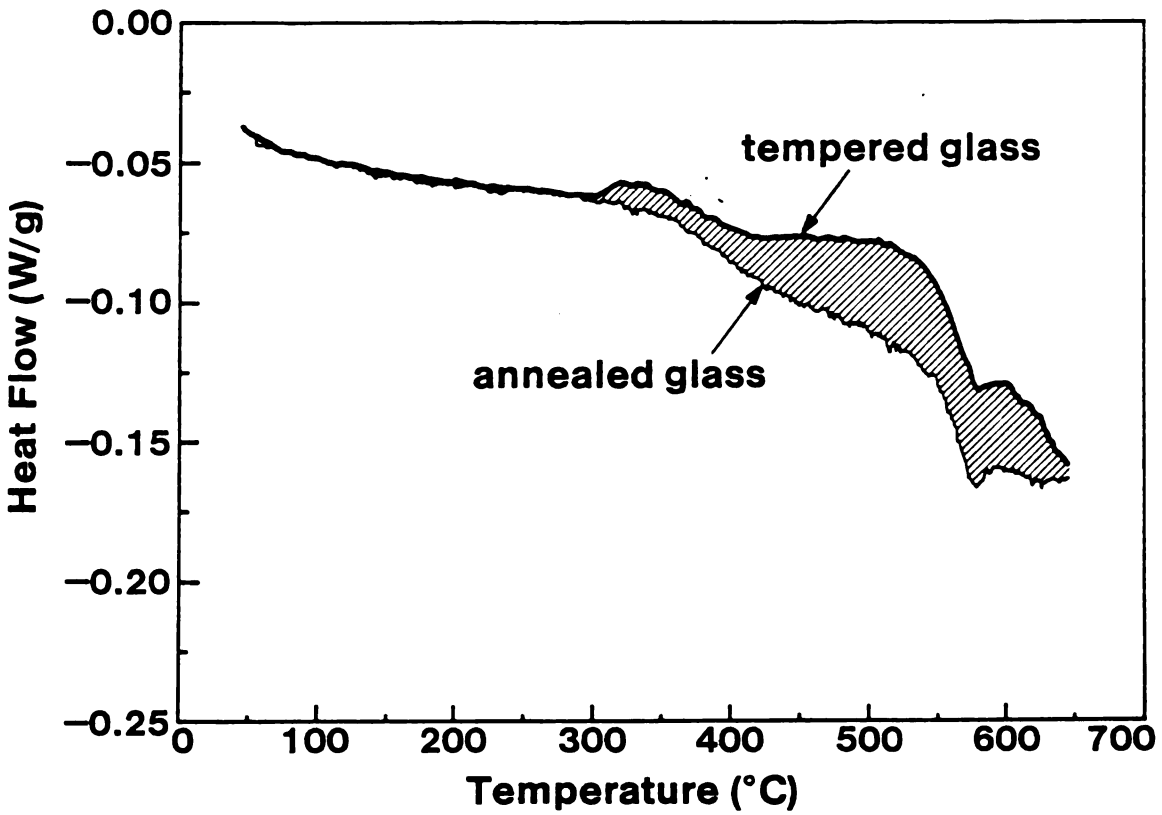

Figure 20. Thermal flow measurement of glass slides using a Differential Scanning Calorimeter.

stressed state of a single glass slide. The annealed and residually stressed states of the glass slide are represented by the solid and dashed lines, respectively. As was the case in the elasticity measurements discussed above, residual stresses in the DSC specimen were induced by a thermal quench of $\Delta T = 680\ ^{o}C$ into a room temperature oil bath.

The cross-hatched region between the curves of the annealed and the residually stressed states is a measure of the stored elastic strain energy released from the residual stresses in the glass slide. As indicated in Figure 20, the residual stress relaxation begins at about 300 ^{o}C, which roughly agrees with the onset of relaxation indicated by the elastic modulus measurements. However, the DSC measurements were made at a heating rate of 10 ^{o}C/minute, while the elasticity measurements were made at a heating and cooling rate of 1 ^{o}C/minute. Future studies should repeat the DSC and elasticity measurements on identically treated slides with identical heating and cooling rates during measurement.

(4.3). Statistical Study of the Effect of Subcritical Crack Growth on Thermal Shock Resistance

In this section subcritical crack growth is investigated by comparing the fracture strength distribution for annealed glass plates to that of quenched (thermally shocked) glass. In addition to single-quench thermal shock testing, subcritical crack growth was evaluated in terms of thermal shock fatigue damage (cyclic thermal shock). Results indicate that subcritical crack growth effects are observable in the shock testing of glass slides via systematic shifts in the retained strength distribution.

(4.3.1) Candidate fracture strength distributions

The strength distribution for a group of monolithic ceramic specimens is related to the distribution of pre-existing critical flaws in the specimens [4,5]. While the Weibull distribution function is typically used to describe fracture strength distributions [18,87], distributions other than the Weibull function may provide a better fit to the strength data in some cases [4,5,88,99]. For example, Doremus found that the normal distribution function fit the static strength data for Pyrex glass better than the Weibull distribution [4]. Shimokawa et al. reported that the lognormal function fit fatigue data for carbon fiber/epoxy matrix composite specimens better than the Weibull function did [88]. In this study, the fracture strength histogram for 239 annealed glass slide specimens is approximately symmetrical so that the normal distribution function is one of the natural candidates to

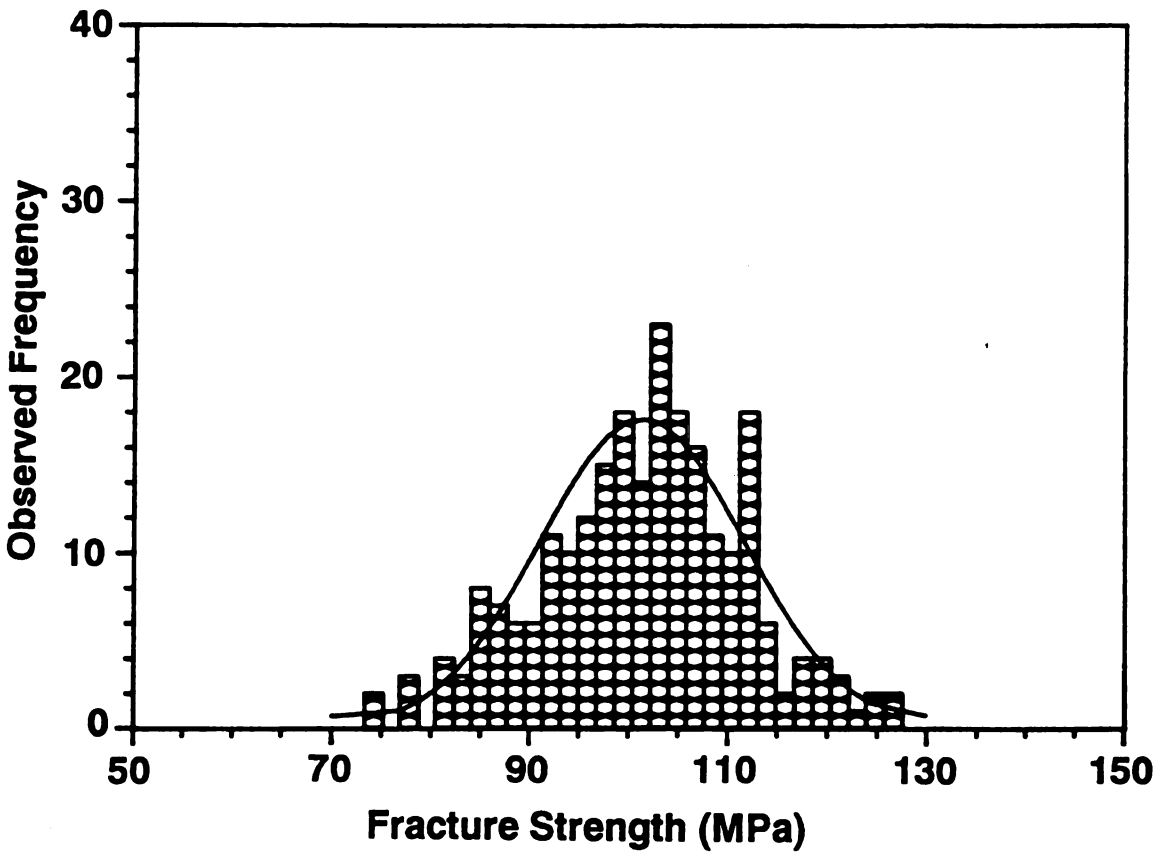

Figure 21. Fracture strength histogram for 239 annealed glass slide specimens fractured in three-point bend.

describe the data (Figure 21). Consequently, in this study the three candidate distribution functions used to analyze the distributions of the fracture strength for the annealed glass slides were the two-parameter Weibull, the normal, and the lognormal functions.

The corresponding probability functions are characterized as follows:

The Normal distribution is described by [90]:

$$f(y) = \frac{1}{\sigma\ (2\ \pi)^{1/2}}\ \exp[-\frac{1}{2}\ (\frac{y\ -\ \mu}{\sigma})^2\ ] \tag{21a}$$

$$F(y) = \int_{-\infty}^{y} f(t)\ \ dt \tag{21b}$$

$$\hat{\mu} = \frac{1}{n}\ \sum_{i=1}^{n}\ y_i \tag{21c}$$

$$\hat{\sigma}^2 = \frac{1}{n}\ \sum_{i=1}^{n}\ (\ y_i\ -\ \hat{\mu})^2 \tag{21d}$$

where f(y), F(y), μ, and σ^2 represent the probability density function (PDF), cumulative distribution function (CDF), mean, and variance, respectively. The $\hat{\mu}$ and $\hat{\sigma}^2$ are the maximum likelihood estimators for μ and σ^2.

The Lognormal distribution with two parameters is characterized by [91]:

$$f(y) = \frac{1}{y\ \sigma\ (2\ \pi)^{1/2}}\ \exp[\ -\ \frac{1}{2}\ (\frac{\log(y)\ -\ \mu}{\sigma})^2\ ] \tag{22a}$$

$$F(y) = \int_0^y f(t)\, dt \tag{22b}$$

$$\hat{\mu} = \frac{1}{n} \sum_{i=1}^{n} \log(y_i) \tag{22c}$$

$$\hat{\sigma}^2 = \frac{1}{n} \sum_{i=1}^{n} (\log(y_i) - \hat{\mu})^2 \tag{22d}$$

where f(y), F(y), μ, and σ^2 have the same definition as that for the Normal distribution. The $\hat{\mu}$ and $\hat{\sigma}^2$ are the maximum likelihood estimators for μ and σ^2.

The Weibull distribution with two parameters is described by [87,92]:

$$f(y) = \left(\frac{m}{b}\right)\left(\frac{y}{b}\right)^{m-1} \exp(-(y/b)^m) \tag{23a}$$

$$F(y) = 1 - \exp(-(y/b)^m) \tag{23b}$$

$$E(y) = b\, \Gamma(1 + 1/m) \tag{23c}$$

$$Var(y) = b^2[\, \Gamma(1 + 2/m) - (\Gamma(1 + 1/m))^2 \,] \tag{23d}$$

where E(y), Var(y), and Γ are the expected value, variance, and gamma function, respectively. Weibull parameters m and b can be calculated according to the maximum likelihood estimators [93]. First, m is calculated iteratively from equation (24a). The b is then computed using equation (24b).

$$\left[\frac{\sum_{i=1}^{n} y_i^m \ln(y_i)}{\sum_{i=1}^{n} y_i^m} - \frac{1}{m} \right] = \frac{1}{n} \sum_{i=1}^{n} \ln(y_i) \qquad (24a)$$

$$b^m = \sum_{i=1}^{n} \frac{y_i^m}{n} \qquad (24b)$$

Applying the maximum likelihood method [90-92] to the annealed glass slide fracture strength data (Table 3) yielded the statistical parameters for the normal, lognormal, and Weibull distribution functions (Table 4). To measure the discrepancy between the fracture strength data and the three candidate distribution functions, a goodness-of-fit test is required. The goodness of fit test employed in this study is based on the empirical distribution function (EDF) and the Kolmogorov-Smirnov test [93,94]. The EDF, $F_n(y)$, is defined as [94]

$$F_n(y) = \frac{\text{number of observation} \leq y}{n} \qquad -\infty < y < \infty \qquad (25a)$$

$$F_n(y) = \frac{i}{n} \qquad y_i \leq y < y_{i+1} \qquad (25b)$$

$$F_n(y) = 0 \qquad y < y_1 \qquad (25c)$$

$$F_n(y) = 1 \qquad y_n \leq y \qquad (25d)$$

$y_1 < y_2 < y_3, \ldots < y_n$ are the order statistics for the fracture strength data y_i for a random sample of size n. $F_n(y)$ is the step function illustrated in Figure 22. The three continuous curves in

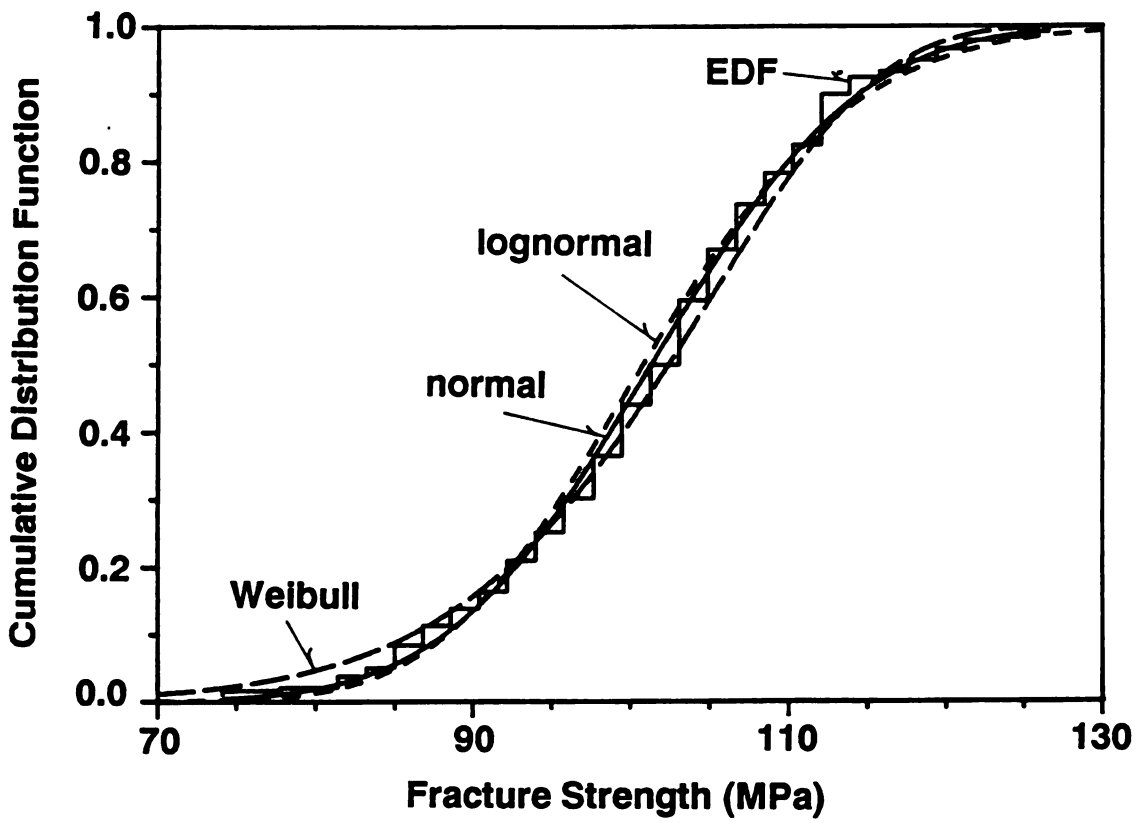

Figure 22. Illustration of cumulative distribution functions and the empirical distribution function for the fracture strength data of annealed glass slides.

Figure 22 represent the cumulative distribution functions (CDF) of the normal, lognormal, and Weibull distributions with the parameters listed in Table 4. In the Kolmogorov-Smirnov test, a good fit requires that D_n be small, where D_n is defined in terms of the greatest vertical difference between the CDF and the EDF [93], such that

$$D_n = \max(D_n^+ , D_n^-) \tag{26a}$$

$$D_n^+ = \max_{1\le i\le n} (F_n(y_i) - F(y_i)) = \max_{1\le i\le n} \left(\frac{i}{n} - F(y_i)\right) \tag{26b}$$

$$D_n^- = \max_{1\le i\le n} \left(F(y_i) - \frac{i-1}{n} \right) \tag{26c}$$

The Kolmogorov-Smirnov statistic (for which the statistical parameters are estimated by maximum likelihood estimators) shows that the normal distribution corresponds to the smallest D_n. However, since the critical value in the Kolmogorov-Smirnov test (two-sided test at significance level $\alpha = 0.05$) is 0.0878, the normal, lognormal, and Weibull distributions all fit this study's strength data for annealed glass slides about equally well (Table 5). For convenience, the normal distribution is used for the thermal shock resistance analysis in the next section.

Table 3. Fracture strength data of annealed glass slides.

S*	f*	S	f	S	f
74.2	2	77.8	3	81.4	4
83.2	3	85.0	8	86.8	7
88.6	6	90.4	6	92.2	11
94.0	10	95.8	12	97.7	15
99.5	18	101.3	14	103.1	23
104.9	18	106.7	16	108.5	11
110.3	10	112.1	18	113.9	6
115.8	2	117.6	4	119.4	4
121.2	3	123.0	1	124.8	2
126.6	2				

* S = fracture strength (MPa).
* f = total number of the specimens which corresponds to the strength, S.

Table 4. Parameters for the normal, lognormal, and Weibull distribution functions, as calculated from maximum likelihood estimators [17-19].

normal :	mean	μ_2 = 101.38 MPa
	variance	σ^2 = 104.90
lognormal :	mean	μ_2 = 4.6137
	variance	σ^2 = 1.0619 X 10^{-2}
Weibull* :	expected value	E(y) = 101.17 MPa
	variance	Var(y) = 127.33
	Weibull parameters	b = 106.00 MPa
		m = 10.834

* The cumulative distribution function of Weibull distribution is:

$$F(y) = 1 - \exp(-(y/b)^m)$$

Table 5. Statisitics of the empirical fracture strength distribution function obtained from goodness of fit test (Kolmogorov-Smirnov test). The statistics D_n^+, D_n^-, and D_n are defined by equations 26 (a) - 26 (c).

	D_n^+	D_n^-	D_n
normal	0.0478	0.0685	0.0685
lognormal	0.0521	0.0867	0.0867
Weibull	0.0787	0.0374	0.0787

(4.3.2) Subcritical crack growth

The literature does not agree on the significance of subcritical crack growth on thermal shock resistance in ceramics [7,51,52]. Therefore, it is appropriate here to review briefly the thermal shock literature as it applies to subcritical crack growth. In his 1969 model of thermal shock damage in ceramics [7], Hasselman proposed that: (1) pre-existing cracks propagate when quenched above a critical quench temperature difference, ΔT_c, (2) cracks are stable (do not grow) below ΔT_c, and (3) dynamic crack growth causes a discontinuous drop in the retained fracture strength at ΔT_c.

Subcritical crack growth's effects on thermal shock, which were not included in Hasselman's 1969 theory [7], are treated for single-quench thermal shock in a 1974 paper by Badaliance, Krohn, and Hasselman [51]. Subcritical crack growth was modeled by taking into account the propagation of pre-existing cracks for quench temperature differences below ΔT_c. The numerical calculation yielded the critical quench temperature difference ΔT_c = 147 ^{o}C. If subcritical crack growth was ignored, a ΔT_c of 238 ^{o}C was obtained. Badaliance inferred that the large discrepancy (91 ^{o}C) was due to thermal shock induced subcritical crack growth. In modeling the ΔT_c change due to subcritical crack growth, Badaliance used K_o = 0.248 MPa $m^{1/2}$ and K_c = 0.749 MPa $m^{1/2}$ for the purposes of numerical calculations, where K_c is the critical stress intensity and K_o is the threshold for subcritical crack growth. The values of K_o and K_c adopted by Badaliance result from static fatigue testing under a mechanical loading [95].

In another key study of the effect of subcritical crack growth on thermal shock behavior, Ashizuka, Easler, and Bradt quenched heated borosilicate glass rods into a room temperature water bath [52]. The retained strength of the shocked borosilicate glass rods was measured in a liquid nitrogen bath and in a room temperature water bath. It was assumed that the moisture-free environment of the liquid nitrogen bath would provide "baseline" values of retained fracture strength, free from subcritical crack growth effects. Ashizuka calculated K_1 associated with the appropriate ΔT by [52]

$$K_1 = Y C^{1/2} \frac{\Delta T \alpha E}{(1 - \nu)} F(B) \tag{27a}$$

$$K_c = \sigma Y C^{1/2} \tag{27b}$$

where K_1, E, α, ν, C, and Y are the stress intensity factor, elastic modulus, thermal expansion, Poisson's ratio, flaw size, and geometric constant, respectively. The F(B) is a function of Biot's modulus, B [61]. To determine the inert strength, σ, both the bend fixture and the specimens were immersed in a liquid nitrogen bath. The specimens were subsequently fractured in four-point bend at a crosshead speed of 0.5 mm/min and an approximate stressing rate of 93.3 MPa/min [52]. Using equations (5a) and (5b), Ashizuka inferred that $K_o \approx 0.9 K_c$ and the subcritical crack growth should be minor [52].

The technique differences in the Badaliance's and Ashizuka's studies were that (1) Badaliance utilized the static fatigue data

to theoretically evaluate the quench-induced subcritical crack growth effect, and (2) Ashizuka experimentally measured fracture strength and then statistically infer the subcritical crack growth effect. Badaliance was engaged in theoretical evaluation and Ashizuka did experimentation.

(4.3.2.1). Evolution of fracture strength degradation

In our study, the fracture strength of annealed glass slides were characterized by a normal distribution. The evolution of the strength distribution for a group of annealed glass slides depended, for example, on whether or not subcritical crack growth was included in the thermal shock damage process. We discuss the evolution of the crack damage (A) neglecting subcritical crack growth, and (B) including subcritical crack growth.

A. No subcritical crack growth effect:

In 1983, Lewis proposed that since the critical flaw sizes of a group of brittle components were characterized by a distribution, the mean retained strength of quenched components should gradually decrease as ΔT increased [38]. Lewis's concept* [38] of the evolution of the fracture strength distribution is experimentally tested in this paper using a large number of glass microscope slides (239 slides were fractured to determine the as-annealed strength distribution and a total of 180 slides were fractured in the single quench tests).

---

* The concept of the evolution of the fracture strength distribution for thermal shock problems was suggested in 1955 by Manson [18].

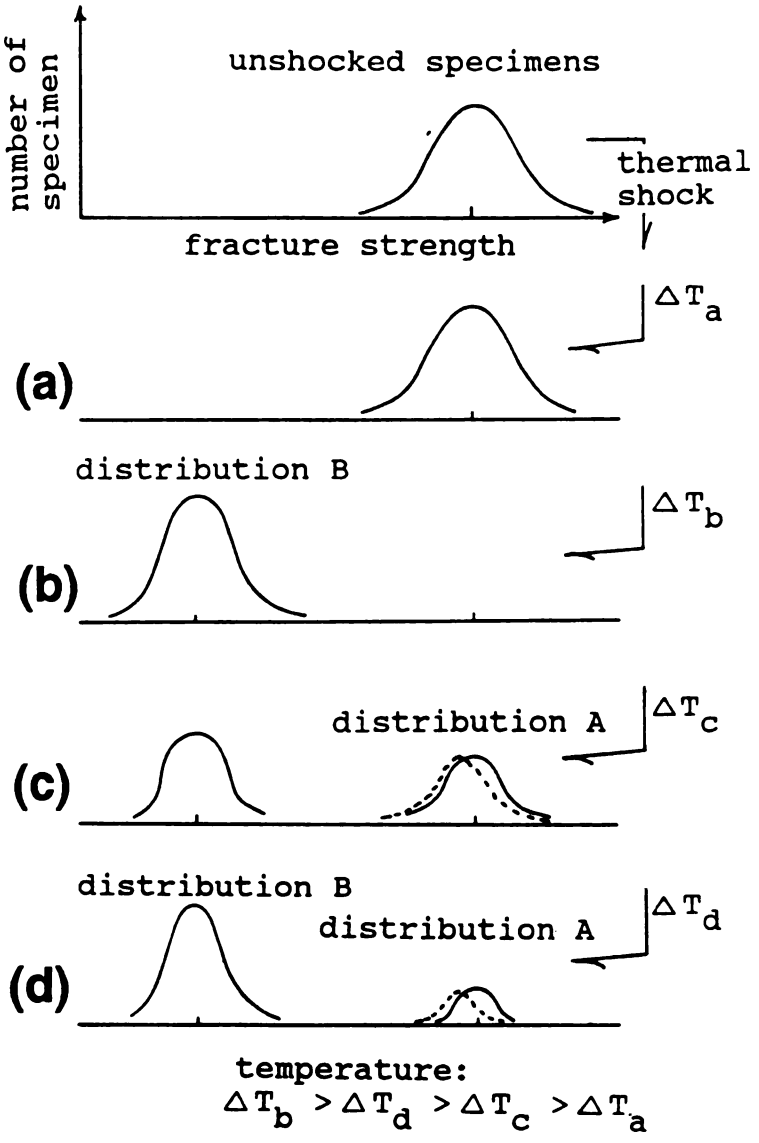

Figure 23. Schematic of the evaluation of fracture strength degradation.

If transient thermal stresses are mild enough ($K_{thermal} < K_c$ for each specimen), then no strength degradation occurs and the initial fracture strength distribution is not altered (Figure 23(a). When thermal stresses are extremely severe ($K_{thermal} > K_c$ for every slide in the total population of glass slides), the strength of each specimen drops as the critical flaws in the specimens extend (Figure 23(b)). When the shock severity is intermediate ($K_{thermal} > K_c$ for some fraction of the slide population), the retained strength distribution breaks into two clusters and becomes bimodal (Figures 23(c) and 23(d)) [38].

In this study, the cluster with lower fracture strength is defined as distribution B (Figures 23(c) and 23(d)). The cluster with higher fracture strength is defined as distribution A. The strength will drop for that fraction of specimens for which $K_{thermal} > K_c$ since the critical flaws extend during thermal shock, while (neglecting subcritical crack growth) the strength remains unchanged for those specimens where $K_{thermal} < K_c$.

B. Subcritical crack growth effect included:

If subcritical crack growth occurs during thermal shock, the evolution of retained fracture strength will differ from that suggested above, in that there will be additional crack growth regimes and an additional crack growth criterion.

If $K_{thermal} > K_c$, the critical flaws are subjected to "pop-in" crack growth at the initial stage of the thermal shock process. Thus, no subcritical crack growth effect on strength degradation is expected (Figure 23(b)). If $K_{thermal} < K_o$ for all slides, then no

crack extension will occur by either subcritical or pop-in growth (Figure 23(a)).

If $K_c > K_{thermal} > K_o$, then critical flaws will not experience pop-in growth, but they can extended subcritically. Since subcritical crack growth typically occurs at a relatively low velocity as compared to a pop-in type crack growth, we would expect subcritical crack growth to produce shifts in the mean strength of distribution A (dashed line in Figures 23(c) and 23(d)), as opposed to the drastic transformations in strength possible in pop-in crack growth.

In order to test for systematic shifts in the retained strength distribution as a function of ΔT, we must first approximate the form of the initial strength distributions. Histograms of the retained fracture strength data (distribution A) for thermally shocked specimens are then compared to the normal distribution determined in section 3.1 (Figure 21) for the annealed specimens.

(4.3.2.2). Experimental results of fracture strength degradation for single-quench thermal shock

The glass microscope slides in a portion of this study were subjected to a single quench into a room temperature water bath. For specimens shocked at a quench temperature difference of 150° C, the retained fracture strength distribution (represented by the solid curve in Figure 24a) shifts slightly to the left when compared to the strength distribution of the annealed glass slides (the dashed line in Figure 24a) (see Appendix C). This small shift to the left (toward lower strengths) in the retained strength

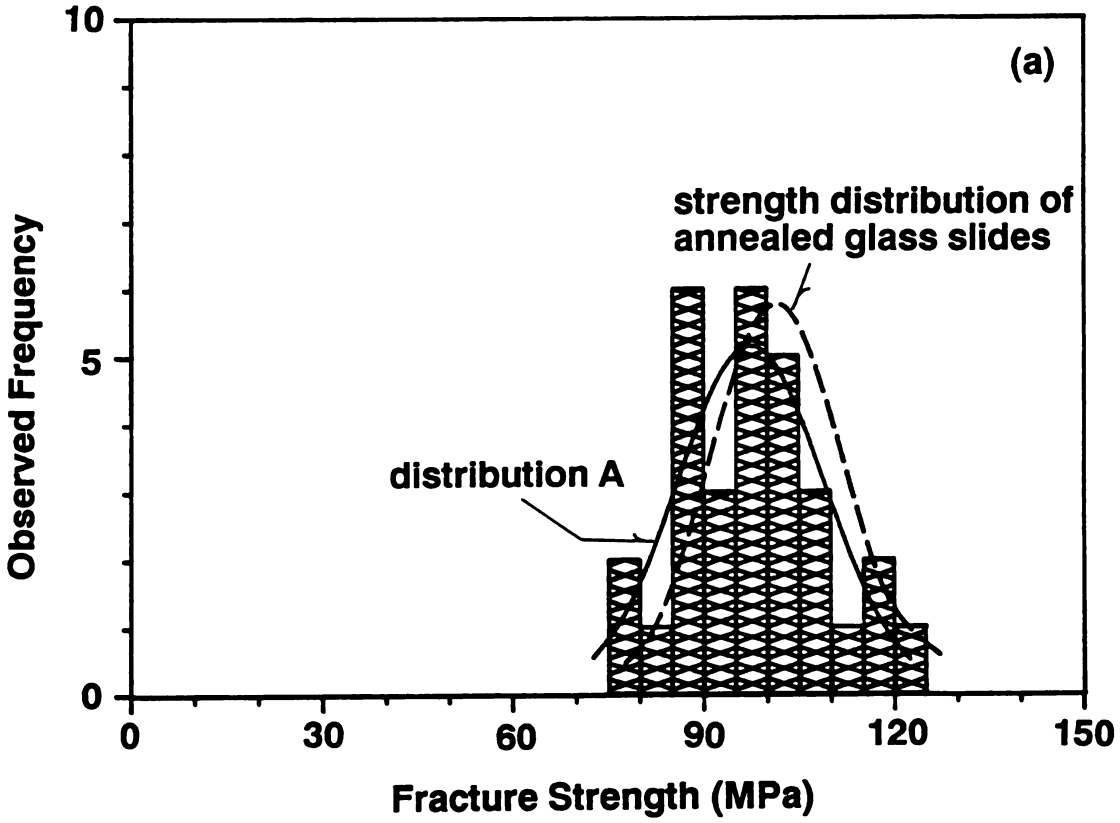

Figure 24(a). Retained fracture strength of glass slides following a single quench into a room temperature water bath at $\Delta T = 150^{o}$ C.

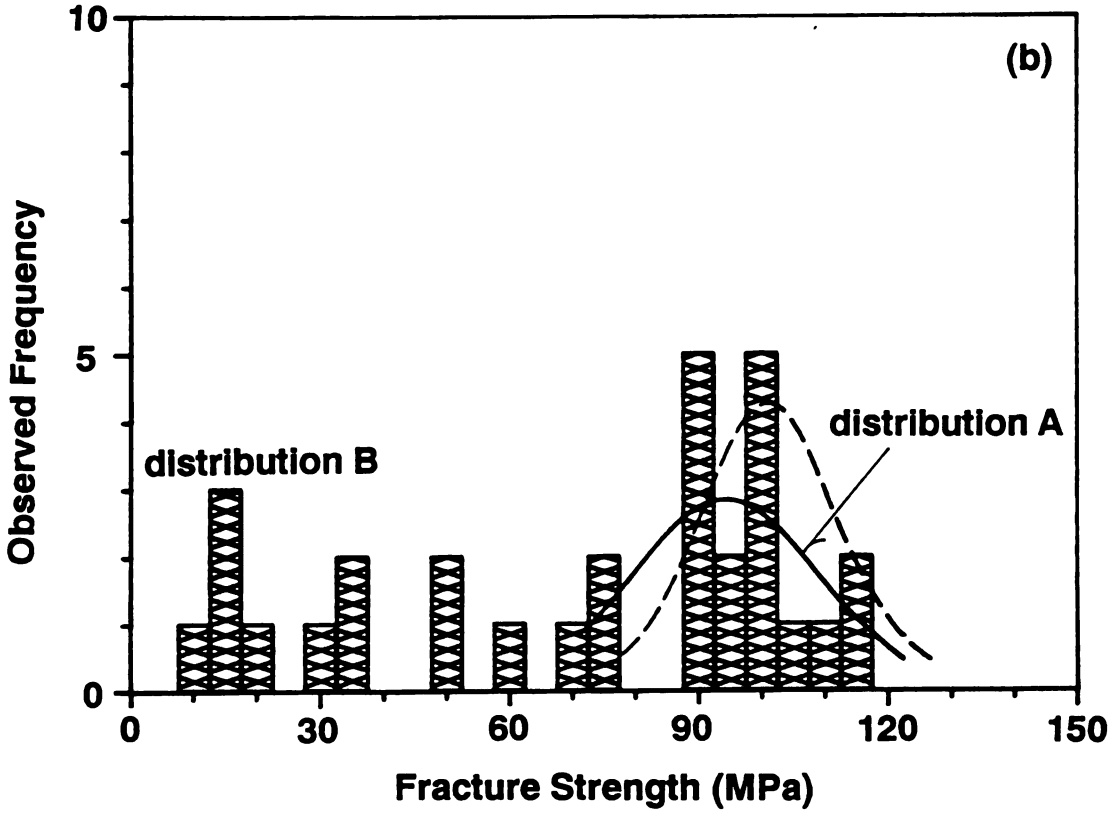

Figure 24(b). Retained fracture strength of glass slides following a single quench into a room temperature water bath at $\Delta T = 160^{\circ}$ C.

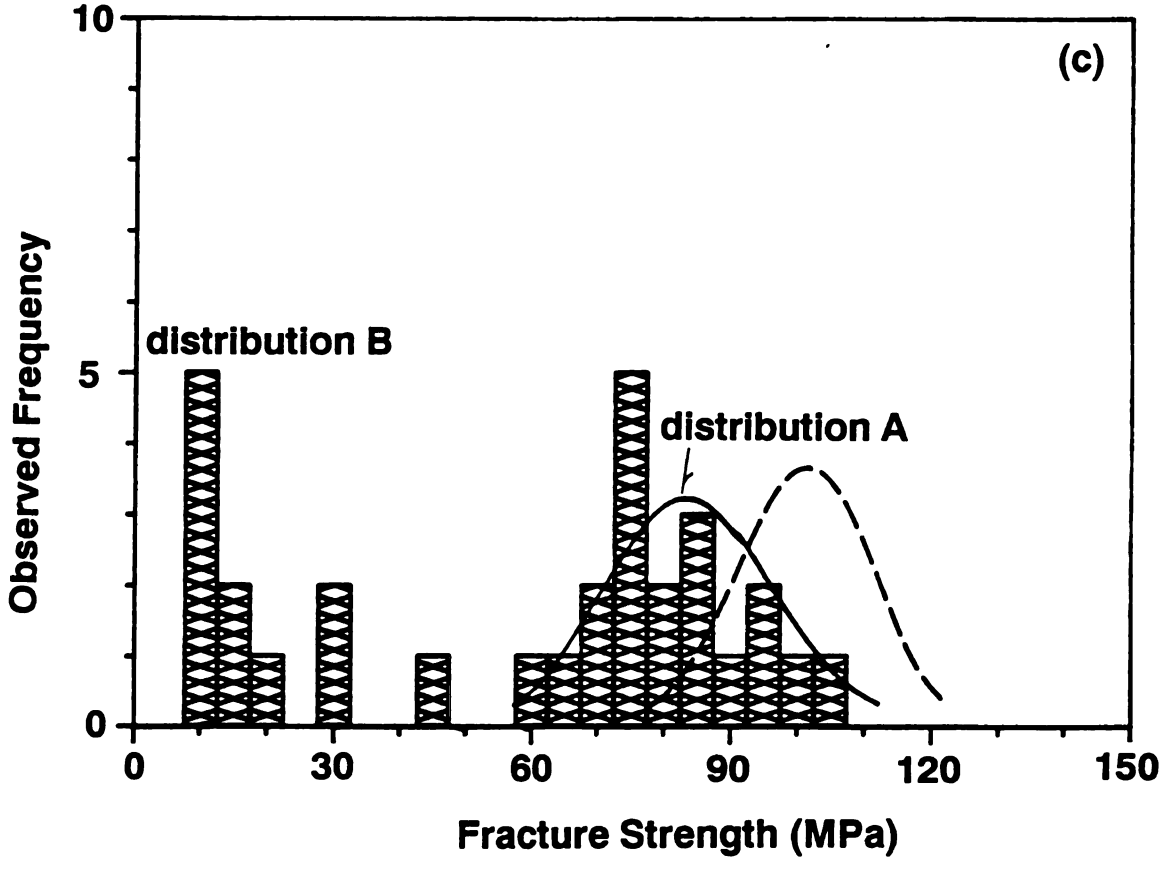

Figure 24(c). Retained fracture strength of glass slides following a single quench into a room temperature water bath at $\Delta T = 170^{\circ}$ C.

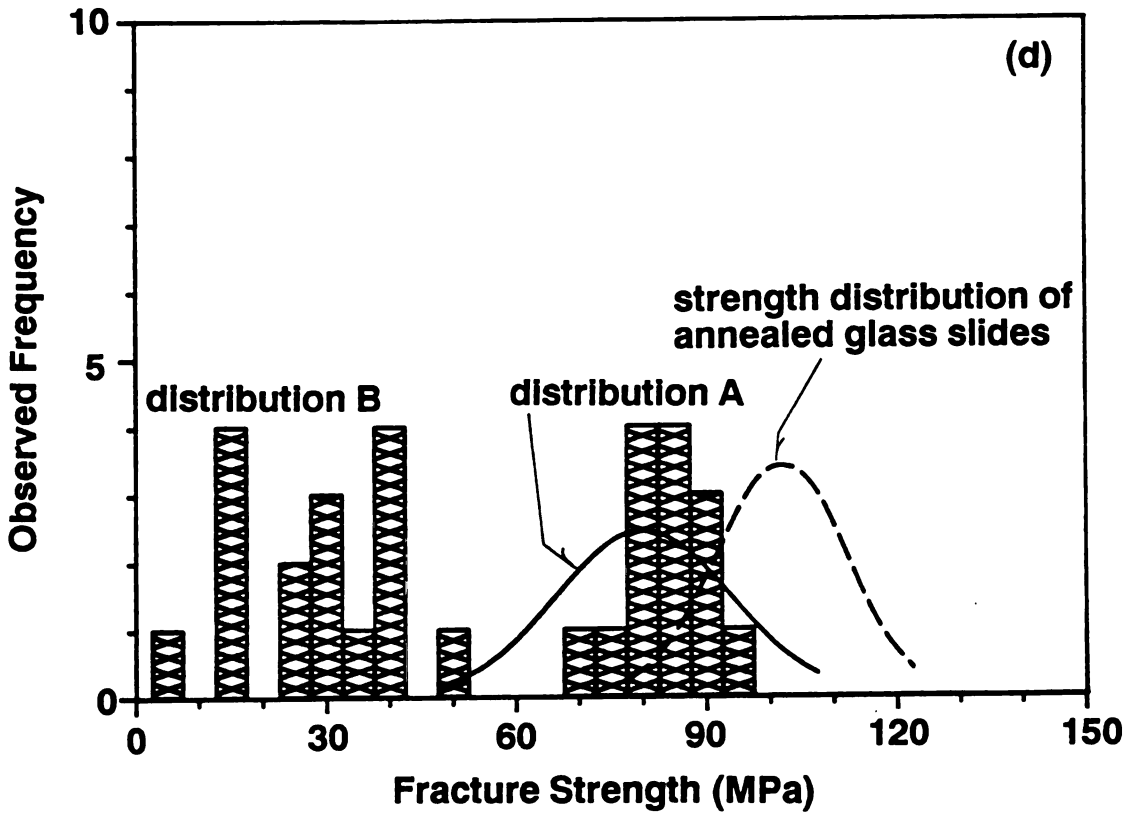

Figure 24(d). Retained fracture strength of glass slides following a single quench into a room temperature water bath at $\Delta T = 180^{o}$ C.

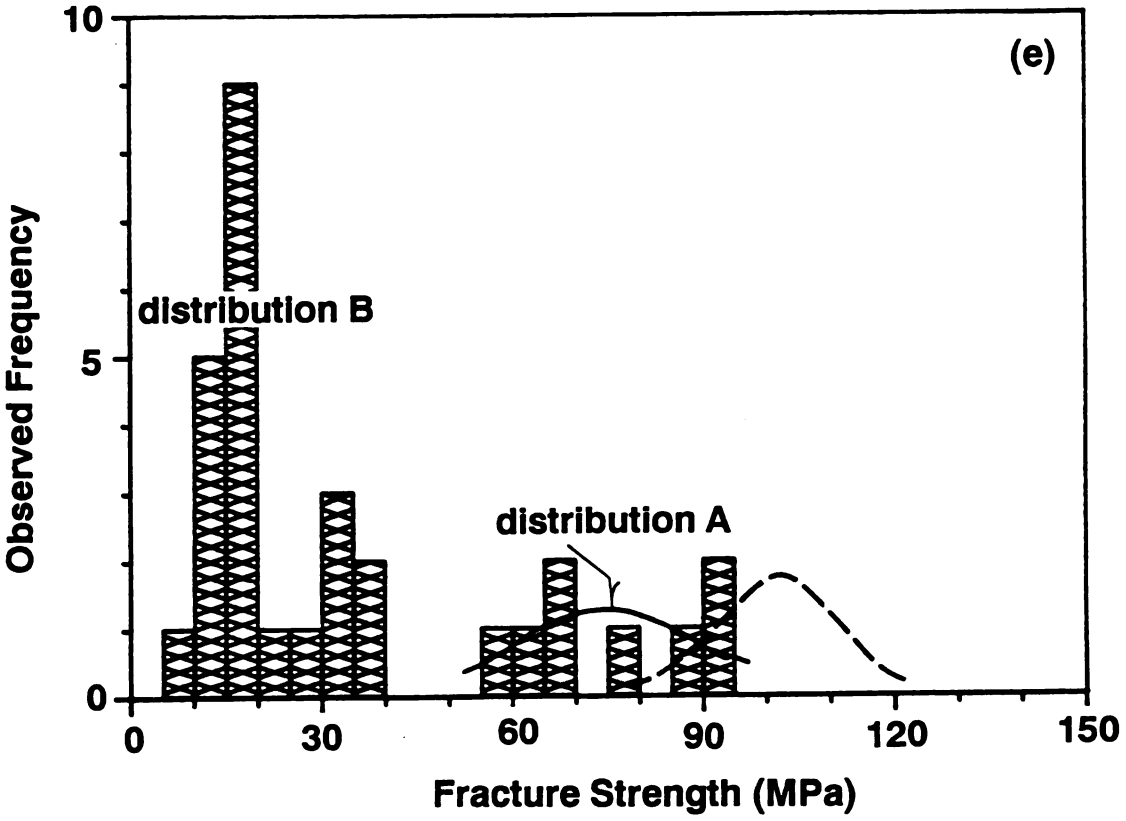

Figure 24(e). Retained fracture strength of glass slides following a single quench into a room temperature water bath at $\Delta T = 190^{o}$ C.

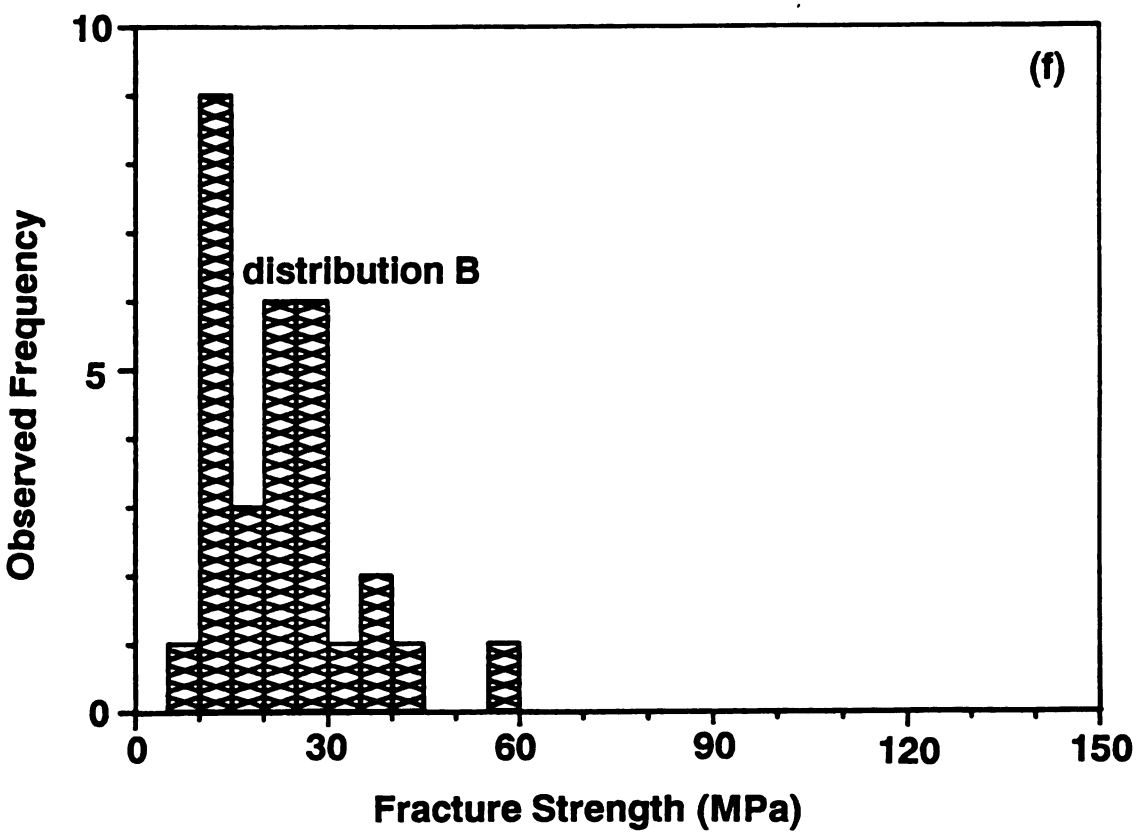

Figure 24(f). Retained fracture strength of glass slides following a single quench into a room temperature water bath at $\Delta T = 200^{\circ}$ C.

distribution is interpreted by the authors as indicative of the onset of strength degradation. The histograms of the retained fracture strength for glass slides shocked at ΔT's of 160° C, 170° C, 180° C, and 190° C show the development of a bimodal distribution (Figures 24(b) - 24(e)). Distribution B (which is similar to the distribution shown schematically in Figures 23(b) and 23(c)), represents the retained fracture strength of slides quenched severely enough to cause pop-in crack growth. In addition, distribution A shifts progressively to the left toward lower strength values, as compared with the strength distribution of annealed glass slides (dashed line). The experimental data in Figures 24(b) - 24(e) breaks into two clusters. The cluster with higher fracture strength is distribution A. The details for determining such distributions are given in Appendix C.

Distribution A disappears in the retained strength data for a ΔT of 200° C (Figure 24(f)). The absence of a distribution of type A suggests that each specimen experienced pop-in crack growth. Thus the entire strength distribution was converted into a distribution of type B, which shows a single mode located at relatively low strength values.

The strength shift for distribution A was attributed to subcritical crack growth. Comparison of the mean strength of distribution A (Figures 24(a) - 24(e)) and the mean strength of annealed glass slides indicates that the strength shift $\Delta\mu$ increases monotonically from 4.28 MPa for a ΔT of 150° C to 26.56 MPa for a ΔT of 190° C (Table 6).

The apparent temperature effect on subcritical crack growth agrees qualitatively with static crack propagation results for silica reported by Sakaguchi et al. [96] and dynamic fatigue results by Ritter et al. [97]. Sakaguchi et al. tested compact tension specimens of fused quartz under static tensile stress in distilled water [96]. Ritter et al. measured the dynamic fatigue of indented soda-lime glass in distilled water using a ring-on-ring test fixture [97]. In both studies the subcritical crack-growth rate increased with increasing water temperature [96,97].

To compensate for the effects of subcritical crack growth, the retained strength data at each ΔT between 150° C and 190° C (Figures 24(a) - 24(e)) were shifted by $\Delta\mu$ (see Table 6 and Figure 5). This shift in strength corresponds to a shift in critical quench temperature difference from the actual quench data $\Delta T_c \approx 175^{\circ}$ C to a "shifted" value $\Delta T_c \approx 190^{\circ}$ C. In this paper, the ΔT corresponding to the 50 percent probability level of failure (see Figures 24(c) and 24(d)) was considered to be the critical quench temperature difference, ΔT_c. The shift in ΔT_c attributable to subcritical crack growth was much less than the subcritical crack growth-induced shift (about 91° C) that Badaliance et al. [52] inferred from their data and computations.

The retained strength evolution for the glass slides shocked in this study indicates that subcritical crack growth does play a role in the thermal shock damage process.

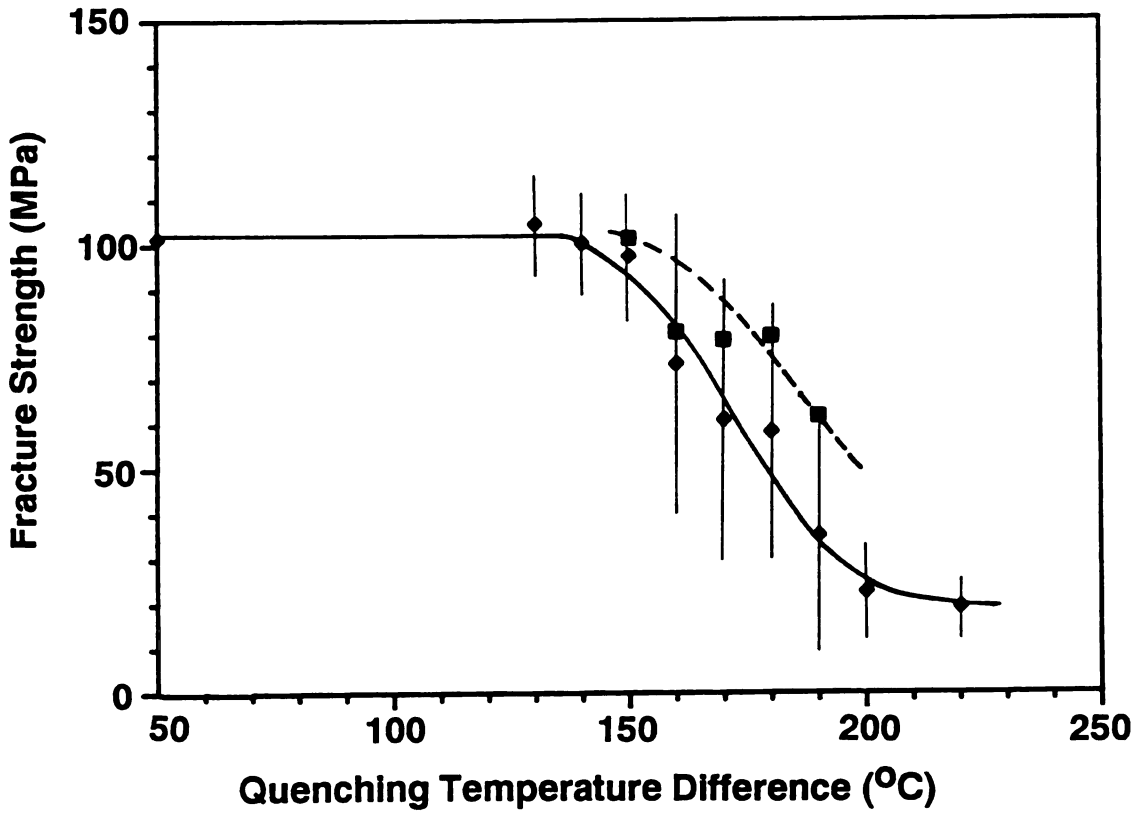

Figure 25. A plot of retained fracture strength versus ΔT. The solid line represents the original strength data curve (single thermal shock), which becomes the dashed line after compensating for subcritical crack growth effects (see Table 6).

(4.3.2.3). Fracture strength degradation during cyclic thermal shock

In addition to the single-quench testing, cyclic thermal shock of the glass slides was analyzed in terms of subcritical crack growth. For single quench testing, the retained fracture strength began to decrease at a ΔT of about 150° C, with an increase in the magnitude of the error bars* for the strength degradation curve at about 160° C (Figure 25). Under cyclic thermal shock conditions, thermal shock damage appeared at temperatures below 150° C. The magnitude of the thermal-shock induced strength drop also increased as the number of thermal shock cycles increased (Figure 26(a)).

---

* The fracture strength distribution of annealed glass slides in this study had a standard deviation σ = 10.2 MPa (Figure 21). Thermal shock damage caused the strength distribution of shocked slides to form two clusters, with one cluster corresponding to slides that underwent pop-in growth and the other cluster corresponding to slides that underwent slow crack growth only (Figures 24(b) - 24(e)). Thus, when ΔT is large enough that the strength distribution becomes bimodal then the standard deviation of shocked slides becomes large in comparison with that of annealed slides. As an example, consider that only five specimens had been thermally shocked at a given ΔT and that three specimens underwent pop-in type crack growth and that the other two specimens experienced subcritical crack growth only. The error bar, which represents two standard deviation in the strength values, would be considerably larger in this case than the corresponding error bars for the as-annealed strength distribution or for the case where all specimens undergo only pop-in growth or only subcritical crack growth.

To make Figure 26(b) more readable, the error bars have been omitted. However, the magnitude of the error bars for Figure 26(b) are shown in the corresponding data points in Figures 25 and 26(a). The presence of thermal fatigue effects implies that pre-existing cracks can extend during each quench cycle, although the growth tends to saturate for the lower ΔT values. For example, the strength of the slides quenched at ΔT's of 130° C and 140° C tend toward a saturated damage level for the number of thermal cycles performed in this study, while the strength drops off precipitously for specimens shocked repeatedly at a ΔT of 150° C. Therefore, Figures 26(a) and 26(b) demonstrate that subcritical crack growth can occur below the critical quench temperature difference (which corresponds to a stress intensity factor below K_c).

Subcritical crack growth is a complex function of temperature and chemical environment. In addition, subcritical crack growth depends on K_o and K_c. For example, as K_c increases, pop-in crack growth decreases. Also, thermal stresses are very strong functions of time and position, thus these stresses are even more difficult to characterize than stresses in quasi-static loading experiments dealing with subcritical crack growth [35-37,95-97]. The relatively small shift in ΔT_c attributable to subcritical crack growth agrees qualitatively with Ashizuka's inference that subcritical crack growth was insignificant to the thermal shock resistance of borosilicate glass rods [52].

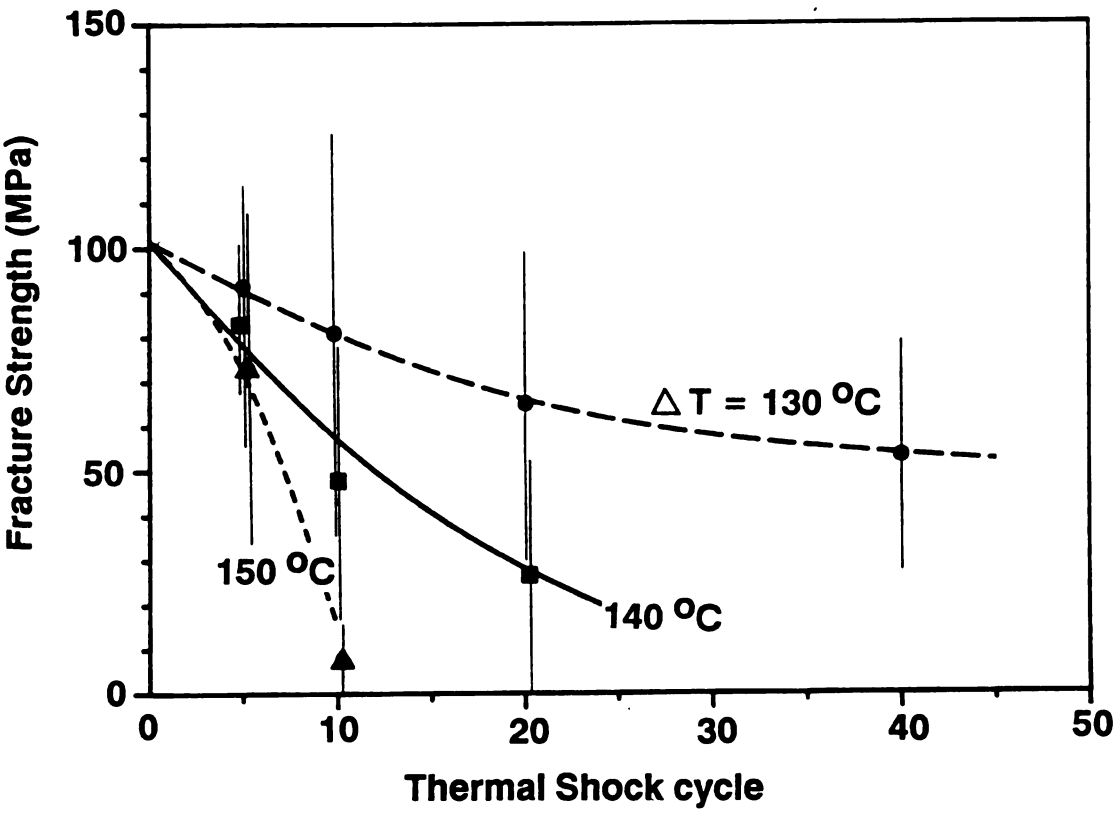

Figure 26(a). Influence of a cumulative number of thermal shock cycles on the retained fracture strength of the glass slides repeatedly shocked below ΔT_c, where ΔT_c is the critical quench temperature difference determined from single-quench testing.

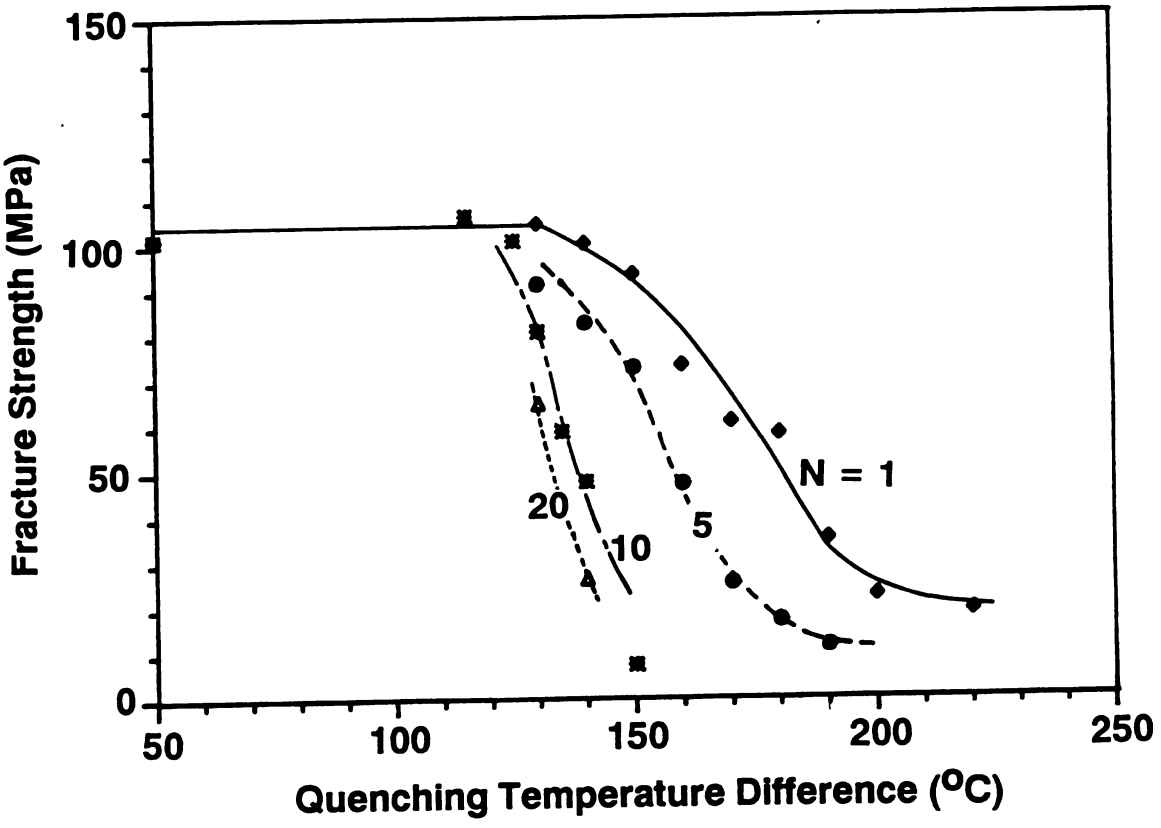

Figure 26(b). Variation of retained fracture strength with respect to ΔT and the cumulative number of thermal shock cycles, N.

Table 6. Thermal shock induced changes in the mean strength μ and the standard deviation σ for the retained strength distribution as a function of the quench temperature difference ΔT. The difference in mean strengths, $\Delta\mu$, measures the extent of slow (subcritical) crack growth. (Units of strength: MPa)

ΔT (^{o}C)	total shocked specimens		part A of bimodal distribution		slow crack growth effect	new distribution without slow crack growth
	$\hat{\mu}$	$\hat{\sigma}$	$\hat{\mu}_a$	$\hat{\sigma}_a$	$\hat{\Delta\mu} = 101.38 - \hat{\mu}_a$	$= \hat{\mu} + \hat{\Delta\mu}$
$\Delta T = 0$	101.38	10.2				
$\Delta T = 150$	97.41	15.3	97.41	11.5	4.28	101.38
$\Delta T = 160$	73.3	34.1	94.25	14.7	7.13	80.43
$\Delta T = 170$	60.75	32.1	83.59	12.1	17.79	78.54
$\Delta T = 180$	58.1	28.8	80.13	13.7	21.25	79.35
$\Delta T = 190$	35	26	74.82	13.7	26.56	61.56
$\Delta T = 200$	22.5	10.7	0		*	

* Since all specimens for $\Delta T = 200\ ^{o}C$ were subject to "pop-in" crack growth, the subcritical crack growth effect could not be evaluated.

(4.4). Computer Simulation of Quench-Induced Strength Degradation in Glass Plates

Hasselman in 1969 proposed a famous model for the calculation of ΔT_c, indicating that crack growth at $\Delta T \geq \Delta T_c$ caused a discontinuous drop in the retained strength [7]. However, Lewis (1983) proposed that since the critical flaw size of a group of brittle components was characterized by a distribution, the mean retained strength of quenched components should exhibit a gradual decrease as ΔT increased [38]. In this section, we extend Lewis' qualitative idea by combining the initial strength distributions, Hasselman's theory (1969), and subcritical crack growth [95,98], to qualitatively model the strength degradation in a group of quenched soda-lime glass specimens. The consequent computer simulation was divided into two parts. Part I of the simulation neglected subcritical crack growth and part II of the simulation included subcritical crack growth.

(4.4.1). Theoretical Consideration

(4.4.1.1). Initial strength distributions

Quench-induced fracture is a stochastic process that depends on the size and spatial distribution of pre-existing flaws. In this study, the initial fracture strength, S, of our group of glass specimens was characterized by a normal distribution with a mean of 101.38 MPa and a standard derivation of 10.2 MPa. (The experimental results were presented in a previous paper section). In the

computer model, the strength distribution used in the computer model was generated using an IMSL (International Mathematics and Statistics Library) random number generator. (The names of subroutines are RNNOR, SSCAL, and SADD, which are shown in Computer program No. 4.) The sample population contained one thousand data points. The corresponding critical crack size, $a = a_o$, was then evaluated by

$$a_o = \pi \left[\frac{K_c}{S\,Y} \right]^2 \tag{23}$$

where K_c and Y are the critical stress intensity factor and a geometrical parameter, respectively. Y was chosen as 1.1215, which is appropriate for a penny-shaped surface flaw where the specimen is loaded quasistatically in uniaxial tension.

(4.4.1.2). No subcritical crack growth effect

For a brittle component that experiences a single thermal shock, Hasselman proposed that pre-existing cracks could propagate if the quench temperature difference, $\Delta T = \Delta T_o$, exceeded the critical value, ΔT_c [7]. In Hasselman's model [7], only "one" specimen was considered and the pre-existing cracks in the one specimen were assumed to have uniform size. In the present study, the 1000 glass specimens included in computer model were assumed to have different critical flaw sizes, $a = a_o$, as determined from equation (23). However, the pre-existing cracks in an individual specimen were also assumed to have the uniform size $a = a_o$, as Hasselman did.

Thus, the critical quench temperture difference, $\Delta T = \Delta T_c$, for the individual specimens was calculated as [7]

$$\Delta T = \left[\frac{\pi\ G\ (1-2\nu)^2}{2\ \alpha^2 E\ (1-\nu^2)} \right]^{1/2} \left[1 + \frac{16\ (1-\nu^2) N a^3}{9\ (1-2\nu)} \right] \left[a^{-1/2} \right] \qquad (29)$$

where N is the crack number density in a component with crack length, a. G is the surface fracture energy required to form a unit area of new crack surface. E, ν, and α are the elastic modulus, Poisson's ratio, and the thermal expansion coefficient, respectively. The required input parameters are listed in Table 7. Therefore, if $\Delta T_o > \Delta T_c$, the resulting "pop-in" crack length, a_1, can be calculated using equation (29). Substituting $\Delta T = \Delta T_c$ into equation (29) gives two positive real solutions: the original crack length, a_o, and a larger crack length, a_{q1}. Crack growth from a_o to a_{q1} is quasi-static, based on Griffith's fracture criterion.

Hasselman proposed that the pop-in cracks extend kinetically to a final length a_f, such that [7]

$$\frac{3(\alpha\Delta Tc)^2 E}{2\ (1-2\nu)} \left[\left[1 + \frac{16(1-\nu^2)Na_o^3}{9\ (1-2\nu)} \right]^{-1} - \left[1 + \frac{16(1-\nu^2)Na_f^3}{9\ (1-2\nu)} \right]^{-1} \right]$$

$$= 2\ \pi\ N\ G\ (a_o^2 - a_f^2) \qquad (30)$$

Equation (29) is a crack instability criterion. Equation (30) determines the kinetic-propagation induced crack length. Although the pre-existing cracks kinetically grow from a_o to a_f, the quench

Table 7. Parameters required for computer simulation

property	magnitude	units	references
elastic modulus (E)	70	GPa	*
Poisson's ratio (ν)	0.18		*
thermal expansion coefficient (α)	6.5×10^{-6}		*
fracture surface energy (G)	4.0	$Pa\ m^{-2}$	[98]
crack density (N)	2×10^{11}	m^{-3}	#
specimen's thickness (2ℓ)	0.0012	m	*
surface heat transfer coefficient (h)	0.4	$W/cm^2\ ^oC$	[61]
thermal conductivity(C)	0.03	$W/cm\ ^oC$	[95]
activation energy (E_*)	1.0×10^{-6}	J/mole	[95]
pre-exponential factor (V_o)	2.9×10^{4}	m/s	[95]
crack growth constant (b)	0.11		[95]
fatigue limit (K_o)	0.248	$MPa\ m^{1/2}$	[95]

* The properties were measured in this study.

\# see Appendix D.

temperature difference, $\Delta T = \Delta T_o$, may be great enough to continuously cause the cracks to quasi-statically propagate [7]. When $\Delta T = \Delta T_o$ is substituted in equation (29), a solution of crack length a_{q2} is obtained. If the a_{q2} is smaller than a_f, the corresponding quasi-static crack propagation does not occur. As a result, the final crack length is a_f rather than a_{q2}. If $a_{q2} > a_f$, the final crack length is a_{q2}, indicating that quasi-static crack growth occurs after the kinetical crack growth. The retained strength, S, is then transformed from the a_q (or a_f) using equation (28).

(4.4.1.3). Subcritical crack growth effect included

For glass slides quenched into a water bath, we approximate the thermoelastic stresses in the slides by using the expression for the thermoelastic stresses in an infinite glass plate of thickness 2ℓ (see page 16)

$$\sigma(Z,t) =$$

$$2\,\frac{\alpha\, E\, \Delta T(Z,t)}{1-\nu}\left\{\sum_{n=1}^{\infty} \exp(-a\,(\delta_n/\ell)^2\, t)\,\frac{\sin(\delta_n)}{\delta_n + \cos(\delta_n)\,\sin(\delta_n)}\left(\frac{\sin(\delta_n)}{\delta_n} - \cos(\delta_n\, Z/\ell)\right)\right\} \tag{10a}$$

$$\delta_n \tan(\delta_n) = B \qquad n = 1,\ 2,\ 3,\ \ldots. \tag{10b}$$

$$\Delta T(Z,t) = \Delta T_o \sum_{n=1}^{\infty} 2\left[\frac{\sin(\delta_n)\,\cos(\delta_n\, Z/\ell)}{\delta_n + \sin(\delta_n)\,\cos(\delta_n)}\right] \exp(-d(\delta_n/\ell)^2\, t) \tag{8b}$$

$\Delta T(Z,t)$ = temperature gradient in a glass slide
t = time
d = thermal diffusivity
δ_n = the root of Eq. (10b)
Z = coordinate in the direction normal to glass plate surfaces
ℓ = half thickness of glass plate. $Z = \ell$ and $Z = -\ell$ on both plate surfaces
B = Biot's modulus

Badaliance, Krohn and Hasselman investigated the interrelation among the stress intensity factor, subcritical crack growth, and quasistatic crack propagation during thermal quench [51]. Pre-existing cracks are suspectable to subcritical crack growth during a thermal quench if the magnitude of the stress intensity factor, $K_{thermal}$, is $K_o < K_{thermal}$, where K_o is the threshold for subcritical crack growth. The crack growth may be described by [51,95,98]

$$da/dt = V_o \exp[(-E_* + b\, K_{thermal})/RT] \tag{31}$$

$$K_{thermal} = 1.1215\, \sigma(\ell,t)\, (\pi\, a_o)^{1/2} \tag{32}$$

where V_o and b are constants. E_*, R, and T represent the activation energy, the universal gas constant, and the absolute temperature, respectively. (Table 7 lists the subcritical crack growth parameters.) Badaliance proposed that the pre-existing surface cracks were subjected to transient thermal stresses equivalent to the surface transient stresses. In the present study, we used Badalinace's approximation to model subcritical crack growth during thermal quench.

In this paper, we used equation (29) to determine whether or not pop-in crack growth occurs. If the initial quench temperature difference ΔT_o exceeded ΔT_c, pop-in crack growth was assumed to occur. (Equation (24) only predicts whether or not the crack growth occurs, without explaining when the crack growth occurs.) In the computer simulation of thermal quench damage in this paper, if pop-in crack growth did not occur, subcritical crack growth mau nor may not occur, subject to the following conditions:

(a) When $K_{thermal}$ was smaller than K_o, no subcritical crack growth occurred.

(b) When $K_{thermal}$ exceeded K_o, the pre-existing cracks grew according to equation (31). Crack propagation was simulated iteratively via equations (10a), (31), and (32).

(c) Subcritical crack growth in pre-existing cracks caused ΔT_c to change with elapsed time. The transient average temperature, T_a, of specimen also decreased with elapsed time. When the critically growing crack satisfied equation (29) ($\Delta T_a > \Delta T_c$), the cracks were allowed to grow according to equation (30) (substituting $\Delta T = \Delta T_a$). Cracks that grow subcritically up to the critical flaw size (for the "current" thermoelastic stress state) can grow by pop-in rather than continuing to grow subcritically. In the computer simulation, when a crack grows subcritically to the critical flaw length, the computation of crack length shifts from the subcritical crack growth subroutine (represented by equation 31) to the pop-in growth subroutine.

(d) The initial time and the final time of the thermal shock simulation were $t = 0$ second and $t = 2.5$ seconds, respectively.

At the end of the thermal shock duration, the retained fracture strength, S, was transformed from the final crack length using equation (23).

(4.4.2). Numerical Results and Discussion

The computer simulation indicates that the evolution of quench-induced crack growth depends on whether or not subcritical crack growth effect is included in the thermal shock damage process. According to Hasselman's model (Equations (29) and (30)) and under the conditions in Table 7, a pre-existing crack with crack length a = $1.2X10^{-5}$m never grows at $\Delta T < 218\ ^{o}C$. However, the crack can grow subcritically at $106\ ^{o}C < \Delta T < 218\ ^{o}C$ (because of $K > K_{o}$). Figure 27(a) illustrates the variation of the crack length with time at different ΔT. Figure 27(b) shows the velocity of crack growth as a function of time. When $\Delta T = 185\ ^{o}C$ and $\Delta T = 195\ ^{o}C$, the crack length increased 0.9 μm and 0.1 μm at the end of the quenching process, respectively (Figure 27). When $\Delta T = 205\ ^{o}C$ and $\Delta T = 215\ ^{o}C$, the subcritically growing cracks become great enough that Griffith's failure criterion is finally satisfied and a pop-in crack growth occurs. According to the computer simulation, subcritical growth effect enhances thermal shock damage.

A thermal shock may cuase the pre-existing crack to propagate, which degrades the fracture strength of the shocked specimens relative to that of the non-shocked specimens. Since the critical flaw size (initial fracture strength) of a group of brittle components is characterized by a distribution, thermal shock testing accordingly requires a large number of specimens to achieve a reliabe

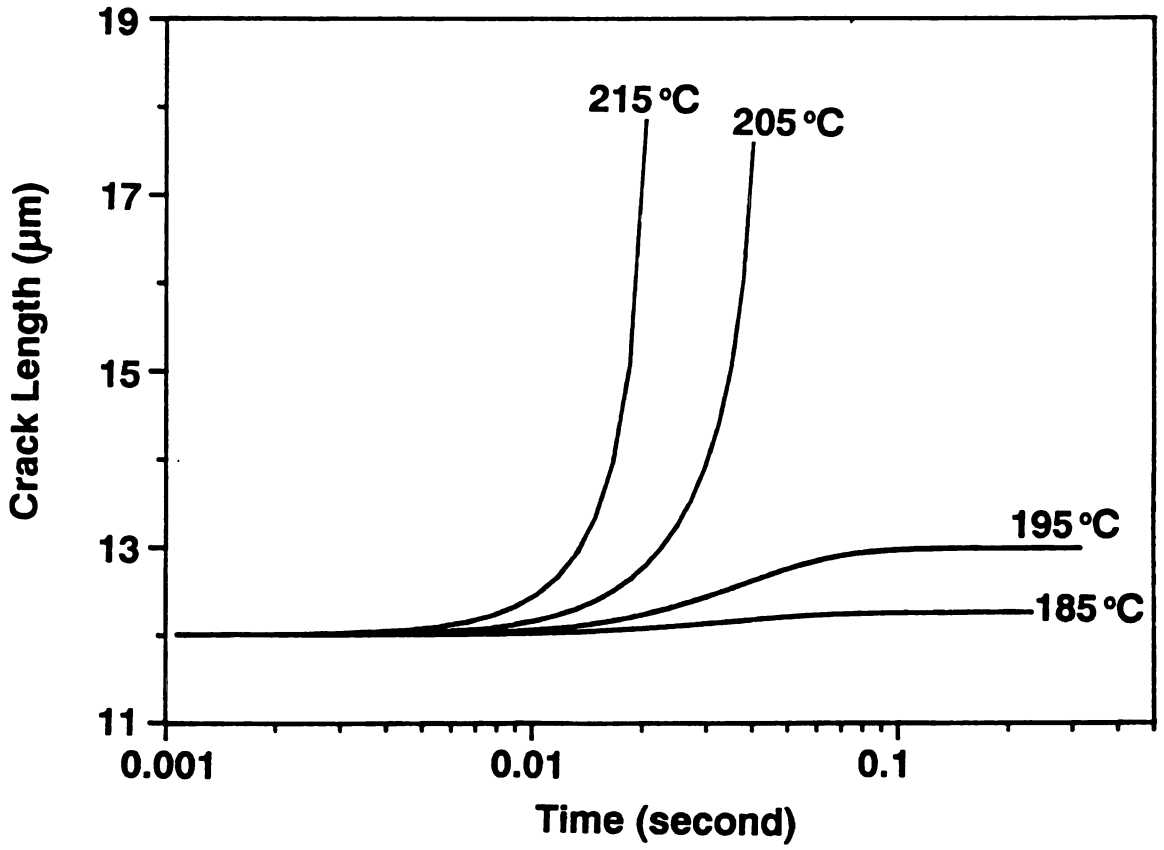

Figure 27(a). Computer simulation of crack length as a function of time for cracks extending subcritically. Note that small differences in quench temperature can induce dramatic changes in the crack growth behavior.

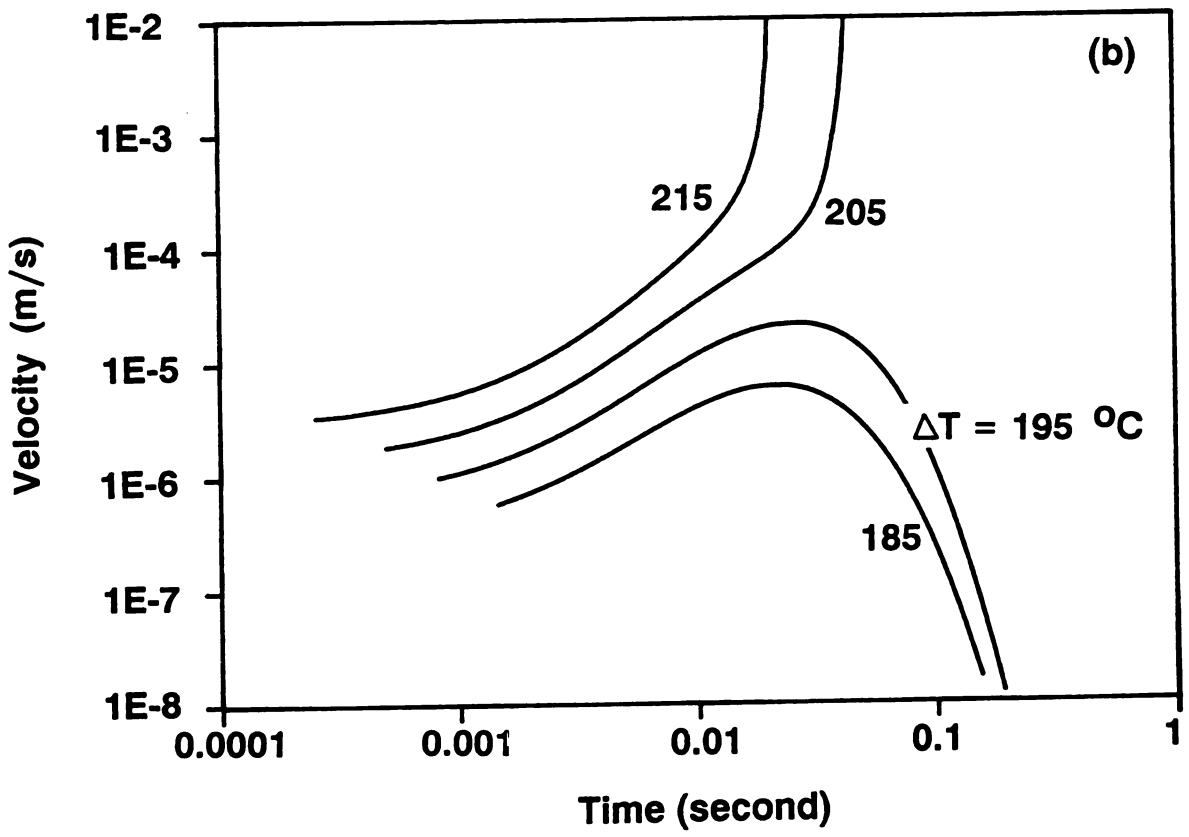

Figure 27(b). Computer simulation of crack growth velocity as a function of time for cracks extending subcritically.

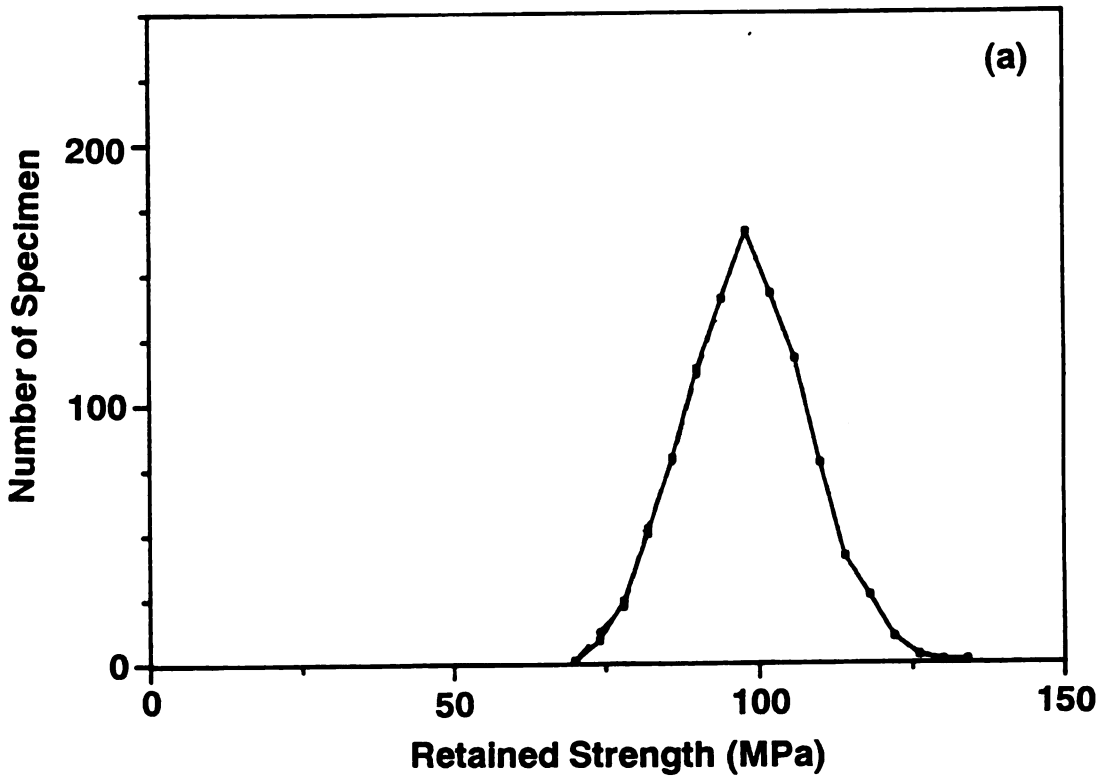

Figure 28(a). Computer simulation of the strength degradation of specimens shocked at $\Delta T = 140\ ^{o}C$. The solid line represents the retained strength without subcritical crack growth effect. The dashed curve represents the retained strength with subcritical crack growth effect.

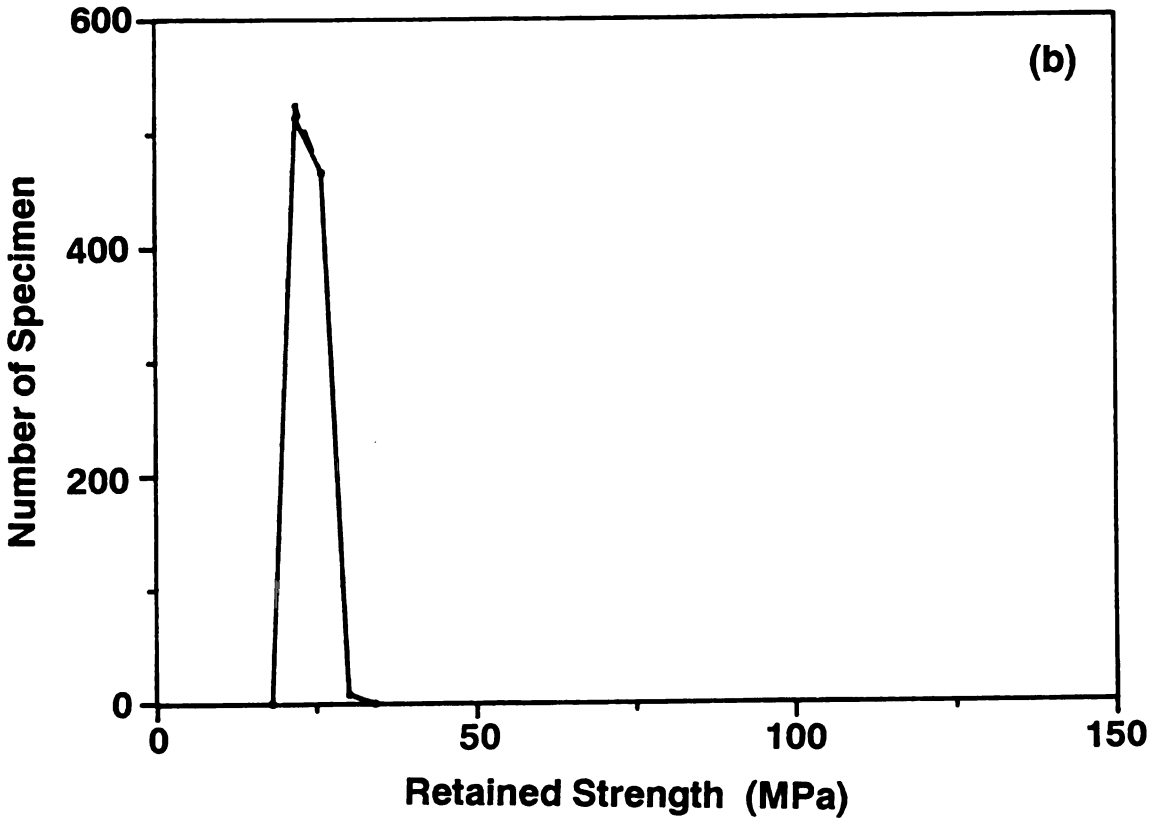

Figure 28(b). Computer simulation of the strength degradation of specimens shocked at ΔT = 240 ^{o}C.

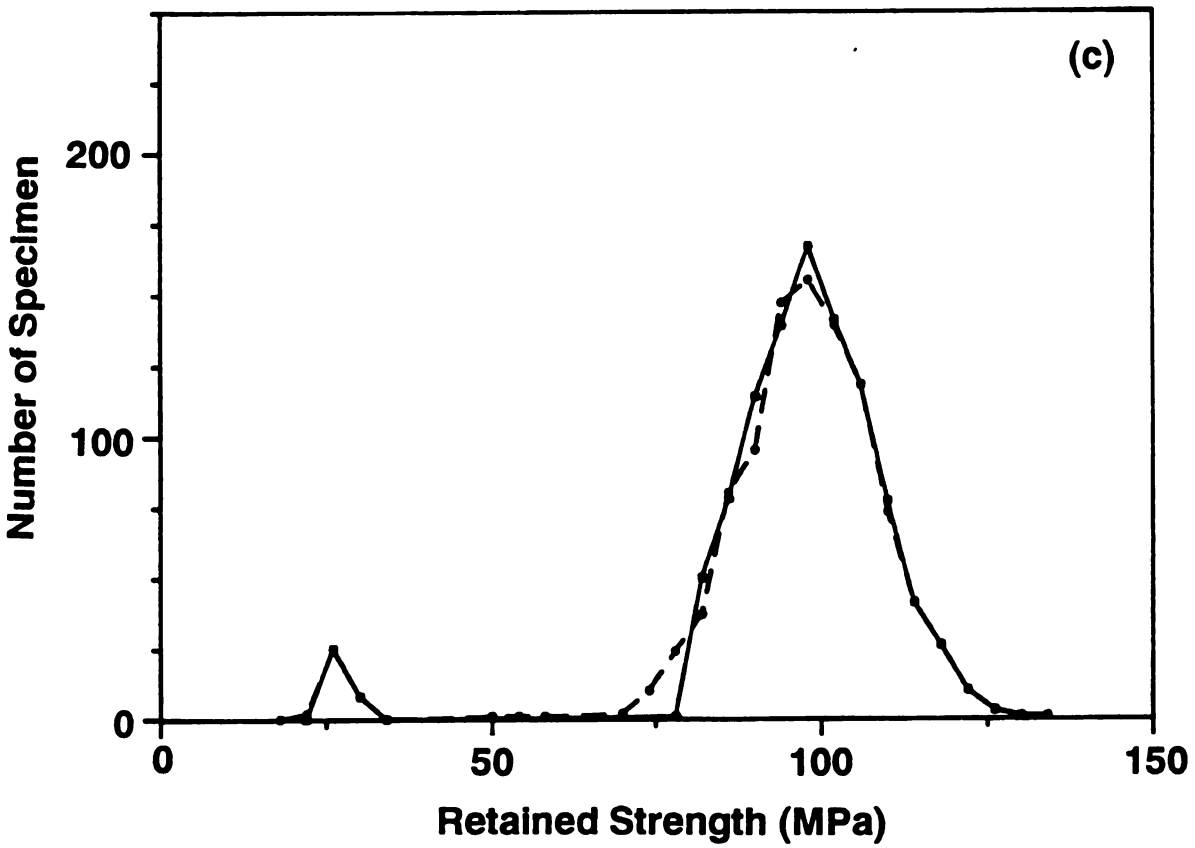

Figure 28(c). Computer simulation of the strength degradation of specimens shocked at $\Delta T = 160\ ^{o}C$.

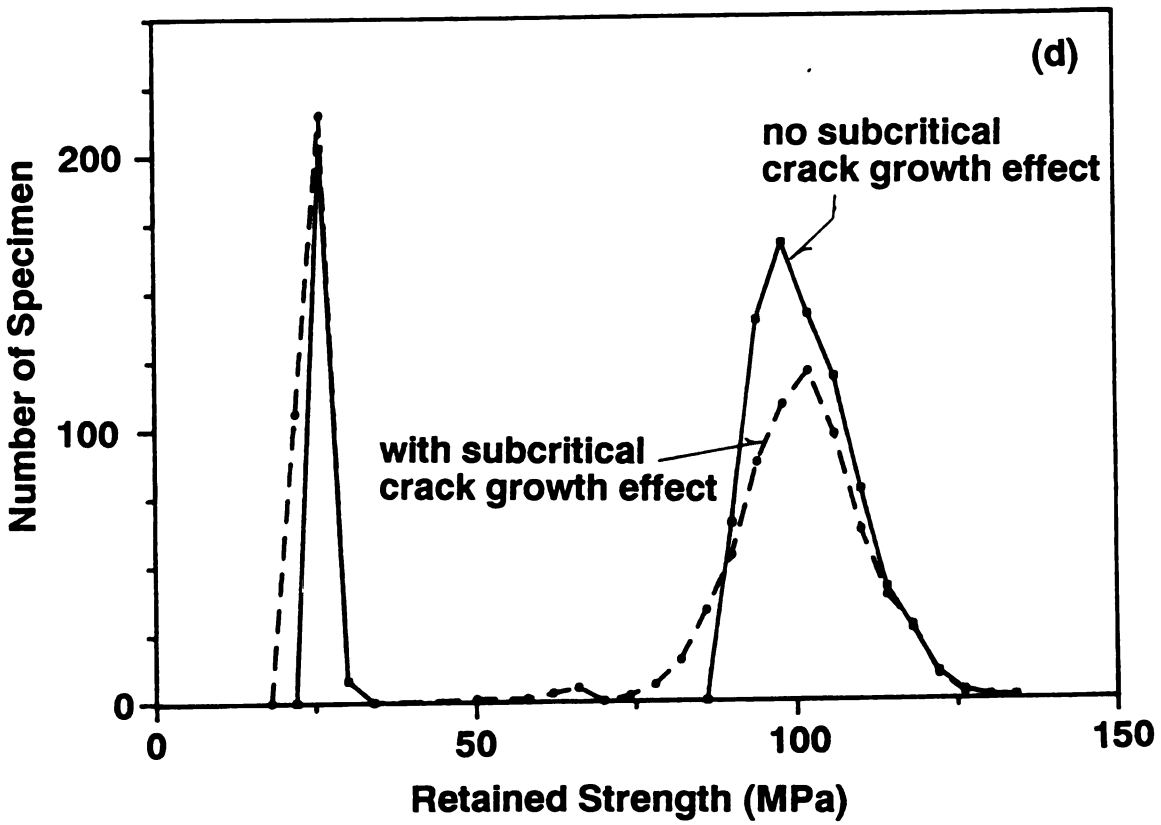

Figure 28(d). Computer simulation of the strength degradation of specimens shocked at ΔT = 180 ^{o}C.

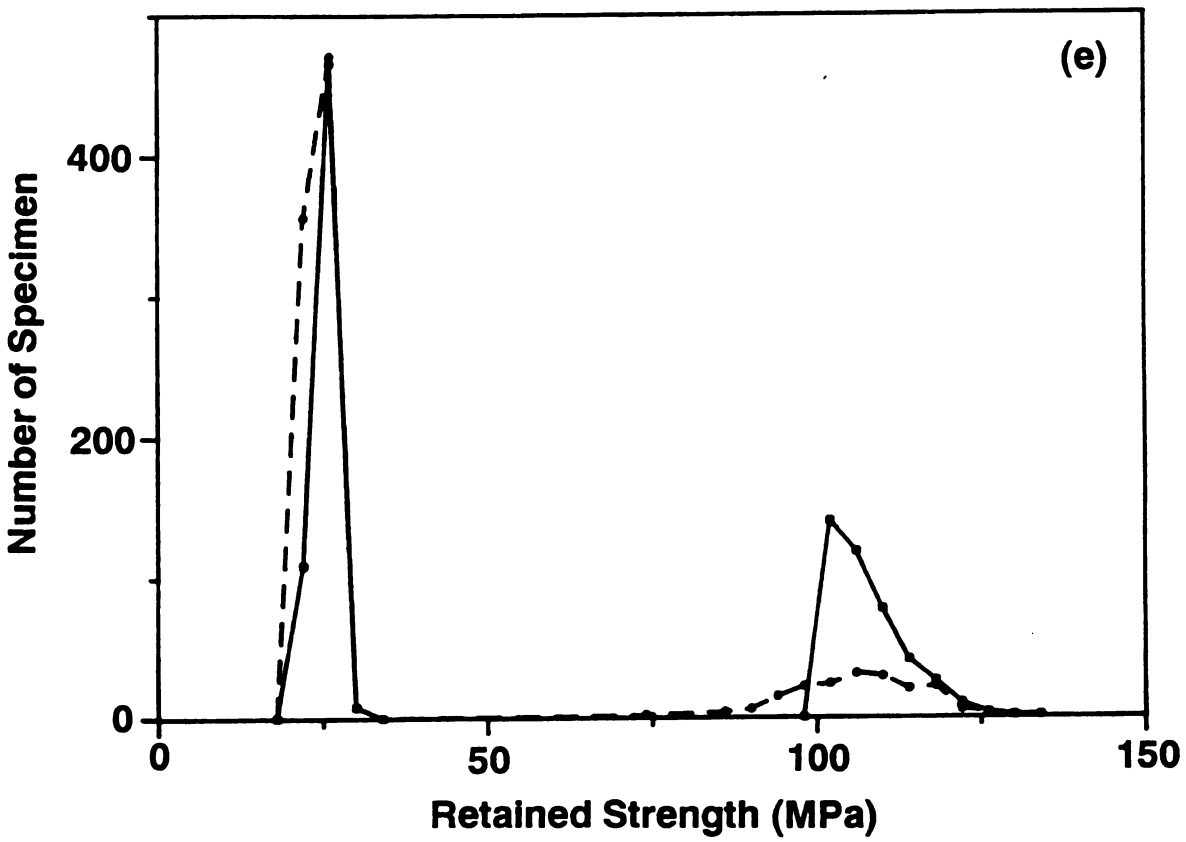

Figure 28(e). Computer simulation of the strength degradation of specimens shocked at $\Delta T = 200\ ^{o}C$.

statistical estimate. The computer simulation results illustrate the strength degradation development of 1000 quenched glass specimens (Figure 28). The solid curves represent no subcritical crack growth and dashed lines represent subcritical crack growth. For simplicity, we shall discuss the evolution of the fracture distribution for two cases: (A) neglecting subcritical crack growth, and (B) including subcritical crack growth.

A. No Subcritical Crack Growth Effect:

Equation (29) yields the critical quench temperature difference for a specimen with a given flaw size $a = a_o$. For the thermal stress conditions listed in Table 1, ΔT_c will vary from specimen to specimen according to the critical flaw size. Figure 29 shows the distribution of ΔT_c corresponding to 1000 glass specimens, which are transformed from the critical flaw size using equations 23 and 29.

When 1000 glass specimens are shocked at $\Delta T = 140\ ^{o}C$, the quench temperature difference is smaller than the ΔT_c for each specimen (see Figure 29). Thus, no strength degradation occurs and the initial fracture strength distribution is not altered (Figure 28(a)). When the glass specimens are shocked at $\Delta T = 240\ ^{o}C$, the quench temperature difference is greater than the ΔT_c for each specimen. Consequently, the strength of each specimen drops as the critical flaws in the specimens extend (Figure 28(b)). When $\Delta T = 160\ ^{o}C$, ($\Delta T = 180\ ^{o}C$, or $\Delta T = 200\ ^{o}C$), some fraction of specimens are subjected to pop-in crack growth. Thus, the retained strength distribution becomes bimodal (Figures 28(c), 28(d), and 28(e)).

B. Subcritical Crack Growth Effect Included:

If subcritical crack growth is present during thermal shock, the evolution of retained fracture strength will differ from that suggested above, in that there will be additional crack growth regimes and an additional crack growth criterion.

When 1000 glass specimens are shocked at $\Delta T = 240\ ^{o}C$, all critical flaws are subjected to pop-in crack growth. Thus, subcritical crack growth will have no effect on strength degradation (Figure 28(b)). If the glass specimens are shocked at $\Delta T = 140\ ^{o}C$, no pop-in crack growth occurs. Furthermore, the transient thermal stress corresponding to $\Delta T = 140\ ^{o}C$ is not great enough to significantly activate subcritical crack growth.

At $\Delta T = 160\ ^{o}C$, $\Delta T = 180\ ^{o}C$, or $\Delta T = 200\ ^{o}C$, subcritical crack growth result in observable shifts in the retained fracture strength (dashed curves in Figures 28(c), 28(d), and 28(e)) in comparison with pop-in crack growth (solid curves). The computer simulation results qualitatively imply that the initial fracture distribution of a group of the specimens shocked at $T = T_o$ can be divided into four domains (Figure 30). Since the ΔT_c of each specimen in domain I is smaller than ΔT_o, all specimens are subjected to pop-in crack growth. Specimens in domain J do not undergo pop-in crack growth initially. Later on, the specimens in domain J are activated from subcritical crack growth into pop-in crack growth. Specimens in domain P only experience subcritical crack growth. Specimens in domain Q do not accumulate thermal shock damage because of $K < K_o$. (If subcritical crack growth were not considered, domains J and P would not exist. As a result, the arrows point out the development of retained strength

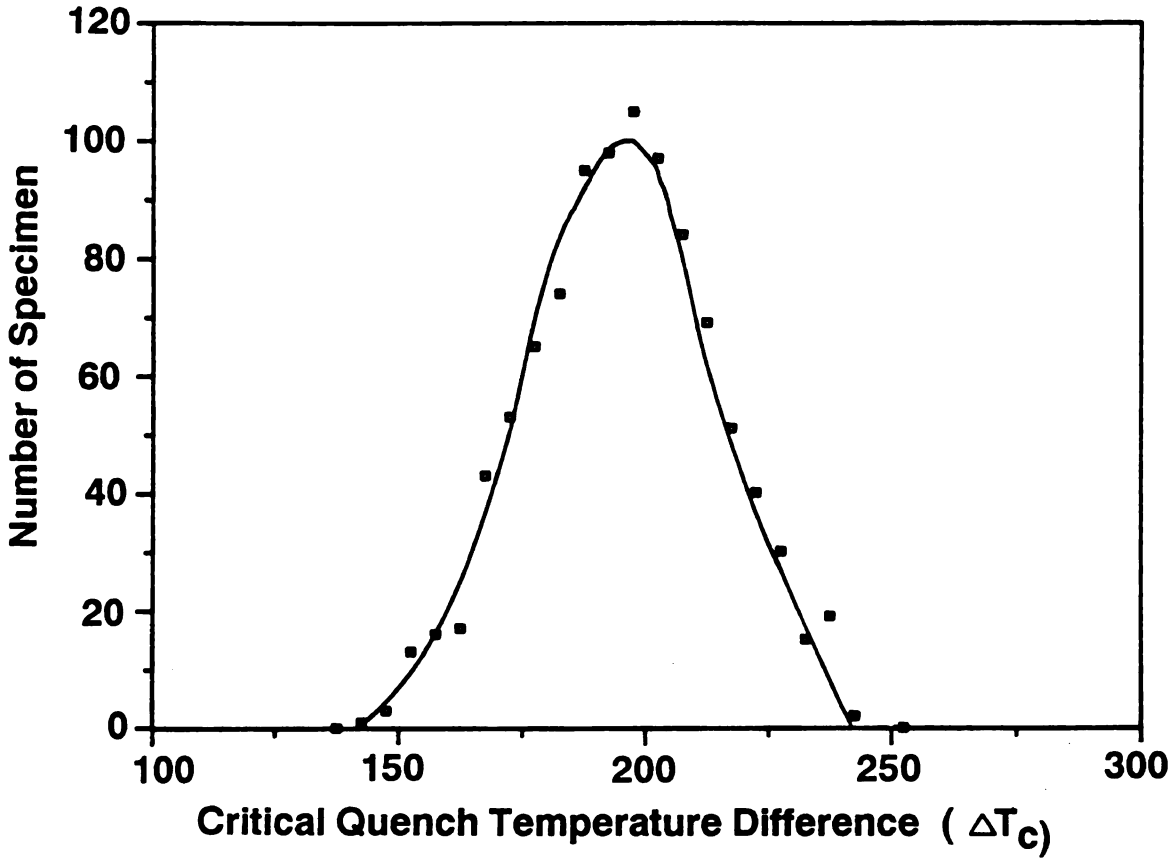

Figure 29. A ΔT_c distribution of 1000 pieces of annealed glass slides, which was calculated from the initial flaw size using equation (29). The initial flaw size was randomly generated through computer program.

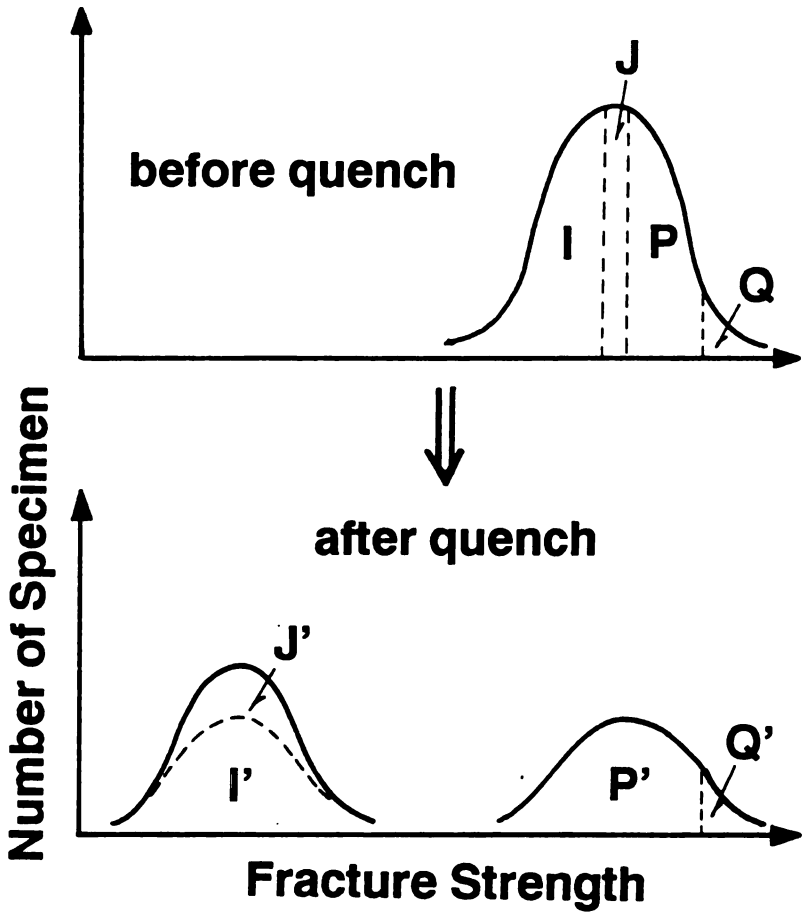

Figure 30. A schematic of illustrating the retained strength degradation in a group of shocked specimens.

distribution, turning into domains L', M', P', and Q'. The populations of domains L, M, P, and Q are determined by the T_o, K_o, and thermal stress conditions.

Figure 31 is a plot of mean retained strength versus ΔT, which corresponds to the retained strength data represented for individual ΔT's given in the series of Figure 28a - 28e. The solid curve does not include subcritical crack growth while the dotted curve does include subcritical crack growth. The strength degradation curves exhibit a smooth strength decrease, rather than a discontinuous drop, in agreement with Lewis' concept. In the present study, the critical quench temperature difference, ΔT_c, was considered to be the ΔT corresponding to the 50 percent probability level of failure. Thus, the solid line yields $\Delta T_c \approx 200\ ^{o}C$ and the dotted line gives $\Delta T_c \approx 190\ ^{o}C$. Subcritical crack growth apparently augments the thermal shock damage, resulting in a decrease in ΔT_c by about $10\ ^{o}C$.

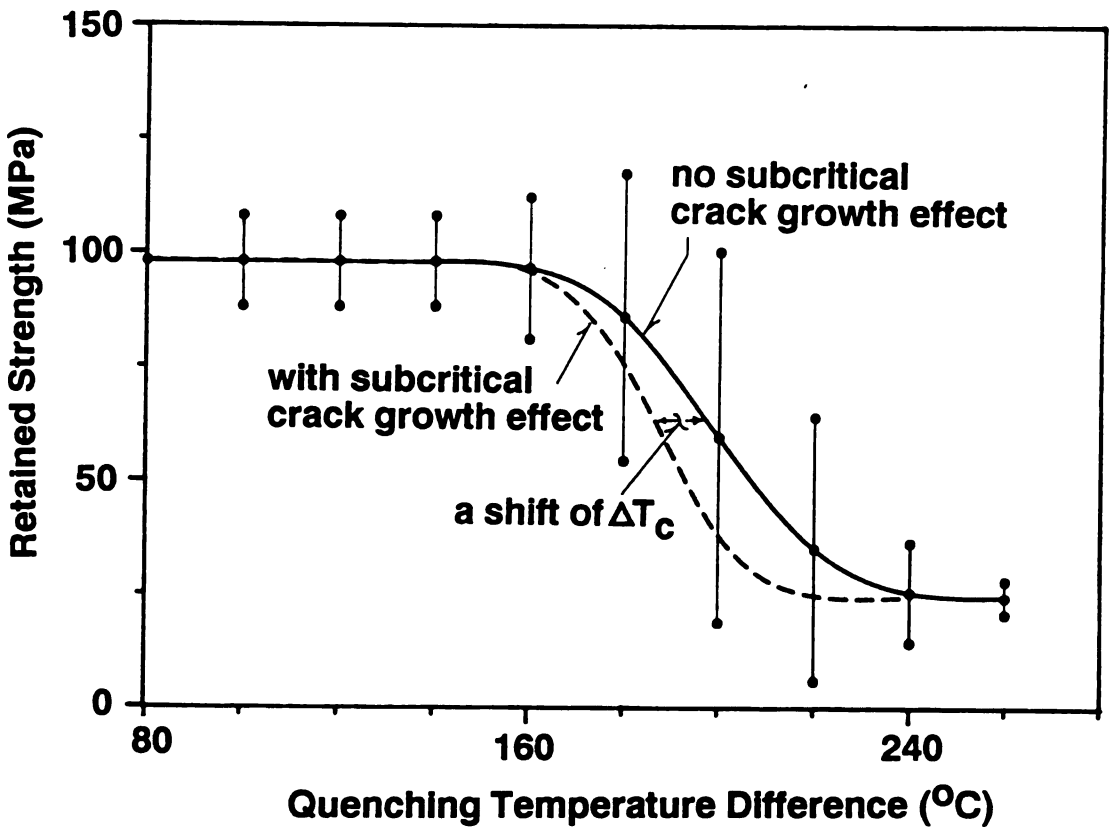

Figure 31. A plot of retained strength versus ΔT. Solid line represents the mean retained strength without subcritical crack growth effect. Dashed line is mean retained strength with the subcritical crack growth effect. The computer simulation data was presented in Figure 28.

5. SUMMARY and CONCLUSIONS

Thermal quenching into a water bath from below the material's annealing temperature is the standard technique for thermal shock testing of brittle ceramics that behave viscoelastically above some elevated temperature [64-73]. The typical thermal stress calculations for such experiments are thermoelastic in nature [21-37]. However, in practice thermal stress conditions for a ceramic component may include a broad quenching temperature ranges, such as thermal quench from above the annealing temperature. Thus, thermal stress calculations should include both thermoelastic theory and viscous flow effects.

In this paper, a thermal shock damage map (Figure 9) was proposed to predict the effect of thermal quench on a glass plate, based on thermoelastic and thermoviscoelastic stress theory. The map indicates that quenching a glass plate may induce either thermal shock damage and/or residual stresses depending on the heat transfer characteristics of the quench bath, the initial material temperature, and material properties. The analysis also indicates that thermal quench from below the glass's annealing temperature increases the probability of thermal shock damage as the quench temperature difference ΔT increases. Viscous flow occurs when a glass is quenched from above the annealing temperature. Viscous flow reduces the transient surface tensile stress, although viscous flow leads to the eventual development of residual tensile stresses in the plate's interior. Thus, a damage-free tempered (quenched) glass plate will be restricted to a certain range of ΔT.

Commercial glass microscope slides were quenched from below and above the annealing temperature. The quenching media include air, oil, and water. The Biot's modulus, B, is ranked as follows: B (water quench) > B (oil quench) > B (air quench). Quenching from below the annealing temperature may lead to thermal shock damage. As the Biot's modulus decreased, the critical quench temperature difference increased. Shock damage decreased the retained fracture strength and elastic modulus, while it increased internal friction. Quenching from above the annealing temperature caused residual stresses and thermal shock damage. For a given quench temperature difference, a decrease in Biot's modulus reduced the magnitude of the quench-induced residual stress and prevented thermal shock damage. The trend in retained fracture strength data agrees with the theoretical analysis (see Figure 9 and reference 61). Thermal quench from above the annealing temperature, without accompanying thermal shock damage, decreases elastic modulus and increases internal friction (Appendix A).

A statistical study of subcritical crack growth during thermal shock damage (for a temperature range of $\Delta T < \Delta T_c$) was also performed in this study. As ΔT was varied in thermal shock experiments on the glass microscope slides, shifts in the retained fracture strength distributions indicate the relative contributions of subcritical (slow) crack growth (Figures 23 and 24). The initial step in the experimental assessment of subcritical crack growth in thermal shock was to determine the strength distribution of a population of unshocked specimens. In this study, a Kolmogorov-Smirnov goodness-of-fit statistic indicated that the normal,

lognormal, and Weibull distributions fit the fracture strength for unshocked, annealed slides about equally well. For convenience, a normal distribution was used for the thermal shock resistance analysis.

The strength degradation observed during thermal shock fatigue tests qualitatively indicated that slow crack growth (subcritical crack growth) occurs below ΔT_c (below K_c). Non-negligible subcritical crack growth during thermal shock was also demonstrated experimentally via a statistical analysis of the retained fracture strength data for single-quenched glass slides. However, for the single-quenched glass slides, the ΔT_c for subcritical crack growth decreased by about 15° C, which is much less than the 91° C shift in ΔT_c reported by Badaliance [51].

A computer model of thermal shock damage was presented, in which a modified form of Hasselman's theory [7] was used to map the initial flaw size (initial strength) into final crack lengths (retained strength). Subcritical crack growth was approximated by superimposing subcritical growth equations on Hasselman's theory. The input parameters used in the computer simulation are experimental data reported on soda-lime glass.

The computer model qualitatively showed that because the initial strength of a group of glass specimens was characterized by a distribution, the strength degradation curve exhibited a gradual decrease with ΔT. Subcritical crack growth effect enhances thermal shock damage and decrease the critical quench temperature difference.

6. REFERENCES

1) T. K. Gupta, "Strength Degradation and Crack Propagation in Thermally Shocked Al_2O_3", J. Amer. Ceram. Soc., 55 [5] 249-253 (1972).

2) D. P. H. Hasselman, "Strength Behavior of Polycrystalline Alumina Subjected to Thermal Shock", J. Am. Ceram. Soc., 53[9] 490-495(1970).

3) R. D. Smith, H. U. Anderson, and R. E. Moore, "Influence of Induced Porosity on the Thermal Shock Characteristics of Al_2O_3", Am. Ceram. Soc., Bull. 55 [11] 979-982 (1976).

4) R. H. Doremus, "Fracture Statistics: A Comparison of the Normal, Weibull, and Type I Extreme Value Distribution", J. Appl. Phys., 54 [1] 193-198 (1983).

5) K. K. Phani and A. K. De, "A Flaw Distribution Function for Failure Analysis of Brittle Materials", J. Appl. Phys., 62 [11] 4433-4437 (1987).

6) Y. Matsuo, K. Kitakami, and S. Kimura, "Crack Size and Strength Distribution of Structural Ceramics after Non-Destructive Inspection", J. Mater. Sci., 22, 2253-2256 (1987).

7) D. P. H. Hasselman, "Unified Theory of Thermal Shock Fracture Initiation and Crack Propagation in Brittle Ceramics", J. Am. Ceram. Soc., 52 [11] 600-604 (1969).

8) F. V. Tooley, pp. 391-409, Handbook of Glass Manufacture, Vol. 1, Ogden Publishing Company, New York, 1961.

9) J. Gebauer and D. P. H. Hasselman, "Elastic-Plastic Phenomena in the Strength Behavior of an Aluminosilicate Ceramic Subjected to Thermal Shock", J. Am. Ceram. Soc., 54 [9] 468-469 (1971).

10) J. Gebauer, D. A. Krohn, and D. P. H. Hasselman, "Thermal-Stress Fracture of a Thermomechanically Strengthened Aluminosilicate Ceramic", J. Am. Ceram. Soc., 55 [4] 198-201 (1972).

11) H. P. Kirchner, pp. 31-79, Strengthening of Ceramics, Marcel Dekker Inc., New York, 1979.

12) J. C. Jaeger, "On Thermal Stresses in Circular Cylinders", Phylosophical Magazine and Journal of Science, 36 [1] 418-428 (1945).

13) W. D. Kingery, "Factor Affecting Thermal Stress Resistance of Ceramic Materials", J. Am. Ceram. Soc., 38 [1] 3-15 (1955).

14) W. B. Crandall and J. Ging, "Thermal Shock Analysis of Spherical Shapes", J. Am. Ceram. Soc., 38 [1] 44-54 (1955).

15) A. F. Emery, G. E. Walker, J. A. Williams, "A Green's Function for the Stress-Intensity Factors of Edge Cracks and Its Application to Thermal Stresses", Transcations of the ASME, J. Basic Engineering, 91 [4] 618-624 (1969).

16) Z. Olesiak and I. N. Senddon, "The Distributions of Thermal Stress in An Infinite Elastic Solid Containing a Penny-Shaped Crack", Arch. for Rational Mechanics and Analysis, 4 [3] 239-254 (1960).

17) M. K. Kassir and G. C. Sih, "Thermal Stresses in a Solid Weakened by an External Circular Crack", Int. J. Solids Structure, 5, 351-367 (1969).

18) S. Manson and R. W. Smith, "Theory of Thermal Shock Resistance of Brittle Materials Based on Weibull's Statistical Theory of Strength", J. Am. Ceram. Soc., 38 [1] 18-27 (1955).

19) J. A. Coppola and R. C. Bradt, "Thermal-Shock Damage in SiC", J. Am. Ceram. Soc., 56 [4] 214-218 (1973).

20) C. C. Seaton and S. K. Dutta, "Effect of Grain Size on Crack Propagation in Thermally Shocked B_4C", J. Am. Ceram. Soc., 57 [5] 228-229 (1974).

21) A. F. Emery, "Thermal Stress in Elastic-Brittle Materials", PP. 95-121, in Thermal Stresses in Severe Environments, Edited by D. H. P. Hasselman, Plenum Press, New York (1980).

22) A. F. Emery and A. S. Kobayashi, "Transient Stress Intensity Factors for Edge and Corner Cracks in Quench-Test Specimens", J. Am. Ceram. Soc., 63[7] 410-415(1980).

23) R. D. Cheverton, P. C. Gehlen, G. T. Hahn, and S. K. Ishander, "Application of Crack Arrest Theory to a Thermal Shock Experiment", in Crack Arrest Methodology and Applications, ASTM STP 711, 392-421 (1980).

24) A. G. Evans and E. A. Charles, "Structural Integrity in Severe Thermal Encironments", J. Am. Ceram. Soc., 60 [1-2] 22-28 (1977).

25) H. F. Nied, "Thermal Shock Fracture in An Edge-Cracked Plate", J. Thermal Stresses, 6, 217-229 (1983).

26) H. F. Nied, "Thermal Shock in An Edge-Cracked Plate Subjected to Uniform Surface Heating", Engineering Fracture Mechanics, 26 [2] 239-246 (1987).

27) V. C. Ting and H. R. Jacobs, "Stress Intensity Factors for Transient Thermal Loading of a Semi-Infinite Medium", J. Thermal Stresses, 2, 1-13 (1979).

28) N. Noda, Y. Matsunaga, amd T. Tsuli, "Thermal Shock Problems of Elastic Bodies with a Crack", J. Thermal Stresses, 12, 369-383 (1989).

29) S. N. Nasser, L. M. Keer, and K. S. Parihar, "Unstable Growth of Thermally Induced Interacting Cracks in Brittle Solids", Int. J. Solids Structural, 14, 409-430 (1978).

30) J. F. Geyer and S. N. Nasser, "Experimental Investigation of Thermally Indiced Interacting Cracks in Brittle Solids", Int. J. Solids Structural, 18 [4] 349-356 (1982).

31) H. A. Bahr and H. J. Weiss, "Heuristic pproach to Thermal Shock Damage due to Single and Multiple Crack Growth", Theoretical and Applied Fracture Mechanics 6, 57-62 (1982).

32) H. A. Bahr, H. J. Weiss, and H. G. Maschke, "Multiple Crack Propagation in a Strip Caused by Thermal Shock", Theoretical and Applied Fracture Mechanics 10, 219-226 (1988).

33) M. V. Swain, "R-Curve Behavior of Magnesia Partially Stabilied Zirconia and its Significance to Thermal Shock", pp. 355-359, in Fracture Mechanics of Ceramics, Vol. 6, edited by R. C. Bradt, Plenum Press, New York, (1983).

34) M. V. Swain, "R-Curve Behavior and Thermal Shock Resistance of Ceramics", J. Amer. Ceram. Soc., 73 [3] 621-628 (1990).

35) G. G. Chell and D. J. F. Ewing, "The role of thermal and Residual stresses in Linear elastic and Post Yield Fracture Mechanics", Int. J. Fracture, 13[4] 467-479(1977).

36) Y. M. Tsai, "Thermal stress in a Transversely Isotropic Medium Containing a Penny-Shaped Crack", J. Appl. Mechanics, 50 [3] 24-28 (1983).

37) B. M. Singh, H. T. Danyluk, and A. P. S. Selvandurai, "Thermal stresses in a Transversely isotropic Elastic Solid Weakened by an External Circular Crack", Int. J. Solids Structures, 23 [3] 403-412 (1987).

38) D. Lewis III, "Thermal shock and Thermal Shock Fatigue Testing of Ceramics with Water Quench Testing", in Fracture Mechanics of Ceramics, Vol. 6, edited by R. C. Bradt et al., Plenum Press, New York, 487-496, 1983.

39) P. F. Becher, D. Lewis, K. R. Carman and A. C. Gonzalez, "Thermal Shock Resistance of Ceramics: Size and Geometry Effects in Quench Tests," Am. Ceram. Soc. Bull., 59 [5] 542-548 (1976).

40) D. Lewis III, "Effect of Surface Treatment on the Strength and Thermal Shock Behavior of a Commerical Glass-Ceramic", J. Am. Ceram. Soc., 58 [6] 599-605 (1979).

41) D. Lewis and R. W. Rice, "Thermal shock Fatigue of Monolithic Ceramics and Ceramic-Ceramic Particulate Composites", Ceram. Eng. Sci. Poc., 2 [7-8] 712-718 (1981).

42) W. P. Rogers, A. F. Emery, R. C. Bradt, and A. S. Kobayashi, "Statistical Study of Thermal Fracture of Ceramic Materials in the Water Quench Test", J. Am. Ceram. Soc., 70 [6] 406-412 (1987).

43) D. Han and J. Mecholsky, "Strength and Toughness Degradation of Tungsten Carbide-Cobalt due to Thermal Shock", J. Am. Ceram. Soc., 70 [6] 406-412 (1987).

44) J. R. Brockenbrough, L. E. Forsythe, and R. L. Rolf, "Reliability of Brittle Materials in Thermal Shock", J. Am. Ceram. Soc., 69 [8] 634-637 (1986).

45) D. J. Walls, M. D. Drory and A. G. Evans, "Evaluation of Reliability of Brittle Components by Thermal Stress Testing", J. Am. Ceram. Soc., 68 [7] 363-367 (1985).

46) R. D. Cheverton and D. G. Ball, "Application of Probabilitic Fracture Mechanics to the Pressurized-Thermal Shock Issue", Fracture Mechanics, ASTM 945, pp. 35-50, American Society for Testing and Materials, (1988).

47) G. C. Wei and J. Walsh, "Hot-Gas-jet Method and Apparatus for Thermal-shock Testing", J. Am. Ceram. Soc., 72 [7] 1286-1289 (1989).

48) Y. W. Mai, "Thermal-Shock Resistance and Fracture-Strength Behavior of Two Tool Carbide", J. Am. Ceram. Soc., 59 [11-12] 491-494 (1976).

49) H. Ohira and R. C. Bradt, "Strength Distributions of a Quench-Strengthened Aluminosilicate Ceramic", J. Am. Ceram Soc., 71 [1] 35-41, (1988).

50) N. A. Travitzky, D. G. Brandon and E. Y. Gutmanas, "Effect of Rapid Cooling on the Microstructure and Mechanical Properties of Commercial 85 wt.% Al_2O_3", Mater. Sci. and Engng., 71, 77-86, (1985).

51) R. Badaliance, D. A Krohn, and D. P. H. Hasselman, "Effect of Slow Crack Growth on the Thermal Stress Resistance of an Na_2O-CaO-SiO_2 Glass", J. Am. Ceram. Soc., 57 [10] 432-436 (1974).

52) M. Ashizuka, T. E. Easler, and R. C. Bradt, "Statistical Study of Thermal Shock Damage of a Borosilicate Glass", J. Am. Ceram. Soc., 66 [8] 542-550 (1983).

53) E. Schreiber, O. L. Anderson, and N. Soga, p. 82, Elastic Constants and Their Measurements, McGraw-Hill, New York (1974).

54) J. B. Wachtman, "Effect of Suspension Position on Apparent Values of Internal Friction Determined by Forster's Method", The Review of Scientific Instruments, 29, 517-520, (1958).

55) H. M. Chou and E. D. Case, "Time-Dependent Recovery of the Elastic Modulus in Thermally Shocked Polycrystalline Yttrium Iron Garnet (YIG)" Mater. Sci. and Eng., 100, 7-14, (1988).

56) B. R. Lawn and D. B. Marshall, "Contact Fracture Resistance of Physically and Chemically Tempered Glass Plates: A Theoretical Model", Phys. Chem. Glasses, 18 [1] 7-18, (1977).

57) D. B. Marshall and B. R. Lawn, "An Indentation Technique for Measuring Stresses in Tempered Glass Surfaces", J. Am. Ceram. Soc., 60 [1-2] 86-87, (1977).

58) D. B. Marshall and B. R. Lawn, "Strength Degradation of Thermally Tempered Glass Plates", J. Am. Ceram. Soc., 61 [1-2] 21-26, (1978).

59) G. R. Anstis, P. Chantikul, B. R. Lawn, and D. B. Marshall, "A Critical Evaluation of Indentation Technique for Measuring Fracture Toughness: I, Direct Crack Measurements", J. Am. Ceram. Soc., 64 [9] 533-538, (1981).

60) Frank kreith, pp. 174, Principles of Heat Transfer, International Textbook Company, Scranton, Pennsylvania, 1965.

61) W. D. Kingery, H. K. Bowen, and D. R. Uhlmann, p. 816-822, Introduction to Ceramics, John Wiley and Sons Inc., New York, (1976).

62) B. A Boley and J. H. Weiner, p. 277, Theory of Thermal Stresses, John wiley and Sons Inc., New York, (1960).

63) R. C. Buchanan, p. 8, Ceramic Materials for Electronics, Marcel Dekker Inc., New York (1986).

64) E. H. Lee, T. G. Rogers, and T. C. Woo, "Residual Stresses in a Glass Plate Cooled Symmetrically from Both Surfaces", J. Am. Ceram. Soc., 48 [9] 480-487, (1965).

65) L. W. Morland and E. H. Lee, "Stress Analysis for Linear Viscoelastic Materials with Temperature Variation", Transaction of the Society of Rheology, 4, 233-263, (1960).

66) R. Muki and E. Sternberg, "On Transient Thermal Stresses in Viscoelastic Materials with Temperature-Dependent Properties", J. Appl. Mech., 28 [6] 193-207, (1961).

67) E. H. Lee and T. G. Rogers, "Solution of Viscoelastic Stress Analysis Problems Using Measured Creep or Relaxation Functions", J. Appl. Mech., 30 [3] 127-133, (1963).

68) O. C. Zienkiewicz, M. Watson, and I. P. King, "A Numerical Method of Visco-Elastic Stress Analysis", Int. J. Mech. Sci., 10, 807-827, (1968).

69) R. L. Frutiger and T. C. Woo, "A Thermoviscoelastic Analysis for Circular Plates of Thermorheologically Simple Material", J. Thermal Stresses, 2, 45-60, (1979).

70) O. S. Narayanaswamy, "Stress and Structure Relaxation in Tempering Glass", J. Am. Ceram. Soc., 61 [3-4] 146-152, (1978).

71) O. S. Narayanaswamy and R. Gardon, "Calculation of Residual Stresses in Glass", J. Am. Ceram. Soc., 52 [10] 554-558, (1969).

72) R. M. Christensen, pp. 5, Theory of Viscoelasticity, Second Edition, Academic Press, New York, (1982).

73) J. H. Batteh, "Effect of Surface Relaxation on Stress Failure in Laser-Irradiated Glass", J. Appl. Phys. 54 (7) 3769-3776, (1983).

74) D. P. H. Hasselman, R. Badaliance, and E. P. Chen, "Thermal Fatigue and Its Failure Prediction for Brittle Ceramics", in Thermal Fatigue of Materials and Components, ASTM STP 612, pp. 55-68, (1976).

75) H. Kamizono, "An Estimation of the Thermal Shock Resistance of Simulated Nuclear Waste Glass under Water Quenching Conditions", J. Mater. Sci. Letters, 3, 588-590, (1984).

76) R. W. Hamming, p. 175, Numerical Methods for Scientists and Engineers, McGraw-Hill Book Company, Inc., New York (1962).

77) E. D. Case, "The Effect of Microcracking upon the Poisson's Ratio for Brittle Materials", J. Mater. Sci., 19, 3702-3712, (1984).

78) K. Matsushita, S. Kuratani, T. Okamoto, and M. Shimada, "Young's Modulus and Internal Friction in Alumina Subjected to Thermal Shock", J. Mater. Sci. Letter, 3, 345-348, (1984).

79) F. P. Mallinder, and B. A. Proctor, "Elastic Constants of Fused Silica as a Function of Larger tensile Strain", Physics and Chemistry of Glasses, 5 [4] 91-103, (1964).

80) J. D. L. Vega and D. C. Bogue, "Mechanical Properties and Residual Stresses in Non-Equilibrium Glasses", Chem. Eng. Comm., 53, 23-31, (1987).

81) N. M. Pavlushkin, S. I. Silvestrovich, V. M. Firsov, and V. D. Kazakov, "Structural State of the Strengthened Surface of Severely Tempered Glass", J. Mater. Sci., 4, 479-484, (1969).

82) J. V. Fitzgerald, "Anelasticity of Glass: Effect of Heat-Treatment on the Internal Friction of Tank Plate Glass", J. Am. Ceram. Soc., 34 [12] 388-391, (1951).

83) D. E. Day and G. E. Rindone, "Internal Friction of Progressively Crystallized Glasses", J. Am. Ceram. Soc., 44 [4] 161-166, (1961).

84) R. E. Reed-Hill, p. 704, Physical Metallurgy Principles, Second Edition, Van Nostrand-Reinhold, New York, (1973).

85) H. S. Carslaw and J. C. Jaeger, p. 24, Conduction of Heat in Solids, Second Edition, Clarendon Press, Oxford, New York, (1959).

86) A. Paul, p. 76, Chemistry of Glasses, Chapman and Hall, Ltd, New York, (1982).

87) W. Weibull, "A Statistical Distribution Function of Wide Applicability", J. Appl. Mech., 18, 293-97 (1951).

88) T. Shimokawa and Y. Hamaguchi, "Distributions of Fatigue Life and Fatigue Strength in Notched Specimens of a Carbon Eight-Hardness-Strain Laminate", J. Composite Mater., 17 [1] 64-76 (1983).

89) W. Hwang and K. S. Han, "Statistical Study of Strength and Fatigue Life of Composite Materials", Composites, 18 [1] 47-53 (1987).

90) R. J. Larsen and M. L. Marx, PP. 104, An Introduction to Mathematical Statistics and Its Application, Prentice-Hall, Englewood Cliffs, New Jersey, (1986).

91) J. Aitchison and J. A. C. Brown, PP. 65, The Lognormal Distribution, The Syndics of the Cambridge University Press, London, (1957).

92) A. C. Cohen, "Maximum Likelihood Estimation in the Weibull Distribution Based on Complete and On Censored Samples", Technometrics, 7 [4] 579-588 (1965).

93) H. R. Neave and P. L. Workthington, PP. 89-99, Distribution-Free Tests, Unwin Hyman Inc., Winchester, Mass USA, (1988).

94) M. A. Stephens, "Tests Based on EDF Statistics", PP. 97-193, in Goodness-of-Fit Techniques, edited by R. B. D'Agostino and M. A. Stephens, Marcel Dekker, New York, (1986).

95) S. M. Wiederhorn and L. H. Bolz, "Stress Corrosion and Static Fatigue of Glass", J. Am. Ceram. Soc., 53 [10] 543-548 (1970).

96) S. Sahaguchi, Y. Sawaki, Y. Abe, and T. Kawasaki., "Delayed Failure in Silica Glass", J. Mater. Sci., 17, 2878-2886 (1982).

97) J. E. Ritter, M. Vicedomine, K. Breder, and K. Jakus, "Dynamic Fatigue of Indented Soda-Lime Glass as a Function of Temperature" J. Mater. Sci., 20, 2868-2872 (1985).

98) G. K. Bansal and W. H. Duckworth, "Fracture Surface Energy Measurements by the Notch-Beam Technique", in Fracture Mechanics Applied to Brittle Materials, ASTM STP 678, pp. 38-46 (1979).

99) J. E. Ritter, M. Vicedomine, K. Breder, and K. Jakus, "Dynamic Fatigue of Indentation, Soda-Lime Glass as a Function of Temperature", J. Mater. Sci., 20, 2868-2872 (1985).

APPENDICES

APPENDIX A

INFLUENCE OF RESIDUAL STRESSES ON THE MEASUREMENT OF THE DYNAMIC ELASTIC MODULUS

Experimental results indicate that thermal quenching of a glass plate from above the annealing temperature can induce residual stresses in the plate and decrease the plate's dynamic resonant frequency (observed as the dynamic elastic modulus, Figure 18). A qualitative analysis, based on dynamic vibration theory and quench-induced nonlinear elasticity can explain the direct relationship between residual stress development and the resonant frequency decrease.

First, the residual stress profile in tempered glass is determined numerically. Figure A-1 illustrates the stress distribution calculated from thermoviscoelastic stress theory. The residual stress distribution is a complex function of initial glass temperature, thermal quench conditions, etc. However, the spatial distribution is symmetric and nearly parabolic. Therefore, we approximate the stress profile in terms of a polynomial

$$\sigma_*(Z) = A_{2n}\, z^{2n} + A_{2n-2}\, z^{2n-2} + A_{2n-4}\, z^{2n-4} + \ldots + A_o \qquad \text{(A-1a)}$$

The residual stress σ_* is subject to the boundary conditions

$$\sigma_*(h/2) - \sigma_*(-h/2) < 0. \qquad \text{(A-1b)}$$

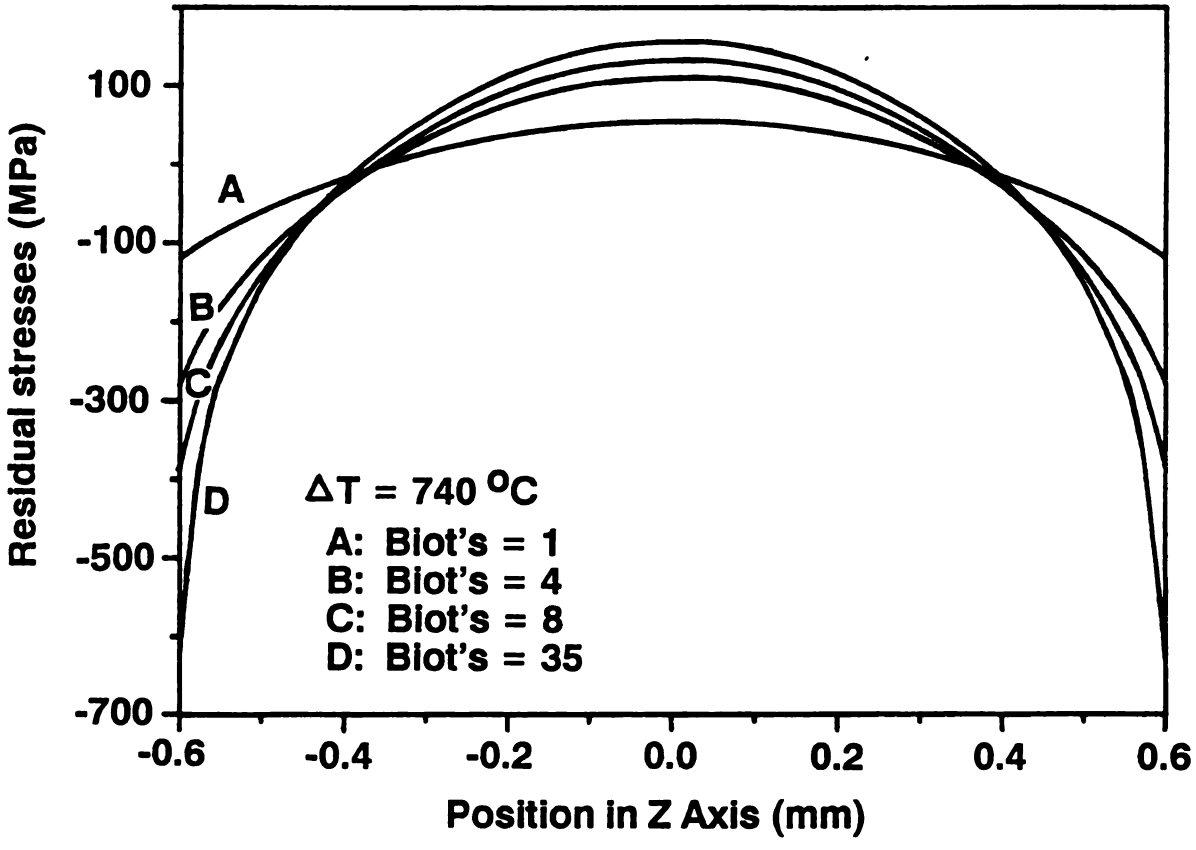

Figure A1. Residual stress profile in a glass plate, as evaluated numerically from thermoviscoelastic theory.

The equilibrium of forces and moments requires that

$$\int_{-h/2}^{h/2} \sigma_*(z)\, dz = 0 \qquad \text{(A-1c)}$$

$$\int_{-h/2}^{h/2} \sigma_*(z)\, z\, dz = 0 \qquad \text{(A-1d)}$$

where σ_* and h represent the quench-induced residual stresses and the thickness of the glass specimen, respectively. In general, a fourth-order polynomial is sufficient to accurately model the residual stress distribution in the glass plates. For example, the calculated residual stress associated with a quench of $\Delta T = 740\ ^{o}C$ and Biot's modulus = 15 can be fitted well by $\sigma_*(Z) = -1864Z^4 - 707Z^2 + 134$ (correlation coefficient = 0.997).

Similarly, if we assume a nonlinear elasticity similar to that observed by Mallinder et al, the thermal strain distribution, $\epsilon_*(z)$, can be approximated by the general form

$$\epsilon_*(z) = B_4\, z^4 + B_2\, z^2 + B_o \qquad \text{(A-2)}$$

The dynamic elastic modulus of materials may be measured by the standing wave resonance technique [14-16]. Therefore, we shall model the effect of the residual stress on the dynamic elastic modulus in terms of a free-free suspended vibrating bar. A free-free suspended vibrating bar (Figure A-2) is the test specimen used in the standing resonance technique [14-16].

According to the dynamics of beams, the governing equation (the Bernoulli-Euler beam equation) is [A1]

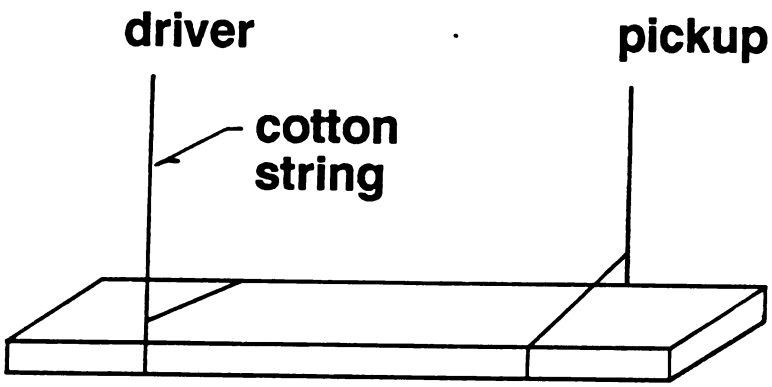

Figure A2. Schematic of specimen suspension for the standing wave resonance technique of elastic modulus measurement.

$$EI \frac{\partial^4 W(x,t)}{\partial x^4} + \frac{a\rho}{g} \frac{\partial^2 W(x,t)}{\partial t^2} = 0 \qquad \text{(A-3a)}$$

The boundary conditions are

$$\frac{\partial^2 W(0,t)}{\partial x^2} = 0 \qquad \frac{\partial^2 W(L,t)}{\partial x^2} = 0 \qquad \text{(A-3b)}$$

$$\frac{\partial^3 W(0,t)}{\partial x^3} = 0 \qquad \frac{\partial^3 W(L,t)}{\partial x^3} = 0 \qquad \text{(A-3c)}$$

where E, ρ, a, L, and I represent the elastic modulus, density, cross sectional area, specimen length, and the second moment of inertia of the cross section of the beam with respect to the neutral axis. (In this derivation, we neglect the effects of shear deformation and rotary inertia, since their effects are not significant for the bar-shaped specimens considered here [A1]). The parameter g is the acceleration due to gravity. W is the transverse deflection of the beam, which is a function of time, t, and position along the longitudinal axis, X. Solving equation A-3 by separation of variables and applying the boundary conditions gives the characteristic equation [A1]

$$W_n(x,t) = w_n(x)\,(C_1\cos(\beta_n t) + C_2\sin(\beta_n t)) \qquad \text{(A-4a)}$$

$$= w_n(x)\,(C_3\cos(\beta_n t + \theta))$$

where C_1, C_2, w_n and β_n are defined as

$$\tan(\theta) = C_2/C_1 \tag{A-4b}$$

$$w_n(x) = \left[\cos(k_n x) + \cosh(k_n x) - \frac{\cos(k_n L) - \cosh(k_n L)}{\sin(k_n L) - \sinh(k_n L)} (\sin(k_n x) + \sinh(k_n x)) \right] \tag{A-4c}$$

$$\beta_n = k_n^2 \left[EI \frac{g}{a \rho} \right]^{1/2} \tag{A-4d}$$

and, in addition

$$\cos(k_n L) \cosh(k_n L) = 1 \tag{A-4e}$$

C_1, C_2, and C_3 are integer constants. Each W_n corresponds to the nth mode of the harmonic transverse vibration with the frequency $f_n = \beta_n/2\pi$. For n = 1, the fundamental vibrational mode, the first root of equation A-4e is $k_1 L = 4.73004$ [A1]. Consequently, the fundamental natural frequency of the glass specimen is given by

$$f = \frac{k_1^2}{2\pi} \left[\frac{E I}{a \rho} \right]^{1/2} \tag{A-5a}$$

Furthermore,

$$E = \frac{0.09652 f^2 L^4 \rho}{h^2} \tag{A-5b}$$

Equation (A-5b) is useful for elastic modulus calculations of bar-shaped specimens, where E is expressed in terms of kgf/m^2 (1 kgf/m^2 = 9.806 Pa).

Experimentally, quenched glass specimens had lower resonance frequencies than the annealed glass specimens. Apparently, residual stresses in the tempered glass lead to the resonant frequency

decrease, and from equation (A-5b), a decrease in resonant frequency implies a decrease in elastic modulus, E. Equation (A-5) (based on linear elasticity) can not explain the experimentally observed decrease in Young's modulus. On the other hand, the energy method applied to the dynamics of beams (Rayleigh's approximation method [A2]) can qualitatively account for the material nonlinearity.

Mallinder et al. [8] indicated that soda glass exhibits nonlinear elasticity under large deformations, such that $E = E_o (1 - 5.11 \epsilon)$, where ϵ is the strain and $E_o = 72.5$ GPa. Meanwhile, Gogotsi et al. [A3] and Swain [A4] also reported nonlinear stress-strain behavior in ceramic materials. Thus, if we assume that the residual stresses in tempered glass can also induce nonlinear effects, namely,

$$E_* = E_o (1 - C \epsilon)$$
$$= E_o ((1 - C (\epsilon_* + \bar{\epsilon})) \qquad \text{(A-6)}$$

where ϵ_* is the thermal residual strain, $\bar{\epsilon}$ is the longitudinal strain due to beam vibration and C is a proportionality constant. E_o corresponds to the slope of the stress-strain curve near the origin (Figure A-3). E_* is the elastic modulus as a function of the residual stresses.

In this study, since the flexural deformation of a free-free suspended vibrating bar, $\bar{\epsilon}$, is small, the geometrical nonlinearity is neglected. The vibration induced deformations of the annealed glass and the tempered glass specimens are assumed to satisfy beam dynamics and classic beam theory. As a result, the observed elastic modulus of an annealed glass bar is $E \approx E_o$. However, residual stresses may lead to nonlinear stress-strain behavior (Figure A-3)

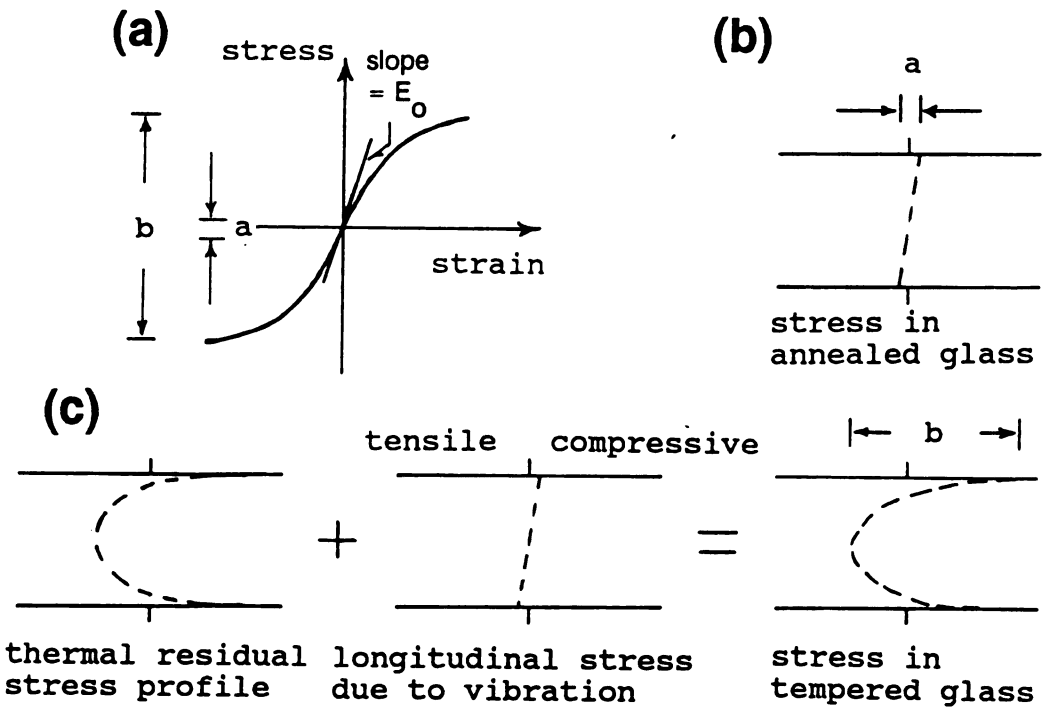

Figure A3. Influence of the thermal residual stresses on the stress-strain range of a standing wave. (a) Nonlinear stress-strain behavior of material. (b) Longitudinal stress due to vibration, where a represents the maximum stress-strain range. (c) Superposition of thermal residual stresses and longitudinal stress, where b is the maximum stress-strain range.

so that the natural frequency calculation should include nonlinear elasticity effect.

Mechanical energy conservation requires the maximum kinetic energy to equal the maximum potential energy [A2]. Thus,

$$T_{max} = U_{max} \tag{A-7a}$$

here,

$$T = \int_0^L \frac{\rho\, a}{2\, g} (\dot{W}_n)^2 \, dx \tag{A-7b}$$

$$U = \int_0^L \frac{E\, I}{2} (W_n'')^2 \, dx. \tag{A-7c}$$

T and U represent the kinetic energy and the potential energy of the annealed glass specimen. $\dot{W}$ and W'' are derivatives with respect to time and x, respectively. From equation (A-7), we obtain

$$T = \int_0^L \frac{\rho\, a}{2\, g} C_3^2\, \beta_n^2 \sin^2(\beta_n t + \theta)\, w_n^2 \, dx \tag{A-8a}$$

$$U = \int_0^L \frac{E\, I}{2} C_3^2 \cos^2(\beta_n t + \theta)\, (w'')^2 dx \tag{A-8b}$$

Equating the maximum values of T and U yields an estimate of f^2, the square of the fundamental natural frequency (n = 1) of annealed glass, such that

$$f^2 = \frac{\beta^2}{4\pi^2} = \frac{g \int_0^L E\, I\, (w'')^2 \, dx}{4\pi^2 \int_0^L \rho\, a\, w^2 \, dx} \tag{A-9}$$

Residual stresses change the effective vibrational potential energy in a quenched (tempered) glass bar. However, the functional form of the equation for kinetic energy does not change, and thus equation (A-7a) is rewritten as

$$T_{max} = (U_{*max} - U_{*resid}). \tag{A-10}$$

U_{*max} is the maximum potential energy in a tempered glass bar undergoing vibration. U_{*max} is the total potential energy arising from the internal thermal residual stresses and the longitudinal stress induced by beam vibration (Figure A-3). U_{*resid} is the thermal residual strain energy of a tempered glass bar in the static or quiescent state. That is, U_{*resid} is the potential energy of the bar when there are no vibrations due to the standing wave resonance measurement technique. Thus, we have

$$U_{*max} - U_{*resid} =$$

$$= b \int_0^L \int_{-h/2}^{h/2} \int [(\sigma_* + \bar{\epsilon} E_*) - \sigma_*] \, d\epsilon \, dz \, dx$$

$$= b \int_0^L \int_{-h/2}^{h/2} \int E_o (1 - C(\epsilon_* + \bar{\epsilon})) \bar{\epsilon} \, d\epsilon \, dz \, dx \tag{A-11}$$

where b is the width of the bar. Combining equations (A-2) and (A-11) yields

$$U_{*max} - U_{*resid}$$

$$= \int_0^L \frac{E_o I}{2} (W_n'')^2 \left[1 - C \left(\frac{3}{112} B_4 h^4 + \frac{3}{20} B_2 h^2 + B_o\right)\right] dx \tag{A-12}$$

Note that if γ is the curvature of the beam with respect to the neutral axis, then $\epsilon = z/\gamma$, $1/\gamma = W''$, and $\int \sigma_* z \, dz = 0$. Substituting equation (A-12) with equation (A-10) and then comparing with equation (A-9) and (A-5b), we get

$$\frac{E_m}{E} = \frac{f_*^2}{f^2} = 1 - C \left(\frac{3}{112} B_4 h^4 + \frac{3}{20} B_2 h^2 + B_o\right) \qquad \text{(A-13)}$$

where E_m is the observed elastic modulus. f_* and f are the fundamental natural frequencies of the tempered glass and of the annealed glass, respectively. Equation (A-13) indicates that, if a tempered glass specimen exhibits nonlinear elastic behavior, the observed elastic modulus may be a function of the residual stress state.

References for Appendix A

A1) E. Volterra and E. C. Zachmanoglou, p. 321, Dynamics of Vibrations, Charles E. Merrill Books Inc., Columbus, Ohio, (1965).

A2) I. H. Shames and C. L. Dym, p. 334, Energy and Finite Element Methods in Structural Mechanics, Hemisphere Publishing Co., New York, (1985).

A3) G. A. Gogotsi, Y. L. Groushevsky, and K. K. Strelov, "The Significance of Non-elastic Deformation in the Fracture of Heterogeneous Ceramic Materials", Ceramurgia International, 4 [2] 113-118, (1978).

A4) M. V. Swain, "R-Curve Behavior and Thermal Shock Resistance of Ceramics", J. Am. Ceram. Soc., 73 [3] 621-28, (1990).

APPENDIX B

PHOTOELASTIC DETECTION OF CRACKS AND THE SUBSEQUENT RESTRICTIONS ON QUENCH CONDITIONS FOR CRACK-FREE SPECIMENS

Photoelasticity is an useful method for detecting the quench-induced cracks in a tempered glass plate. The cracks, which may be, say, 2 mm in length, are sometimes invisible to the unaided eye for specimens quenched from above the annealing temperature, although cracks of a similar length are typically detected much more easily in specimens quenched from below the annealing temperature. The difficulty in detecting cracks in glass slides quenched from above the annealing temperature likely stems from a decrease in crack opening displacement as a function of the surface compressive stresses that arise when glass plates are quenched from above their annealing temperature (Figures 18(a) and 18(b)).

However, cracks locally disturb the residual stress field of the tempered glass specimens so that photoelastic stress measurements yield fringe patterns that are characteristic of the stress release and redistribution [B1,B2]. In the study of the effect of residual stresses on the observed elastic modulus changes, tempered glass specimens were examined photoelastically in order to eliminate the specimens with cracks. By not measuring the elastic modulus for specimens having detectable quench-induced cracks, we attempted to eliminate the crack-modulus effects and focus on the effect of residual stress upon the elastic modulus (see Appendix A also).

For quenching into room temperature oil (SAE 20W 50), about 1/5 of the specimens quenched at $\Delta T = 680\ ^{o}C$ were eliminated from the elasticity measurement due to cracking, and about 4/5 of the specimens quenched at $\Delta T = 660\ ^{o}C$ were eliminated because of cracking. Oil quenching for the ΔT interval $550\ ^{o}C < \Delta T < 640\ ^{o}C$ did not provide a non-cracked specimen. For air quench (cooling freely in air), all quenched specimens successfully developed residual stresses without cracking, although due to the lower surface heat transfer coefficient, h, the air quench produced a much lower residual stress than did the oil quench. However, neither quenching route provided specimens with residual stresses, S_r, in the range of $40\ MPa < S_r < 100\ MPa$. Thus, the data in Figure 18 form two clusters, the cluster of $S_r < 40$ MPa corresponds to the air Quenched specimens and the cluster where $S_r > 100$ MPa corresponds to the oil quenched specimens.

References for Appendix B

B1) C. W. Smith, "Photoelasticity in Fracture Mechanics", Experimental Mechanics, 20 [11] 390-396, (1980).

B2) A. Shukla and J. W. Dally, "A Photoelastic Study of Energy Loss During a Fracture Event", Experimental Mechanics, 21 [4] 163-168, (1981).

APPENDIX C

DETERMINATION OF DISTRIBUTION A IN A STATISTICAL ANALYSIS OF RETAINED FRACTURE STRENGTH

For certain ranges of quench temperature difference ΔT, the schematics in Figures 23(c) and 23(d) depict the retained strength distribution as separating into two clusters. In Figures 23(c) and 23(d), the two clusters (also labeled as distribution A and distribution B) are clearly distinguisable. However, in practice the distributions may not exhibit such a clear separation (Figure 24(b)). This appendix proposes a systematic way of approaching this problem.

In order to proceed with the analysis, We assumed that: (1) The shocked specimens without pop-in crack growth (distribution A) exhibits a normal strength distribution similar to that of the annealed specimens, and (2) Subcritical crack growth only shifts distribution A, without changing its shape. Consequently, we describe distribution A by a normal distribution with the same standard deviation as the annealed specimens.

In this paper, we determined distribution A as follows:

(1) The retained strength data for n specimens were ranked in ascending order such that $y_1 < y_2 < y_3 \ldots\ldots < y_{n-1} < y_n$.

(2) Distribution A is a subset of the retained strength data. The subset consists of the ordered strength data for (n - j + 1) specimens, which is y_j, y_{j+1}, y_{j+2}, ..., y_{n-1}, y_n. The jth strength values is selected such that the standard deviation of the subset, $\hat{\sigma}_A$, is approximately equal to, σ, the standard deviation of the strength distribution for the annealed glass slides. In this study, σ for the annealed slide glass

population was 10.2 MPa.

(3) After determining the strength values to include in distribution A, the mean strength, $\hat{\mu}_A$, is then calculated.

In Figure 5, the solid curves represent the normal distributions with mean μ_A and standard deviation σ_A for the (n - j + 1) specimens that underwent subcritical crack growth. The dashed curves in Figure 5 illustrates the normal distribution for the (n - j + 1) specimens, but with the mean and standard deviation of the unshocked annealed glass slides (μ = 101.38 MPa and σ = 10.2 MPa). The dashed curve thus presents the distribution "as it would have been" without the shift in the strength distribution produced by subcritical crack growth in the glass slides.

APPENDIX D

THE INFLUENCE OF CRACK NUMBER DENSITY ON STRENGTH DEGRADATION OF SHOCKED COMPONENTS

The knowledge of the crack number density, N, in shocked components is required for the determination of ΔT_c (see equation (29)). Since N is difficult to evaluate experimentally, N becomes an arbitrary variable in the computer simulation. Figure. D1 illustrates the effect of N on the strength degradation curve. The essential characteristics of strength degradation curve do not vary as N changes. In this study, $N = 2 * 10^{11}$ $1/m^3$ was adopted.

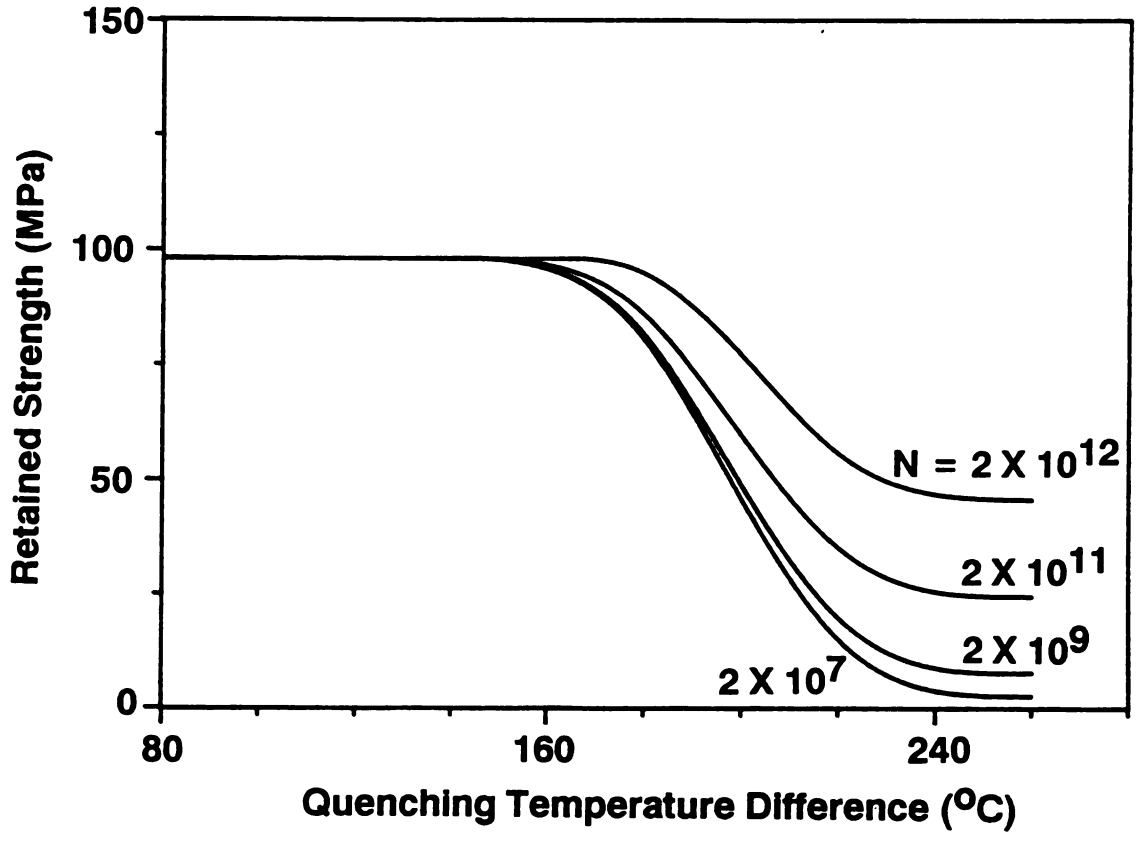

Figure D1. The effect of crack number density, N, on subcritical crack growth.

APPENDIX E

ELASTIC MODULUS DETERMINATION OF COATING LAYERS AS APPLIED TO LAYERED CERAMIC COMPOSITES

This Appendix develops relationships for determining the in-plane elastic modulus of a coating by two experimental techniques: (1) dynamic resonance and (2) static bend. Dynamic resonance measurements on model two-layer and three-layer composite beams (consisting of bonded strips of alumina and glass) agree well with the relationships developed. In addition, the dynamic resonance and static bend techniques are applied to a SiC coating/graphite substrate composite, where the two methods give statistically similar results for the elastic modulus of the SiC coatings.

1. INTRODUCTION:

Coatings as a protective layer may improve the surface properties of the substrate, such as the wear resistance and the high temperature corrosion resistance [E1,E2]. The stress-strain behavior [E2,E3], contact stress field [D4], integrated surface hardness [E5], coating delamination [E6,E7], cracking [E8], spalling, bending, and residual stress state of coated systems [E9-E12] are all functions of the elastic modulus of the coating. As a result, the in-plane elastic modulus of coatings is a basic parameter for characterizing coating performance.

Watkins et al. measured the elastic modulus of coatings using the four point bend test [E13]. King indicated that the modulus

could be estimated from the indentation test [E14], while other researchers determined the modulus by measuring the coating-induced curvature of the substrate [E15-E17].

Dynamic resonance is a simple technique to measure the elastic modulus of homogenous materials [E18,E19]. Dynamic resonance can also be useful in the measurement of the elastic moduli of coating/substrate composites if the formulae associated with the elastic modulus calculation are modified. This paper extends the resonance method to evaluate the in-plane elastic modulus of coatings, using the Bernoulli-Euler beam equation [E20,E21]. In addition, a static surface strain-bending moment method is also presented for determining the elastic moduli of coatings.

2. THEORETICAL BACKGROUND

2.1 Static bend test

The neutral axis of a homogenous rectangular beam coincides with the centroid of cross section when the beam is subjected to symmetrical bending [E22]. If one of the beam's surfaces is coated with a material of different elastic modulus, the beam is no longer homogenous and the neutral axis shifts from the centroid of cross section of the composite beam [E22]. (If the coating had the same modulus as the substrate, the neutral axis would still coincide with the centroid of the composite beam.) Thus, the in-plane elastic modulus of the coating can be evaluated from the shift of the neutral axis.

Figure E1(a) illustrates the cross section of the composite beam. The thickness of the coating and the substrate are ℓ_c and ℓ_s

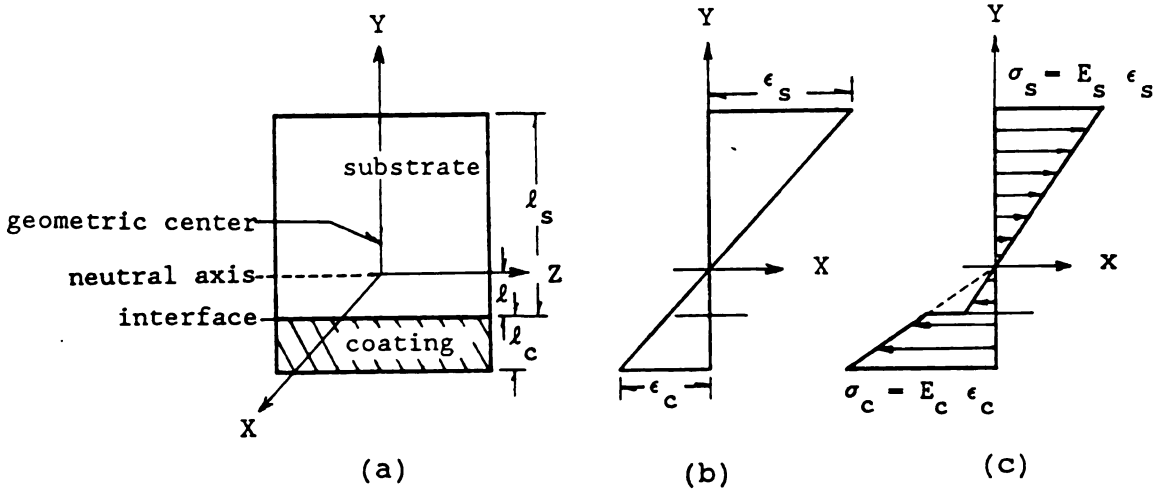

Figure E1. Stress-strain relationship in a composite beam subjected to a pure bending moment. (a) Cross section of composite beam; (b) strain development in axial direction; (c) stress in axial direction.

respectively. The distance from the neutral axis to the coating-substrate interface is ℓ. For convenience, assume that the coating has a larger modulus than the substrate. The neutral axis then deviates from the centroid and approaches the interface. In this study, perfect interfacial bonding is assumed for stress translation between coatings and substrate. When the beam is subjected to a pure bending moment, normal strain in the longitudinal direction develops (Figure E1(b)) [E22], where the strain curve passes through the neutral axis. Based on the trigonemetric relations (Figure E1(b)), surface strains ϵ_c and ϵ_s in the coating and substrate satisfy the following equation

$$-\frac{\epsilon_s}{\epsilon_c} = \frac{\ell_s - \ell}{\ell_c + \ell} \qquad \text{(E-1a)}$$

or

$$\ell = \ell_s - \left(\frac{K}{1+K}\right)(\ell_s + \ell_c) \qquad \text{(E-1b)}$$

where

$$K = -\frac{\epsilon_s}{\epsilon_c}$$

K is the relative strain, which is always positive. Figure E1(c) shows the normal stress in the longitudinal direction (the X axis in Figure E1(c)). In the bent composite beam, the dependence of the normal stresses σ_c and σ_s (where "c" and "s" denote coating and substrate, respectively) upon the transverse coordinate Y is described by [E22]

$$\sigma_c = \frac{E_c Y}{r}$$

$$\sigma_s = \frac{E_s Y}{r} \qquad \text{(E-2)}$$

where r is the radius of curvature of the neutral axis, and E_c and E_s are the elastic moduli of coatings and substrate. From equilibrium of the axial forces [E22], the following equation has to be satisfied

$$\int_{-\ell}^{\ell_s - \ell} \sigma_s \, dA + \int_{-\ell - \ell_c}^{-\ell} \sigma_c \, dA = 0 \qquad \text{(E-3)}$$

where A is the cross sectional area. Substituting equation (E-2) into (E-3) yields

$$\ell = \frac{E_s \ell_s^2 - E_c \ell_c^2}{2 E_s \ell_s + 2 E_c \ell_c} \qquad \text{(E-4)}$$

Combining equations (E-1b) and (E-4), we have

$$E_c = E_s R \frac{KR + 2K - R}{2R - K + 1} \qquad \text{(E-5)}$$

here

$$R = \frac{\ell_s}{\ell_c}$$

R is the relative thickness. The in-plane elastic modulus of the coating, E_c, can be calculated from equation (E-5). In practice, E_s

can be determined in a separate experiment on the substrate material itself, before the coating is applied.

Since equation (E-5) was derived assuming a pure bending moment, a test method involving pure bend is needed. A pure bending moment can arise from a four point bending fixture. Consequently, E_c can be evaluated from the surface strains, ϵ_c and ϵ_s, which can be detected using a strain gage attached to a specimen loaded in four-point bend. Figure E2 shows the relationship between relative strain, relative modulus and elastic modulus. For a given coating/substrate material system (E_c/E_s = constant), the relative strain approaches one with the increase of the relative thickness. If the experimental error due to the strain measurement is constant, the uncertainty of the measured modulus data increases with the increasing R. Consequently, a small R is recommended in measuring the elastic modulus of coatings.

2.2 Dynamic resonance

In dynamic beam vibration theory, the Bernoulli-Euler beam equation can approximately describe beam vibrations [E20,E21,E23]. In the present study, the coatings' elastic modulus is calculated using the Bernoulli-Euler beam equation [E20,E21].

$$EI \frac{\partial^4 W(x,t)}{\partial x^4} + \frac{a\rho}{g} \frac{\partial^2 W(x,t)}{\partial t^2} = 0 \qquad \text{(E-6)}$$

Equation (E-6) corresponds to the free, undamped vibration of a monolithic beam with constant cross sectional area, a. E, ρ, and I represent the elastic modulus, density, and the second moment

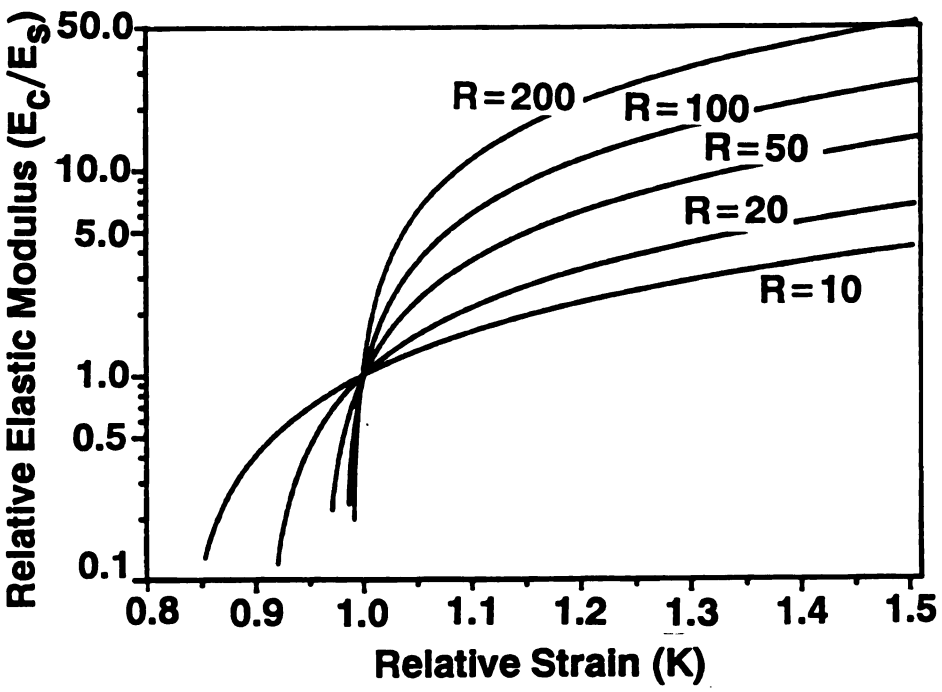

Figure E2. Relationship between relative strain, K, relative thickness, R, and relative elastic modulus, E_c/E_s, for the in-plane modulus measurement of coatings.

inertial of the cross section of the beam with respect to the neutral axis. The parameter g is the acceleration due to gravity. W is the transverse deflection of the beam, which is a function of time, t, and position along longitudinal axis, X. For a comoposite beam, if the interface bonding of coating-substrate is perfect, equation (E-6) becomes

$$(E_c I_c + E_s I_s) \frac{\partial^4 W(x,t)}{\partial x^4} + \left(\frac{a_c \rho_c + a_s \rho_s}{g} \right) \frac{\partial^2 W(x,t)}{\partial t^2} = 0 \qquad \text{(E-7)}$$

where the subscripts c and s refer to the material parameters associated with the coatings and substrate respectively. In practice, the $(a_c\rho_c+a_s\rho_s)/g$ term can be expressed as AD/g, according to

$$\frac{a_c \rho_c + a_s \rho_s}{g} = (a_c + a_s) \frac{a_c \rho_c + a_s \rho_s}{(a_c + a_s)\, g}$$

$$= A \frac{D}{g} \qquad \text{(E-8)}$$

where A and D are the cross sectional area and average bulk density of the composite beam.

Dynamic resonance modulus measurements were performed using rectangular composite beams with free ends (Figure E3). Since the bending moment and the shear force are zero at both free ends, the boundary conditions of the transverse vibration are given by

$$\frac{\partial^2 W(0,t)}{\partial x^2} = 0 \qquad \frac{\partial^2 W(L,t)}{\partial x^2} = 0 \qquad \text{(E-9a)}$$

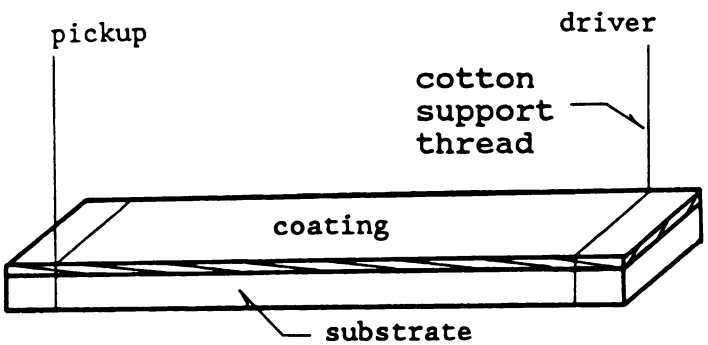

Figure E3. Illustration of the composite beam whose elastic modulus is determined by the dynamic resonance method.

$$\frac{\partial^3 W(0,t)}{\partial x^3} = 0 \qquad \frac{\partial^3 W(L,t)}{\partial x^3} = 0 \tag{E-9b}$$

where L is the length of the composite beam. Solving equation (E-7) by the method of separation of variables and applying the boundary conditions gives the characteristic equation [E20,E21]

$$W_n(x,t) = (C_1\cos(\beta_n t) + C_2\sin(\beta_n t))\left[\cos(k_n x) + \cosh(k_n x) - \frac{\cos(k_n L) - \cosh(k_n L)}{\sin(k_n L) - \sinh(k_n L)}(\sin(k_n x) + \sinh(k_n x))\right] \tag{E-10}$$

where

$$\beta_n = k_n^2 \left[(E_c I_c + E_s I_s)\frac{g}{A\,D}\right]^{1/2} \tag{E-11}$$

$$\cos(k_n L)\cosh(k_n L) = 1 \tag{E-12}$$

C_1 and C_2 are integer constants. Each W_n corresponds to a harmonic transverse vibration with the frequency, $f = \beta_n/2\pi$. The n represents the nth mode of vibration. For n=1, the fundamental vibrational mode, the first root of equation (E-12) is $k_1 L = 4.73004$ [E21,E22]. Consequently, the fundamental vibration frequency of the composite beam is given by

$$f = \frac{k_1^2}{2\pi}\left[(E_c I_c + E_s I_s)\frac{g}{A\,D}\right]^{1/2} = \frac{11.15}{L^2}\left[\frac{E_c I_c + E_s I_s}{A\,D}\right]^{1/2} \tag{E-13}$$

For a composite beam with the cross section shown in Figure E1(a), the second moment of inertia with respect to the neutral axis is

$$I_s = \int_{-\ell}^{\ell_s - \ell} Y^2 \, dA$$

$$I_c = \int_{-\ell-\ell_c}^{-\ell} Y^2 \, dA \qquad \text{(E-14)}$$

Combining equations (E-4), (E-13), and (E-14) gives

$$E_c = \frac{1}{\ell_c^3}\left[0.02413 \, f^2 L^4 D \, (\ell_c + \ell_s) - E_s \ell_s^3 + \frac{3(E_s \ell_s^2 - E_c \ell_c^2)^2}{4 \, (E_s \ell_s + E_c \ell_c)} \right] \qquad \text{(E-15)}$$

Thus, for the elastic modulus of a "single-sided" coating (Figure E1(a)), the in-plane elastic modulus of coatings can be evaluated using equation (E-15) in which the adopted units are Hertz, meter, and kilogram. The elastic moduli, E_c and E_s, are expressed in terms of kgf/m^2 (1 kgf/m^2 = 9.806 Pa). Although Equation (E-15) is in implicit form, it can Be solved using a numerical iteration method.

If a composite beam has coating layers on both the upper and lower substrate surfaces (Figure E4), the neutral axis still coincides with the centroid of cross section. As a result, the second moment of inertia is

$$I_s = \int_{-\ell_s/2}^{\ell_s/2} Y^2 \, dA \qquad \text{(E-16a)}$$

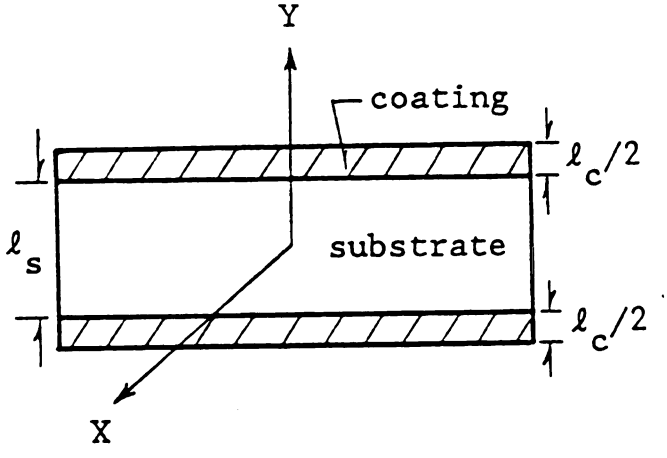

Figure E4. Cross section and dimensions of a composite beam with two coating layers.

$$I_c = \int_{-(\ell_c+\ell_s)/2}^{(\ell_c+\ell_s)/2} Y^2 \, dA - \int_{-\ell_s/2}^{\ell_s/2} Y^2 \, dA \qquad \text{(E-16b)}$$

Combining Equation (E-13) and (E-16), we get an expression for the coatings' in-plane modulus for a substrate with a coating on both the upper and lower faces (Figure E4).

$$E_c = \frac{1}{(\ell_c+\ell_s)^3 - \ell_s^3} \left[0.09652 \, f^2 L^4 D \, (\ell_c+\ell_s) - E_s \ell_s^3 \right] \qquad \text{(E-17)}$$

(It is reemphasized that the unit of elastic modulus is kgf/m^2.) Equation (E-17), in explicit form, may be evaluated directly, in constrast to the implicit form (equation (E-15)). When ℓ_s becomes zero, equations (E-15) and (E-17) become equation (E-18), which corresponds to the modulus E_c of a homogenous beam composed of the coating material

$$E_c = \frac{0.09652 \, f^2 L^4 D}{\ell_c^2} \qquad \text{(E-18)}$$

Equation (E-18) is similar in form to the ASTM standard test method for the elastic modulus of a monolithic beam [E-19], with the exception of the correction factor for effects of shear deformation and rotatory inertia [E19-E21,E23]. However, the importance of the correction factor is minor when the ratio of beam length to thickness exceeds thirty. For instance, the error is only 0.8% if the correction factor is neglected for a beam whose length to thickness ratio is thirty [E19].

3. EXPERIMENTAL PROCEDURE

The static and dynamic modulus measurements included in this study were performed on SiC coating/graphite substrate materials in addition to a number of glass/glass and alumina/glass model composite beam specimens that were prepared in order to more rigorously test the theory.

3.1 Model composite beam preparation

The following three types of model composite beam specimens were prepared for this study: a two-layer glass/glass composite, a two-layer alumina/glass composite, and a three-layer alumina/glass/alumina composite. The glass layers in the composite beams were 7.6 cm X 0.8 cm X 0.127 cm strips cut by a low speed diamond saw from glass microscope slides. After annealing at 600 ^{o}C for 30 minutes in air in an electric furnace, the furnace power was shut off and the cut glass strips were allowed to free-cool to room temperature. The alumina layers in the model composite beams were 7.6 cm cm X 0.8 cm X 0.064 cm strips cut from an as-received alumina substrate (Saxonburg Ceramics Inc., Monroe, NC) with a mass density of 3.707 gm/cm^3 and an average grain size of about 18 μm. After sectioning, the alumina specimens were annealed at 1100 ^{o}C for 10 hours in hour in an electric furnace.

Two layer glass/glass composite beam specimens were prepared by two adhesion methods: (1) by sintering and (2) by adhesion via gluing. Two annealed glass strips, placed so that their 7.6 cm X 0.8 cm faces were superimposed, were sintered at 740 ^{o}C for 30 minutes in air. During heating, the glass strips were set on a flat

aluminosilicate refractory board to minimize possible deformation of the glass strips. Super glue (Ross Adhesives, Conros Corporation, Detroit, MI) was also used to bond additional glass/glass two layer composites.

The thermal expansion mismatch between glass slides and the alumina substrates made sintering difficult so that only glue bonding was feasible for the two and three layer alumina/glass and alumina/glass/alumina composite beams. Glued composite alumina/glass and alumina/glass/alumina composite beams were fabricated from the annealed alumina and glass strips described above.

3.2 SiC coating/graphite substrate composite specimens, monolithic graphite specimen, and free-standing SiC Coatings

Using a low speed diamond saw, billets of SiC coating/graphite composite material were cut into composite beams 8 cm X 0.8 cm X 0.3 cm with coating on a single 8 cm X 0.8 surface. (The SiC coated graphite billets were prepared by a chemical vapor deposition technique by M. B. Miller, Material Technology Cororation, Dallas, Texas.) The uncoated surfaces of the graphite substrate were polished using 600 grit SiC polishing paper. One 8.57 cm X 0.805 cm X 0.285 cm graphite monolithic substrate specimen (without the SiC coating) was also cut from the as-received billets.

Ten of the SiC coating/graphite composite beams were heated in air in an electric furnace at 550 ^{o}C until the graphite substrates were totally removed by oxidation in order to produce free-standing SiC layers from the coatings. The free-standing SiC coatings were

approximately 5 cm X 0.8 cm X 0.011 cm. X ray diffraction measurements between 10 degrees 2θ and 75 degrees 2θ indicated that the SiC layers was not modified significantly by the oxidation anneal.

3.3 Elasticity measurements

The fundamental frequency of the transverse vibrational mode of the specimens was measured using the dynamic resonance method, which is described elsewhere [E18,E19]. The elastic moduli of the annealed glass, alumina strips (prior to bonding the strips together), and the monolithic graphite specimen were calculated according to equation (E-18). The moduli of the glass/glass and multilayer alumina/glass composite beams were determined according to equations (E-15) and (E-17). The in-plane elastic moduli of the SiC coatings were determined from the measured fundamental flexural frequency using equation (E-15). The elastic moduli of the free-standing SiC coatings were measured by dynamic resonance from equation (E-18).

The in-plane elastic modulus of the SiC coating/graphite beam composites and the modulus of monolithic graphite specimen were also measured using a static bend test in a four point bend fixture with a 2.4 cm inner span and a 7.2 cm outer span. Strain gauges (EA-06-125BZ-350, Measurements Group Inc., Raleigh, NC) were attached parallel to the beam axes on the upper and lower faces on the composite beam (Figure 5). The strains were recorded and the elastic modulus for the model composite beams and for the SiC coatings were determined from equation (E-5).

Both the static (equation (E-5)) and the dynamic (equations (E-15) and (E-17)) techniques require accurate knowledge of the specimen dimensions and (when applicable) the coating thickness. Dimensions of the glass/glass and multilayer alumina/glass composites were determined to within ± 0.004 cm using a micrometer. The average thickness of the SiC coatings on the sectioned SiC/graphite composites was measured with an optical microscope to an accuracy of ± 5 μm.

4. RESULTS AND DISCUSSION

Measurements of the in-plane elastic modulus of coatings in this study agree well with the relationships developed in section 2 of this paper for modulus determinations by dynamic resonance (equations (E-15) and (E-17)) and by static bend (equation (E-5)). Section 4.1 presents results of the elasticity measurements on the glass/glass, alumina/glass and alumina/glass/alumina model composite beams. Section 4.2 discusses the results of the measurements on the SiC coating/graphite composite beams and subsequent measurements on the free-standing SiC films produced from the composite beams via oxidation of the graphite substrate.

4.1 Model composite beam elasticity results

For the two layer glass/glass model composite beams, the elastic modulus of each of the original glass strips (labeled as A and G in Figure E6) was measured prior to bonding. After bonding the composite beam via either gluing or sintering, E_c, the in-plane modulus of the composite beam was measured. Strip G was considered

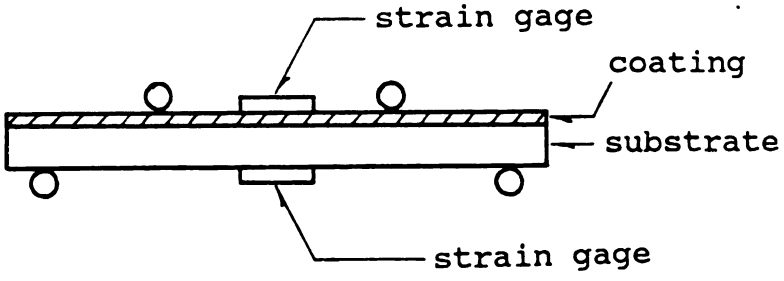

Figure E5. Schematic of the static four point bend apparatus used for the in-plane modulus measurement of SiC coatings.

a) Two-layer model composites

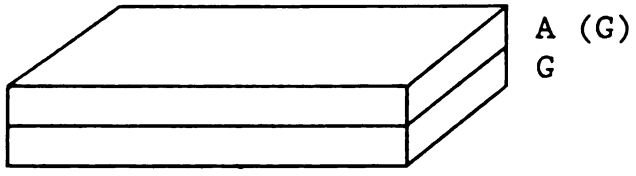

Alumina/glass and glass/glass composites

b) Three-layer model composites

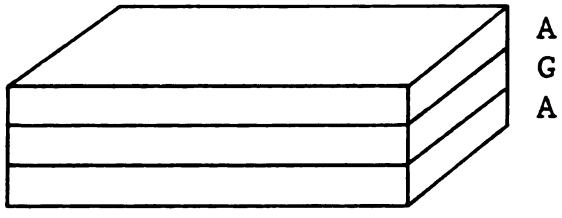

Alumina/glass/alumina composites

A= alumina substrate.
G= glass strip.

Figure E6. Illustration of two-layer and three layer-model composites.

to be the "substrate" and strip A was treated as the "coating" for both the glued and sintered composite beams. E_c (the elastic modulus of the coating strip "A" in Figure E6) was computed from equation (E-15) for each of the five glued glass/glass composite beams. The values of E_c obtained from equation (E-15) agreed to within ± 1.2 percent with the modulus of strip "A" measured prior to bonding (Table E1). However, E_c for five sintered glass/glass two-layer composites differed by up to 7.2 percent from the moduli of the corresponding "A" strips prior to bonding (Table E1). The larger deviation for the sintered glass composites may stem from slight deformations or stresses that can occur during sintering or during the cooling subsequent to sintering. (The two layer glass/glass specimens were sintered at 740 ^{o}C, which is considerably higher than the 600 degree anneal temperature of given the glass slides used in the other composite beam specimens).

Since equations (E-15) and (E-17) assume perfect bonding, the effects of the imperfect adhesion also were explored. As expected, the measured in-plane modulus of the two layer glass/glass composite beams decreased monotonically (Figure E7) as the relative fraction of the glue-bonded interface decreased. (Since the glass specimens are transparent, the glue-bonded interface can be observed directly). Poor adhesion impedes the stress transfer between the coating and the substrate, decreasing the integrated elastic stiffness [E22].

As was the case for the glass/glass composites, the elastic modulus of the individual alumina and glass strips was measured prior to glue-bonding the alumina/glass and the alumina/glass/alumina composite beams. For the alumina/glass and

Table E1. Dynamic resonance measurements of the in-plane elastic moduli of two-layer glass/glass composites (units: GPa)

Substrate glass G	"Coating" glass A	In-plane modulus of glass A	Deviation*
		glass/glass prepared by sintering	
67.9	68	72.9	7.2%
66.7	69.4	73.7	6.2%
68.9	67.6	70.8	4.7%
67.8	67.1	67.7	0.9%
66.3	66.5	71.2	7.1%
		mean: 71.3±2.1	
		prepared by glue adhesion	
68.6	67.6	67.3	-0.4%
66.4	67.8	67.3	-0.7%
66.3	68.6	67.8	-1.2%
67.9	66.3	66.5	0.3%
67.8	67.9	68.6	1.0%
mean: 67.6±0.9		mean: 67.5±0.7	

* Deviation = (original modulus of glass A - in-plane modulus of glass A)/original modulus of glass A * 100%.

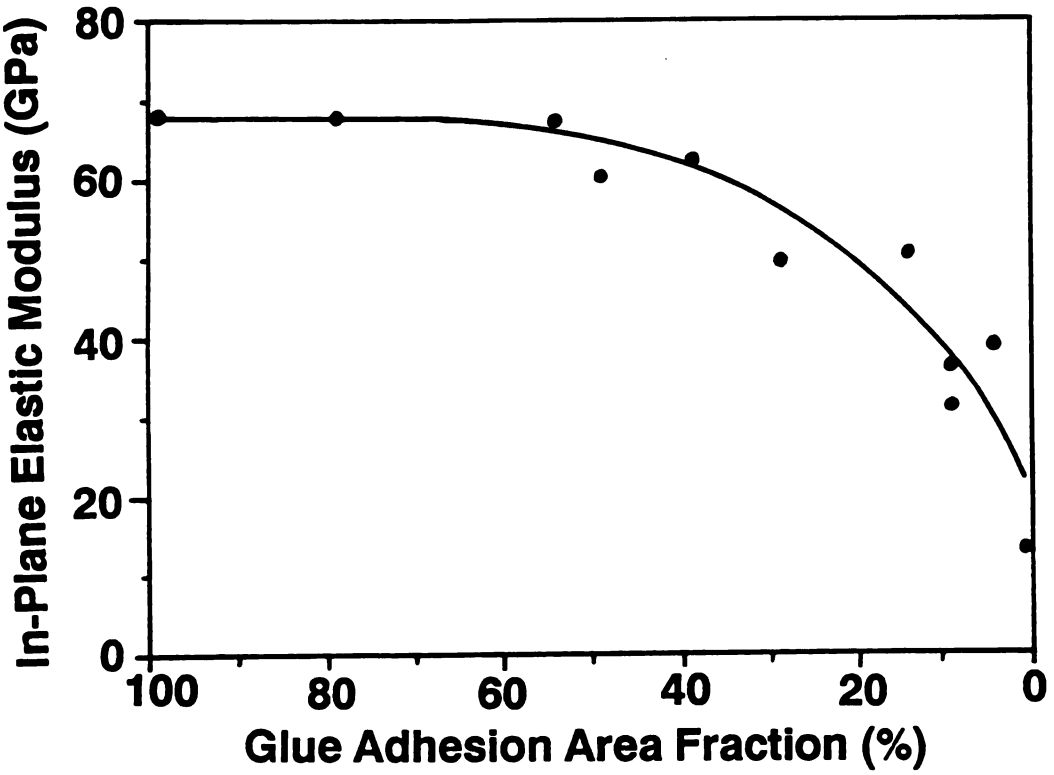

Figure E7. Influence of glue adhesion area fraction on the measured elastic modulus of two-layer glass/glass composite beams.

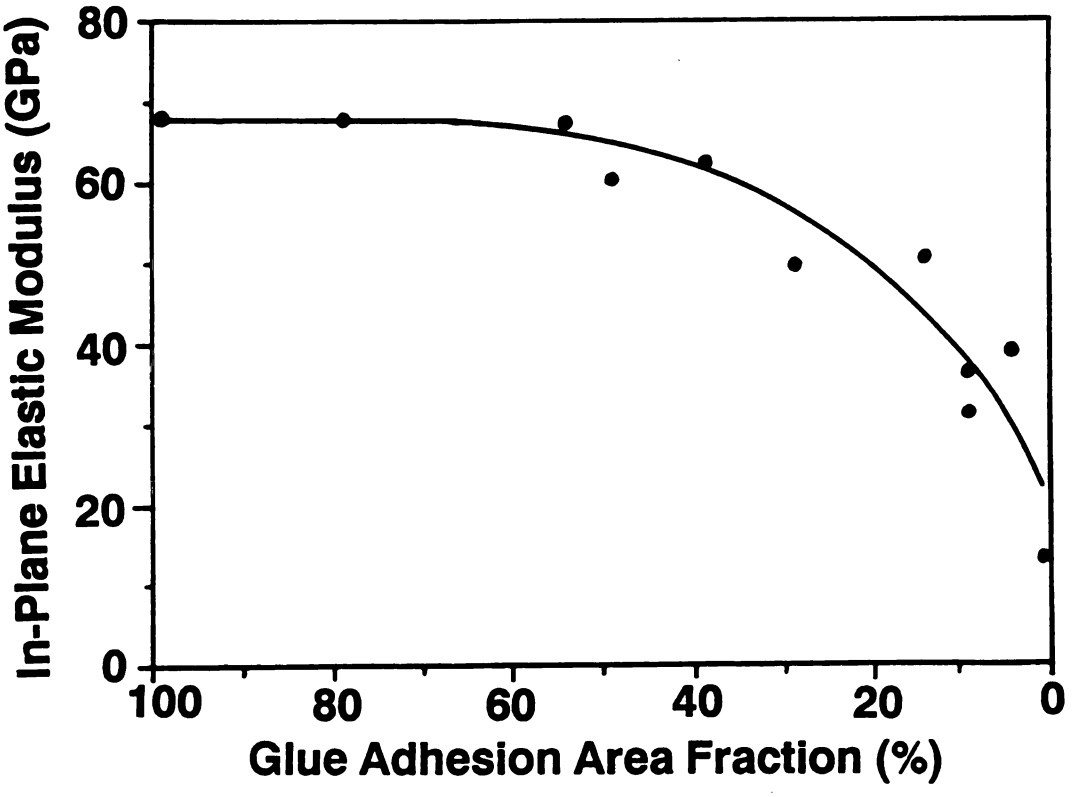

Figure E7. Influence of glue adhesion area fraction on the measured elastic modulus of two-layer glass/glass composite beams.

alumina/glass/alumina beams, the alumina strips were considered to be the "coatings" while the intermediate glass layer (labeled as G in Figure E6) was considered be to the "substrate" for purposes of the modulus calculations. For the four alumina/glass composite beams, the in-plane elastic moduli E_c of the alumina "coatings" computed from equation 15 were within 3 percent of the pre-bond modulus of the same alumina strips (Table E2). For the each of the three alumina/glass/alumina composite beams, the average modulus of the two alumina coating layers calculated from equation (E-17) agrees to within 1 percent with the average modulus for the corresponding pairs of alumina strips measured prior to bonding them to the glass substrate (Table E3).

4.2 SiC/graphite composites and free-standing SiC layers elasticity

The dynamic resonance and the static bend test gave 10.36 and 9.97 Gpa, respectively, for the elastic modulus of the monolithic (uncoated) graphite substrate. For the purpose of the subsequent calculations of the in-plane elastic moduli of the SiC coatings, we selected the statically-determined value of 9.97 GPa as E_s, the elastic modulus of the graphite substrate. (Recall that, as discussed in Section 3.2, the graphite substrate specimen was cut from the same as-received billet of CVD SiC coated graphite as were the SiC/graphite composite specimens.)

The in-plane elastic modulus of the SiC coatings on the commercially coated SiC/graphite composite beams was determined via both the static bend test and the dynamic resonance technique (Table C4). For ten SiC/graphite composite beams, dynamic resonance gave

Table E2. Dynamic resonance measurements of the in-plane elastic moduli of the alumina in Al_2O_3/glass composites (units: GPa)

Unbonded modulus of alumina strip	In-plane modulus of alumina	Deviation*
307.5	297.9	-3.1%
307.2	306.8	-0.1%
304.7	295.0	-3.1%
306.3	300.3	-1.9%
mean: 306.4±1.1	mean: 300.0±4.3	

* Deviation = (unbounded modulus - in-plane modulus)/ unbounded modulus * 100%

Table E3. Dynamic resonance measurements of the in-plane elastic moduli of the alumina in Al_2O_3/glass/Al_2O_3 composites (units: GPa)

Unbonded modulus of alumina strip (two strips per composite specimen)		In-plane modulus of alumina	Deviation
303.6	308.9	308.9	1%
303.1	305.7	306.7	1%
309.3	306.3	305.2	-1%
mean: 306.2±2.4		mean: 306.9±1.5	

an average in-plane elastic modulus of 379.5 GPa, while the static bend test on the same ten SiC/graphite specimens gave an average modulus of 359.6 GPa. The mean elastic modulus of the ten monolithic (free-standing) SiC coatings was 367.0 GPa, as measured by the dynamic resonance method. The SiC coatings measured under three different test conditions (dynamic measurements on composite beams, static measurement on composite beams, and dynamic measurements on the free standing coatings) present somewhat different mean values for the elastic modulus of the SiC coating (Table E4). Therefore, further analysis is required to determine whether or not the differences in the means are statistically significant.

Using the Krushal-Wallis test [24], the null hypothesis was that the three test conditions gave the same value for the elastic modulus of the SiC coating. At a significance level of α=0.05, there is no difference in the three data populations from which the samples are taken. Thus, there are no statistically significant differences among the SiC coatings' in-plane elastic modulus values, as determined in the three test conditions listed in Table E3.

4.3 Comparisons between the model composite beam results and the SiC coating results

The elastic modulus data for the glass/glass composite beams shows a coefficient of variation CV (where CV is the standard deviation/mean) of only 0.01 (Table E1). Considering the alumina/glass and the alumina/glass/alumina composite beams as a single group, the CV of the data for the in-plane modulus of the

Table E4. A comparison of in-plane elastic modulus data of SiC coatings (units: GPa)

static bend test	dynamic resonance method	
composite beam	composite beam	monolithic SiC coating layer
337.7	407.5	406.3
412.5	378.3	332.7
411.9	294.8	317.2
371.9	387.2	404.1
340.8	377.4	345.2
365.4	433.6	355.2
332.9	411.0	389.0
321.9	369.0	362.0
342.0	340.4	415.0
358.8	395.7	342.9
mean: 359.6±31.6	mean: 379.5±39.2	mean: 367±34.3

alumina coatings was 0.016 (Tables E2 and E3). However, CV of the SiC coatings is about 0.098 (Table E4). The relatively large CV for the SiC coatings may be due to the uncertainty in the data for the SiC coating thickness. For the model composite beams, the thickness of the glass slides and alumina substrates is uniform to within about 0.127±0.0005 cm and 0.064±0.0005 cm, respectively. This thickness can be measured easily prior to bonding together the individual layers of the model composites. In contrast to the model composites, the billets of SiC graphite/composite materials, prepared by chemical vapor deposition, show a slight coating thickness gradient between the corner and the central surface. The SiC coating thickness ranges from 89 to 103 μm (extreme values), which is observed from all of the composite beams cut from the billets.

5. CONCLUSIONS

Relationships have been developed for the determination of the in-plane elastic modulus of coatings by a dynamic resonance technique (equations (E-15) and (E-17)) and by a static bend method (equation (E-5)). Dynamic resonance modulus measurements of model composite systems, including two-layer glass/glass composite beams (bonded by either gluing or by sintering) and of two-layer alumina/glass beams (bonded by glue) agree well with predictions of the coating modulus based on equation 15. The coating's elastic modulus for the three-layer alumina/glass/alumina composite beams are well described by equation (E-17). The in-plane elastic modulus

of the SiC coatings on SiC coating/graphite composite beams were determined by both the dynamic resonance and the static bend techniques. The graphite substrate was then removed from the SiC/graphite beams, leaving a free-standing SiC layer. A Krushal-Wallis test showed no statistically significant differences among the three sets for the elastic modulus calculated for of the SiC coating (that is, for measurements done statically and dynamically on intact composite beams, as well as dynamic resonance on free-standing SiC layers).

In this study, the ratio R of substrate thickness to coating thickness (ℓ_s/ℓ_c) varied from 1.0 for the two layer glass/glass model composites to 2.0 for the alumina/glass two-layer composites, to about 27 in the case of the two-layer SiC/graphite composites. The ratio E_s/E_c of the elastic moduli of the substrate and coating, respectively, varied from 1.0 for the glass/glass model composites, to about 0.2 for the alumina/glass model composites, to about 0.027 for the CVD SiC/graphite composites. Thus, for a considerable range of relative coating thickness and relative elastic moduli for layered ceramic composites, the equations and techniques presented in this paper provide a reasonably accurate means of determining the elastic modulus of the coating layer. For completeness, future studies should include measurements on which the coating modulus is less than the substrate modulus, although in many applications the materials of interest are as those trested here (that is, where the coating modulus is equal to or greater than the substrsate modulus).

References for Appendix E

E1) R. F. Bunshah, pp. 158, Deposition Technologies for Films and Coatings, Noyes Publication, Park Ridge, New Jersey, (1982).

E2) H. W. Grunling, K. Schneider, and L. Singheiser, "Mechanical Properties of Coated Systems", Mater. Sci. and Eng., 88: 177-189 (1987).

E3) T. Shikama, H. Shinmo, M. Fukutomi, M. Fujitsuka, and M. Okada, "Mechanical Properties of Molybdenum Coated with Titanium Carbide Film", J. mater. Sci., 18[10]: 3092-3098 (1983).

E4) R. B. King and T. C. O'Sullivan, "Sliding Contact Stresses in a Two-Dimensional Layered Elastic Half-Space", Int. J. Solids Structures, 23[5]: 581-597 (1987).

E5) A. K. Bhattacharya and W. D. Nix, "Analysis of Elastic and Plastic Deformation Associated with Indentation Testings of Thin Films on Substrates", Int. J. Solids Structures, 24[12]: 1287-1298 (1988).

E6) D. B. Marshall and A. G. Evans, "Measurement of Adherence of Residually Stressed Thin Films by Indentation. I: Mechanics of Interface Delamination", J. Appl. Phys., 56[10]: 2632-2638 (1984).

E7) A. G. Evans and J. W. Hutchinson, "On the Mechanics of Delamination and Spalling in Compressed Films", Int. J. Solids Structures, 20[5]: 455-466 (1984).

E8) A. K. Sinha, H. J. Levinstein, and T. E. Smith, "Thermal Stresses and Cracking Resistance of Dielectric Films (SiN, Si_3N_4, and SiO_2) on Si Substrates", J. Appl. Phys., 49[4]: 2423-2426 (1978).

E9) A. Brenner and S. Senderoff, "Calculation of Stress in Electrodeposits from the Curvature of a Plated Strip", Journal of Research of National Bureau of Standards, 42: 105-123 (1949).

E10) P. H. Townsend and D. M. Barnett, "Elastic Relationships in Layered Composite Media with Approximation for the Case of Thin Films on a Thick Substrate", J. Appl. Phys. 62[11]: 4438-4444 (1987).

E11) A. V. Virkar, J. L. Huang, and R. A. Cutler, "Strengthening of Oxide Ceramics by Transformation-Induced Stresses", J. Am. Ceram. Soc., 70[3]: 164-70 (1987).

E12) R. L. Mullen, R. C. Hendricks, and G. McDonald, "Interface Roughness effect on Stresses in Ceramic Coatings", Ceram. Eng. Sci. Proc., 8[7-8]: 559-571 (1987).

E13) T. R. Watkins, D. J. Green, and E. Rybe, "Measurement of the In-Plane Young's Modulus and Residual Stresses in CVD SiC Coatings", presented at 91st Annual Meeting of the American Ceramic Society, (1989).

E14) R. B. King, "Elastic Analysis of Some Punch Problems for a Layered Medium", Int. J. Solids Structures, 23[12]: 1657-1664 (1987).

E15) A. G. Vannie, "A Method for the Determination of the Stress in, and Young's Modulus of Silicon Nitride Passivation Layers", Solid State Technology, 23[1]: 81-84 (1980).

E16) D. S. Williams, "Elastic Stiffness and Thermal Expansion Coefficient of Boron Nitride Films", J. Appl. Phys., 57[6]: 2340-2342 (1985).

E17) E. M. Corcoran, "Determining Stresses in Organic Coatings Using Plate Beam Deflection", Journal of Paint Technology, 41[538]: 635-640 (1969).

E18) E. Schreiber, O. L. Anderson, and N. Soga, pp. 82, Elastic Constants and Their Measurement, McGraw-Hill, New York, (1974).

E19) "Standard Testing Method for Young's Modulus, Shear Modulus, and Poission's Ratio for Glass and Glass-Ceramics by Resonance", ASTM, Designation: C623-71 (Reapproved 1981).

E20) E. Volterra and E. C. Zachmanoglou, pp. 321, Dynamics of Vibrations, Charles E. Merrill Books, Inc., Columbus, Ohio, (1965).

E21) S. K. Clark, pp.75-87, Dynamics of Continuous Elements, Prentice-Hall, Inc., Englewood Cliffs, New Jersey, (1972).

E22) S. P. Timoshenko and D. H. Young, pp. 113, Strength of Materials, Fourth Edition, Van Nostrand Reinhold Co., Princeton New York, (1962).

E23) C. W. D. Silva, "Dynamic Beam Model with Internal Damping Rotatory Inertia and Shear Deformation", AIAA Journal, 14[5]: 676-680 (1976).

E24) H. R. Neave and P. L. Worthington, pp. 243, Distribution-Free Tests, Unwin Hyman Ltd., London, (1988).

COMPUTER PROGRAM

Computer program No. 1

```
C       This is a part of pgograms to calculate the "thermoelastic
C       stress in glass plates".  This program can evaluate the
C       relationship between Biot's modulus and critical quench
C       temperature difference if the fracture strength of specimen
C       is pre-determined.


C       B = Biot's modulus  ; 2H = thickness of plate
C       EX = thermal expansion  ;  EL = elastic modulus
C       CFS = critical fracture strength : DI = diffusivity
C       TEMP = quench temperature difference  ; TEMP = T1 - T0
C       T1 = initial temperature ; T0 = quenching medium temperature
        DO 78  L = 1, 2
         STREN = 60 + 80 *(L-1)
        DO 30  M = 1 , 20
           TEMP = 80 +  20 * M
             T1 = 100 + 20 * M
             T0 = 20
        DO 10, N = 1 , 10
        B = 0.1 * N**3
        B1 = B
        KK = 1
        IF (N .EQ. 1) THEN
         B3 = 0.05
         ELSE
          B3 = 0.1  * (N-1)**3
        END IF
        CALL CHIUCH(B,XG, TEMP, T1, T0)
         IF (XG .LT. STREN) THEN
           GO TO 10
         ELSE
           B2 = (B1 + B3)/2
           B = B2
          END IF
 120     CALL CHIUCH(B,XG, TEMP, T1, T0)
         KK = KK + 1
         IF((ABS(XG - STREN)/STREN .LT. 0.001) .OR. (KK .EQ. 20)) THEN
          WRITE (2,*) TEMP, B , KK, XG
          PRINT *, TEMP, B , KK , XG
         GO TO 30
          ELSE
           IF(XG . GT. STREN) THEN
             B1 = B2
             B2 = (B1 + B3)/2
             B = B2
           ELSE
             B3 = B2
             B2 =(B1 + B3)/2
             B = B2
            END IF
           END IF
         GO TO 120
 10     CONTINUE
        PRINT *, TEMP
 30     CONTINUE
       WRITE(2 ,*) STREN
  78    CONTINUE
        STOP
        END
```

```
      subroutine chiuch(B,XG, TEMP, T1 , T0)
      REAL X(0:12) , T(205)
C     INPUT OF SOME PARAMETERS
        H = 1.0E-3
        DI = 4.8E-7
        EX = 8.0E-6
        EL =7.0E+10
C     eignvalue calculation using half-interval tech.
C                              :  X(M) * TAN(X(M)) = B
      DO 10 , E = 0 , 10
         XM1 = 0 + 3.14159 * E
         XM2 = 1.570795 + E * 3.14159
       DO 20 , W = 1 , 50
          XM3 = (XM1 + XM2)/2
          IF (ABS(XM1 - XM2) .LT. 0.0000003) THEN
             GO TO 15
          ELSE
             XMM1 = XM1 * TAN(XM1) - B
             XMM2 = XM2 * TAN(XM2) - B
             XMM3 = XM3 * TAN(XM3) - B
          END IF
          IF ((XMM1 * XMM3) .GT. 0.0) THEN
             XM1 = XM3
             XM2 = XM2
          ELSE
             XM1 = XM1
             XM2 = XM3
          END IF
 20     CONTINUE
 15       X(E) = XM3
 10    CONTINUE

C   TO CALCULATE THERMOELASTIC STRESSES
        XG = 0.0
       DO 22  M = 1 , 200
          XRR = 0.0
           T(M) = 0.000001 * 1.1**M
        DO 60 , E = 0 , 10
          XPP = EXP(-DI * (X(E)/H)**2 * T(M))
           XA = SIN(X(E))/(X(E) + COS(X(E))* SIN(X(E)))
           XB = SIN(X(E))/X(E) - COS(X(E)*H/H)
          XRR = XPP * XA * XB + XRR
 60      CONTINUE
         STRESS = 2 * EX*EL* TEMP/(1-0.25) * XRR/1000000
         IF (STRESS .GT. XG) THEN
           XG = STRESS
           ELSE
           GO TO 80
         END IF
 22      CONTINUE

 80      RETURN
        END
```

Computer program No. 2

```
C       This is a part of pgograms to calculate the "transient
C       thermoviscoelastic stress"


C       B = Biot's modulus  ; 2H = thickness of plate  ;  DI = diffusivity
C       EX = thermal expansion  ;  EL = elastic modulus
C       CFS = critical fracture strength
C       TEMP = quench temperature difference  ; TEMP = T1 - T0
C       T1 = initial temperature   ;  T0 = quenching medium temperature
C       T(M) is real time
C       CCT(L,M) is reduced time ; L = position variable , M = time variable
        REAL A(0:22,0:1302), STRESS(0:22,0:1302), STRAIN(0:1302)
        REAL T(0:1302) , CCT(0:22,0:1302) , TTT(0:22,0:1302)
        REAL X(0:12)
C       A IS A SPECIAL FUNCTION WHICH IS USED IN THERMOELASTIC STRESS CAL.
C       INPUT OF SOME PARAMETERS
          B = 10
          H = 1.0E-3
          DI = 4.8E-7
          EX = 8.0E-6
          EL =7.0E+10
          TEMP = 670
          T1 = 690
          T0 = 20
C       To calculate the temperature distribution
C       eignvalue calculation using half-interval tech. :  X(M) * TAN(X(M)) = B
        DO 10 , E = 0 , 10
           XM1 = 0 + 3.14159 * E
           XM2 = 1.570795 + E * 3.14159
         DO 20 , W = 1 , 50
            XM3 = (XM1 + XM2)/2
            IF (ABS(XM1 - XM2) .LT. 0.0000003) THEN
               GO TO 15
            ELSE
               XMM1 = XM1 * TAN(XM1) - B
               XMM2 = XM2 * TAN(XM2) - B
               XMM3 = XM3 * TAN(XM3) - B
            END IF
            IF ((XMM1 * XMM3) .GT. 0.0) THEN
               XM1 = XM3
               XM2 = XM2
            ELSE
               XM1 = XM1
               XM2 = XM3
            END IF
   20     CONTINUE
   15       X(E) = XM3
   10     CONTINUE
C       To calculate the reduced time and temperature gradient
C       Loop F is related to the position along plate thickness.
C       The half thickness of glass plate includes 21 points.
C       T(M) loop is real time.  Real time is divided into 1300 points
C       in 17 seconds.
        DO  40 , F = 0 , 20
          CCT(F,0) = 0.0
          TTT(F,0) = T1
          STRESS(F,0) = 0.0
   40   CONTINUE
        T(0) = 0.0
        DO  30 , F = 0 , 20
          Z = H * F /20
C         Since we divide the half thickness to be 20 division, the equation
C         above has " / 20".
C         Z is the corrodinate in the direction of plate thickness
          XSS = 0.0
```

```
      DO 50 , M = 1 , 1300
        T(M) = 0.00001 * M**2
        XRR = 0
       DO 60 , E = 0 , 10
         XPP = EXP(-DI * (X(E)/H)**2 * T(M))
          XA = SIN(X(E))* COS(X(E)* Z/ H)
          XB = X(E)+ SIN(X(E))* COS(X(E))
         XQQ = XA/XB
         XRR = XPP * XQQ + XRR
60     CONTINUE
       TTT(F,M) = T0 + TEMP * 2 * XRR
       XT = EXP(0.0889028* TTT(F,M-1))+ EXP(0.0889028* TTT(F,M))
       CCT(F,M) = 1.68974E-21 * XT * (T(M) - T(M-1))/2 + CCT(F,M-1)
50     CONTINUE
30    CONTINUE
C     To calculate the thermoviscoelastic stresses
C     (1) To Calculate the A(J,L) ;  a simplied function in calculating
C     precedure.
      DO 70 , I = 1 , 1300
       DO 80 , F = 0 , 20
        A(F,I) = EXP((-CCT(F,I) + CCT(F, I-1))/1400)
80     CONTINUE
70    CONTINUE
C     (2)
      STRAIN(0) = 0.0
      DO 82 , I = 1 , 1300
        XQ = 0.0
        XR = 0.0
        XS = 0.0
       DO 84 , J = 1 , 20
        XQ = A(J,I) + A(J-1,I) + XQ
        XA = (TTT(J,I) - TTT(J,I-1)) * A(J,I)
        XB = (TTT(J-1,I) - TTT(J-1,I-1)) * A(J-1,I)
        XR = XA + XB  + XR
        XC = (A(J,I))**2 * STRESS(J,I-1)
        XS = XC + (A(J-1,I))**2 * STRESS(J-1,I-1) + XS
84     CONTINUE
        XA = STRAIN(I-1)* EL/(1-0.25)* XQ+ EX* EL/(1-0.25)* XR- XS
         XB = EL/(1-0.25)*XQ
       STRAIN(I) = XA/XB
       DO 86 , F = 0 , 20
        XA = STRAIN(I)- STRAIN(I-1)- EX *(TTT(F,I)-TTT(F,I-1))
         HH = EL/(1-0.25)* XA * A(F,I)
         STRESS(F,I) = HH + (A(F,I))**2 * STRESS(F,I-1)
86     CONTINUE
82     CONTINUE
       PRINT * , '  POSITION            MPa    '
       DO 90 , WK =  0 , 40
          W = WK - 20
        XL = W/20 * H * 1000
C      THE UNIT IS mm and MPa
        XG = STRESS(ABS(W),1300)/1000000
        WRITE(1, *) XL, XG
        PRINT * ,   XL, XG
 90    CONTINUE
       STOP
       END
```

Computer program No. 3

```
C       This is a part of programs to calculate the "thermoviscoelastic
C       stress in glass plates".  This objective of this program is to
C       evaluate the relationshiop between Biot's modulus and critical
C       quench temperature difference when the fracture strength of slides
C       are pre-determined.  ----thermoviscoelastic stress------

C       B = Biot's modulus  ; 2H = thickness of plate
C       EX = thermal expansion  ;  EL = elastic modulus
C       CFS = critical fracture strength : DI = diffusivity
C       TEMP = quench temperature difference  ; TEMP = T1 - T0
C       T1 = initial temperature ; T0 = quenching medium temperature
C       T(M) is real time , M = time variable
C       CCT(L,M) is reduced time ; L = position variable
        DO 78  L = 1, 2
         STREN = 60 + 80 *(L-1)
        DO 30  M = 1 , 7
           TEMP = 580 +  20 * M
             T1 = 600 + 20 * M
             T0 = 20
        DO 10, N = 1 , 10
        B = 0.2 * N**3
        B1 = B
        KK = 1
        IF (N .EQ. 1) THEN
         B3 = 0.05
         ELSE
          B3 = 0.2  * (N-1)**3
        END IF
        CALL CHIUCH(B,XG, TEMP, T1, T0)
         IF (XG .LT. STREN) THEN
           GO TO 10
         ELSE
           B2 = (B1 + B3)/2
           B = B2
          END IF
 120     CALL CHIUCH(B,XG, TEMP, T1, T0)
         KK = KK + 1
         IF((ABS(XG - STREN)/STREN .LT. 0.001) .OR. (KK .EQ. 14)) THEN
          WRITE (3,*) TEMP, B , KK, XG
          PRINT *, TEMP, B , KK , XG
         GO TO 30
          ELSE
           IF(XG . GT. STREN) THEN
             B1 = B2
             B2 = (B1 + B3)/2
             B = B2
           ELSE
             B3 = B2
             B2 =(B1 + B3)/2
             B = B2
            END IF
           END IF
          GO TO 120
 10     CONTINUE
        PRINT *, TEMP
 30     CONTINUE
        WRITE(3 ,*) STREN
 78     CONTINUE
        STOP
        END


        subroutine chiuch(B,XG, TEMP, T1 , T0)
        REAL A(0:22,0:1302), STRESS(0:22,0:1302), STRAIN(0:1302)
```

```
      REAL T(0:1302) , CCT(0:22,0:1302) , TTT(0:22,0:1302)
      REAL X(0:12)
C     A IS A SPECIAL FUNCTION WHICH IS USED IN THERMOELASTIC STRESS CAL.
C     INPUT OF SOME PARAMETERS
        H = 1.0E-3
        DI = 4.8E-7
        EX = 8.0E-6
        EL =7.0E+10
C     To calculate the temperature distribution
C     eignvalue calculation using half-interval tech.
C                                 :  X(M) * TAN(X(M)) = B
      DO 10 , E = 0 , 10
         XM1 = 0 + 3.14159 * E
         XM2 = 1.570795 + E * 3.14159
       DO 20 , W = 1 , 50
          XM3 = (XM1 + XM2)/2
          IF (ABS(XM1 - XM2) .LT. 0.0000003) THEN
             GO TO 15
          ELSE
             XMM1 = XM1 * TAN(XM1) - B
             XMM2 = XM2 * TAN(XM2) - B
             XMM3 = XM3 * TAN(XM3) - B
          END IF
          IF ((XMM1 * XMM3) .GT. 0.0) THEN
             XM1 = XM3
             XM2 = XM2
          ELSE
             XM1 = XM1
             XM2 = XM3
          END IF
 20     CONTINUE
 15     X(E) = XM3
 10   CONTINUE
C     To calculate the reduced time and temperature gradient
C     Loop F is related to the position along plate thickness.
C     The half thickness of glass plate includes 21 points.
C     T(M) loop is real time.  Real time is divided into 1300 points
C     in 17 seconds.
      DO  40 , F = 0 , 20
        CCT(F,0) = 0.0
        TTT(F,0) = T1
        STRESS(F,0) = 0.0
 40   CONTINUE
      T(0) = 0.0
      DO  30 , F = 0 , 20
        Z = H * F /20
C       Since we divide the half thickness to be 20 division, the
C       equation above has " / 20".
C       Z is the corrodinate in the direction of plate thickness
        XSS = 0.0
       DO 50 , M = 1 , 1300A
         T(M) = 0.00001 * M**2
         XRR = 0
        DO 60 , E = 0 , 10
          XPP = EXP(-DI * (X(E)/H)**2 * T(M))
           XA = SIN(X(E))* COS(X(E)* Z/ H)
           XB = X(E)+ SIN(X(E))* COS(X(E))
          XQQ = XA/XB
          XRR = XPP * XQQ + XRR
 60      CONTINUE
         TTT(F,M) = T0 + TEMP * 2 * XRR
         XT = EXP(0.0889028* TTT(F,M-1))+ EXP(0.0889028* TTT(F,M))
         CCT(F,M) = 1.68974E-21 * XT * (T(M) - T(M-1))/2 + CCT(F,M-1)
 50    CONTINUE
 30   CONTINUE
C     To calculate the thermoviscoelastic stresses
```

```
C       (1) To Calculate the A(J,L);  a simplied function in calculating
C       precedure.

        XG = 0.0

        DO 70 , I = 1 , 1300
         DO 80 , F = 0 , 20
          A(F,I) = EXP((-CCT(F,I) + CCT(F, I-1))/1400)
  80     CONTINUE
  70    CONTINUE
C       (2)
        STRAIN(0) = 0.0
        DO 82 , I = 1 , 1300
          XQ = 0.0
          XR = 0.0
          XS = 0.0
         DO 84 , J = 1 , 20
          XQ = A(J,I) + A(J-1,I) + XQ
          XA = (TTT(J,I) - TTT(J,I-1)) * A(J,I)
          XB = (TTT(J-1,I) - TTT(J-1,I-1)) * A(J-1,I)
          XR = XA + XB  + XR
          XC = (A(J,I))**2 * STRESS(J,I-1)
          XS = XC + (A(J-1,I))**2 * STRESS(J-1,I-1) + XS
  84     CONTINUE
          XA = STRAIN(I-1)* EL/(1-0.25)* XQ+ EX* EL/(1-0.25)* XR- XS
           XB = EL/(1-0.25)*XQ
         STRAIN(I) = XA/XB
         DO 86 , F = 0 , 20
          XA = STRAIN(I)- STRAIN(I-1)- EX *(TTT(F,I)-TTT(F,I-1))
           HH = EL/(1-0.25)* XA * A(F,I)
           STRESS(F,I) = HH + (A(F,I))**2 * STRESS(F,I-1)
  86     CONTINUE
         XGGG = STRESS(20,I)/1000000
           IF (XGGG .GT. XG) THEN
              XG = XGGG
               GO TO 82
            ELSE
              IF(((XG-XGGG)/XG) .LT. 0.01) GO TO 82
            GO TO 156
           END IF
  82     CONTINUE
C         PRINT * , '  POSITION            MPa    '
C         DO 90 , WK =  0 , 40
C            W = WK - 20
C          XL = W/20 * H * 1000
C       THE UNIT IS mm and MPa
C          XG = STRESS(ABS(W),1300)/1000000
C          WRITE(1, *) XL, XG
C          PRINT * ,   XL, XG
C   90    CONTINUE

C           DO 231 I =  1 , 1300
C               XGGG = STRESS(20, I)/1000000
C            IF (XGGG .GT. XG) THEN
C             XG = XGGG
C             END IF
  231       CONTINUE


  156   RETURN
        END
```

Computer program No. 4

```
C       This is a part of programs is perform the "computer simulation
C       of strength degradation of shocked glass plates"
C       Purpose : to create a distribution of initial fracture strength
C                 (a distribution of initial crack flaw size) using the
C       random number generater of IMSL program.  (normal distribution)


C       Statistic parameter:  mean = 101.4. standard deviation = 10.24
C       Kc : critical intensity factor.  Y : geometric parameter

        CHARACTER*15 CRACKLEN
        REAL X(1000) , Z(1000) , KC, XX

        Y = 1.1215
        KC = 0.78E+6

C  1 :  random generation of fracture strength, X( ), using IMSL program
        DO 5 N = 1 , 1000
          CALL RNNOR(1, XX)
          CALL SSCAL(1, 10.24, XX, 1)
          CALL SADD(1, 101.4, XX, 1)
          X(N) = XX
 5      CONTINUE

        OPEN (UNIT = 1, FILE = 'CRACKLEN' , STATUS = 'NEW' )

C  2 :  transformation from X( ) to initial crack length,  Z( )
        DO 10  N = 1 , 1000
          Z(N) = (Kc/Y/(X(N)* 1E+6))**2 / 3.14159
          WRITE (1,*) Z(N)
 10     CONTINUE

          CLOSE (UNIT = 1)

        STOP
        END
```

Computer program No. 5

```
C      This is a part of programs to perform the 'computer simulation
C      of strength degradation of shocked glass plates'
C      Purpose : to simulate the retained strength degradation
C   -----      (1) without subcritical crack growth


C      Stress intensity factor Kc = 0.78E+6.
C      geometric parameter Y = 1.1214
C      thermal expansion = EX.  elastic modulus = E.
C      Poission ratio = V.  Fracture surface energy = G.
C      crack density = XN.  fatigue limit = KO
C      quench temperature difference = DELTAT (arbitrary)
C------   DATA FILE OF INITIAL CRACK LENGTH:  CRACKLEN

       CHARACTER*15  CRACKLEN
       DOUBLE PRECISION  X(1000), XF1(1000), XF2(1000)
       DOUBLE PRECISION  Z1(1000),  Z2(1000), Z3(1000)
       DOUBLE PRECISION A, B, C, D, ZT1 ,ZT2 ,ZT3 , W1, W2, W3 ,Tc
       DOUBLE PRECISION TT, LENGTH
       INTEGER J, II(0:53) , I1(0:53) , I2(0:53)

       KC = 0.75E+6
       Y = 1.1214
       EX = 6.5E-6
       E = 70E+9
       V = 0.25
       G = 4
C       XN = 2E +11

       OPEN (UNIT = 1, FILE = 'CRACKLEN' , STATUS = 'OLD')
        DO 1  N = 1 , 1000
          READ(1, *) X(N)
 1      CONTINUE
       CLOSE (UNIT = 1)

C      The purpose of loop 888 is to repeatedly calculate the
C      strength degradation related to different deltat.

        DO 777  , III = 1, 4

        XN = 2E+5 * 100**III
        IF (III .EQ. 4) THEN
          XN = 2E+12
        END IF

       DO 888 IJK = 1 , 10
          DELTAT = 80 + (IJK - 1) *20
               PRINT * , ' DELTAT = ', DELTAT

C      The purpose of loop 3 and 4 is to clearn all variables
C      in order for the repeated calculation of loop 888.

         DO 3 , N = 1 , 1000
             Z1(N) = X(N)
             XF1(N) = 0.0
             XF2(N) =0.0
             Z2(N) =0.0
             Z3(N) =0.0
   3     CONTINUE

         DO 4 , WN = 0 , 53
             II(WN) = 0.0
             I1(WN) = 0.0
             I2(WN) = 0.0
   4   CONTINUE
```

```
C 1.1 :  transformation from Z1( ) to final crack length, Z2( )
C        Z1( ) is the initical crack length

         B = 2* 3.14159* XN* G
         C = 16 *(1-V**2) * XN /9/(1-2*V)
         D = 3.14159*G*(1-2*V)**2/2/E/EX**2/(1-V**2)
C    definition of A, B, C and D, are given in Hasselman's paper(1969)

C    To find the final crack length due to kinetic behavior using
C    Hasselman's Eq. (4) and (7).
C    Numercial technique:  interval-halving mothod
C    Tc is the critical temperature for kinetic crack growth.

       K = 0
       KK = 0
C      K represents the total number of specimens without crack growth
C      KK is the total number with crack growth

       DO 30 M = 1 , 1000

          Tc = D**0.5 *(1+ C*Z1(M)**3) / Z1(M)**0.5
                          A = 3*(EX * Tc)**2 * E/2/(1- 2*V)
          IF (Tc .GT. DELTAT) THEN
             K = K + 1
 501         Z2(K) = Z1(M)
             GO TO 30
          END IF
C     The physical meaning of statement 501 is 'no crack growth'.
C     It means that Z2( ) represents the part of intial flaws
C     without crack growth.
CB     After statment 502, the other part of initial crack 'grows'.

 502      ZT1 = Z1(M) * 1.001
          DO 20 N = 1 , 35
            CALL CHIUCH(A, B, C, Z1(M), ZT1, W1)
             IF (N .EQ. 1) THEN
               W3 = W1
               ZT3 = ZT1
               GOTO 20
             ELSE
               IF (W1*W3 .GT. 0.0) THEN
                 W3 = W1
                 ZT3 = ZT1
                 ZT1 = Z1(M) * 3**N
                 GO TO 20
               ELSE
                 GO TO 25
               END IF
             END IF
 20       CONTINUE
C      The purpose of loop 20 is to find an interval in which
C      the solution exists.  The solution will be calcualted in
C      loop 28 using interval-halving method.

 25       DO 28 NM = 1 , 30
            ZT2 = (ZT1 +ZT3)/2
            CALL CHIUCH(A, B, C, Z1(M), ZT2, W2)
            IF (W3*W2 .GT. 0.0) THEN
               W3 = W2
               ZT3 = ZT2
               ZT2 = (ZT1+ZT3)/2
            ELSE
               W1 = W2
               ZT1 = ZT2
               ZT2 = (ZT1 + ZT3)/2
```

```
            END IF
            IF (ABS(ZT1 - ZT3) .LT. 0.0000000001) GO TO 19
 28       CONTINUE
 19        KK = KK + 1
           Z3(KK) = ZT2
 30    CONTINUE

C       Z3( ) represents the final crack length due to kinetic
C       crack growth.


C 1.2 : To find the final quasi-static crack length according to
C       to Eq. (4)

         DO 200 N = 1, KK
          TT = D**0.5*(1+C*Z3(KK)**3)/Z3(KK)**0.5
          IF (TT .LT. DELTAT) THEN
            GO TO 477
          ELSE
            GO TO 200
          END IF

C     To find final crack length using interval-halving method
 477       ZT1 = Z3(KK) * 1.001
           DO 40 NN = 1 , 35
             CALL CHIUCH(A, B, C, Z3(KK), ZT1, W1)
              IF (N .EQ. 1) THEN
                W3 = W1
                ZT3 = ZT1
                GO TO 40
              ELSE
                IF (W1*W3 .GT. 0.0) THEN
                  W3 = W1
                  ZT3 = ZT1
                  ZT1 = Z3(KK) * 3**NN
                  GO TO 40
                ELSE
                  GO TO 45
                END IF
              END IF
 40        CONTINUE

 45          DO 48 M = 1, 30
              ZT2 = (ZT1 + ZT3)/2
              CALL CHIUCH(A, B, C, Z3(KK), ZT2, W2)
               IF (W3*W2 .GT. 0.0) THEN
                 W3 = W2
                 ZT3 = ZT2
                 ZT2 = (ZT1 + ZT3)/2
               ELSE
                 W1 = W2
                 ZT1 = ZT2
                 ZT2 = (ZT1 + ZT3)/2
               END IF
               IF (ABS(ZT1 - ZT3) .LT. 0.0000000001) GO TO 44
 48        CONTINUE
 44             Z3(KK) = ZT2
 200       CONTINUE


C  4 :  transformation from Z2( ) and Z3( ) to final strength,
C       Xf1 and XF2(  ) , respectively.
C       Sorting of retained fracture strength
        DO 46 N = 1 , 1000
         DD = Kc/Y/(3.14159*X(N))**0.5 / 1E+6
```

```
        J = DD/4
        II(J) = II(J) + 1
46    CONTINUE
        XMEAN = 0.0
      IF (K .EQ. 0) GO TO 155
      DO 50 N = 1 , K
        XF1(N) = Kc/Y/(3.14159*Z2(N))**0.5/1E+6
         XMEAN = XMEAN + XF1(N)
        J = XF1(N)/4
        I1(J) = I1(J) +1
50    CONTINUE
155    IF (KK .EQ. 0) GO TO 157
      DO 60 N = 1 , KK
        XF2(N) = Kc/Y/(3.14159*Z3(N))**0.5/1E+6
        XMEAN = XMEAN + XF2(N)
        J = XF2(N)/4
        I2(J) = I2(J) +1
60    CONTINUE
157   DO 49 WN = 0, 35
       WRITE (3,*) WN*4+2 , II(WN) , I1(WN) , I2(WN)
49    CONTINUE

       XMEAN = XMEAN/(K+KK)
       VAR = 0.0
       IF (K .EQ. 0) GOTO 72
       DO 71 N = 1, K
         VAR = (XMEAN - XF1(N))**2 + VAR
71     CONTINUE
72     DO 73 N = 1, KK
         VAR = (XMEAN -XF2(N))**2 + VAR
73     CONTINUE
        STAND = (VAR/(K+KK))**0.5
       WRITE (3, *)
       WRITE (3, *)  DELTAT, XN, XMEAN, STAND
       WRITE (3 , *)
       WRITE (3, *)
888   CONTINUE
777   CONTINUE
      STOP
      END


      SUBROUTINE CHIUCH(A, B, C, Z1 , ZT , ZTRIAL)
      DOUBLE PRECISION A , B, C, Z1, ZT, ZTRIAL
      ZTRIAL = A*(1/(1+C*Z1**3)-1/(1+C*ZT**3))-B*(ZT**2-Z1**2)
      RETURN
      END
```

Computer program No. 6

```
C      This is a part of programs to perform "computer simulation
C      of strength degradation of shocked glass plates"
C      Purpose : to simulate the retained strength degradation
C   -----      (2) with subcritical crack growth


C      Stress intensity factor Kc = 0.75E+6.
C      geometric parameter Y = 1.1215
C      thermal expansion = EX.  elastic modulus = E.
C      Poission ratio = V.  Fracture surface energy = G.
C      crack density = XN.  fatigue limit = KO
C      quench temperature difference = DELTAT (arbitrary)
C-----   DATA FILE OF INITIAL CRACK LENGTH:  CRACKLEN

       CHARACTER*15  CRACKLEN
       DOUBLE PRECISION  X(1000), XF1(1000), XF2(1000)
       DOUBLE PRECISION  Z1(1000),  Z2(1000), Z3(1000)
       DOUBLE PRECISION A, B, C, D, ZT1 ,ZT2 ,ZT3 , W1, W2, W3 ,Tc
       DOUBLE PRECISION TT, LENGTH, FINAL, DELTAT
       INTEGER J, II(0:53) , I1(0:53) , I2(0:53)

       Kc = 0.75E+6
       Y = 1.1215
       EX = 6.5E-6
       E = 70E+9
       V = 0.25
       G = 4.
       XN = 2E +11

       OPEN (UNIT = 1, FILE = 'CRACKLEN' , STATUS = 'OLD')
        DO 1  N = 1 , 1000
          READ(1, *) X(N)
 1      CONTINUE
       CLOSE (UNIT = 1)

C      The purpose of loop 888 is to repeatedly calculate the strength
C      degradation related to different deltat.

       DO 888 IJK = 1 , 8

          DELTAT = 100 + (IJK - 1) *20
               PRINT * , ' DELTAT = ', DELTAT

C      The purpose of loop 3 and 4 is to clearn all variables
C      in order for the repeated calculation of loop 888.

         DO 3 , N = 1 , 1000
             Z1(N) = X(N)
             XF1(N) = 0.0
             XF2(N) =0.0
             Z2(N) =0.0
             Z3(N) =0.0
   3     CONTINUE

         DO 4 , WN = 0 , 53
             II(WN) = 0.0
             F1(WN) = 0.0
             I2(WN) = 0.0
   4   CONTINUE


C 1.1 :  transformation from Z1( ) to final crack length, Z2( )
C        Z1( ) is the initical crack length

       B = 2* 3.14159* XN* G
       C = 16 *(1-V**2) * XN /9/(1-2*V)
```

```
        D = 3.14159*G*(1-2*V)**2/2/E/EX**2/(1-V**2)
C     definition of A, B, C and D, are given in Hasselman's paper (1969)

C     To find the final crack length due to kinetic behavior by means of
C     Hasselman's Eq. (4) and (7).
C     Numercial technique:  interval-halving mothod
C     Tc is the critical temperature for kinetic crack growth.

        K = 0
        KK = 0
C       K represents the total number of specimens without crack growth
C       KK is the total number with crack growth

        DO 30 M = 1 , 1000

           Tc = D**0.5 *(1+ C*Z1(M)**3) / Z1(M)**0.5
                          A = 3*(EX * Tc)**2 * E/2/(1- 2*V)
           IF (Tc .GT. DELTAT) THEN
              K = K + 1
  501         Z2(K) = Z1(M)
              GO TO 30
           END IF

C      The physical meaning of statement 501 is 'no crack growth'.
C      It means that Z2( ) represents the part of intial flaws
C      without crack growth.
C      After statment 502, the other part of initial crack 'grows'.

  502      ZT1 = Z1(M) * 1.001
           DO 20 N = 1 , 35
             CALL CHIUCH(A, B, C, Z1(M), ZT1, W1)
              IF (N .EQ. 1) THEN
                W3 = W1
                ZT3 = ZT1
                GOTO 20
              ELSE
                IF (W1*W3 .GT. 0.0) THEN
                  W3 = W1
                  ZT3 = ZT1
                  ZT1 = Z1(M) * 3**N
                  GO TO 20
                ELSE
                  GO TO 25
                END IF
              END IF
  20        CONTINUE

C       The purpose of loop 20 is to find an interval in which
C       the solution exists.  The solution will be calcualted in
C       loop 28 using interval-halving method.

  25        DO 28 NM = 1 , 30
              ZT2 = (ZT1 +ZT3)/2
              CALL CHIUCH(A, B, C, Z1(M), ZT2, W2)
              IF (W3*W2 .GT. 0.0) THEN
                 W3 = W2
                 ZT3 = ZT2
                 ZT2 = (ZT1+ZT3)/2
              ELSE
                 W1 = W2
                 ZT1 = ZT2
                 ZT2 = (ZT1 + ZT3)/2
              END IF
              IF (ABS(ZT1 - ZT3) .LT. 0.0000000001) GO TO 19
  28        CONTINUE
  19         KK = KK + 1
```

```
          Z3(KK) = ZT2
 30     CONTINUE

C        Z3( ) represents the final crack length due to kinetic crack
C        growth.


C 1.2 : To find the final quasi-static crack length according to Eq. (4)

         DO 200 N = 1, KK
          TT = D**0.5*(1+C*Z3(KK)**3)/Z3(KK)**0.5
          IF (TT .LT. DELTAT) THEN
            GO TO 477
          ELSE
            GO TO 200
          END IF

C      To find final crack length using interval-halving method
 477       ZT1 = Z3(KK) * 1.001
          DO 40 NN = 1 , 35
            CALL CHIUCH(A, B, C, Z3(KK), ZT1, W1)
             IF (N .EQ. 1) THEN
               W3 = W1
               ZT3 = ZT1
               GO TO 40
             ELSE
               IF (W1*W3 .GT. 0.0) THEN
                 W3 = W1
                 ZT3 = ZT1
                 ZT1 = Z3(KK) * 3**NN
                 GO TO 40
               ELSE
                 GO TO 45
               END IF
             END IF
 40       CONTINUE

 45          DO 48 M = 1, 30
              ZT2 = (ZT1 + ZT3)/2
              CALL CHIUCH(A, B, C, Z3(KK), ZT2, W2)
               IF (W3*W2 .GT. 0.0) THEN
                 W3 = W2
                 ZT3 = ZT2
                 ZT2 = (ZT1 + ZT3)/2
               ELSE
                 W1 = W2
                 ZT1 = ZT2
                 ZT2 = (ZT1 + ZT3)/2
               END IF
               IF (ABS(ZT1 - ZT3) .LT. 0.0000000001) GO TO 44
 48       CONTINUE
 44            Z3(KK) = ZT2
 200      CONTINUE


C   THE SUBROUTINE HRONG is to study the effect of subcritical crack
C   growth on the retained strength degradation.  It means that Z2( )
C   will enter the subsroutine.  The chage in Z2(  ), resulting from
C   the calculation of subroutine, is due to subcritical crack growth.

        NUMB = 0
        DO 65 N = 1, K
         CALL HRONG(Z2(N),A,B,C,D, DELTAT, FINAL, NUMB)
         Z2(N) = FINAL
 65     CONTINUE
```

```
        PRINT *, 'STUPID --- STUPID ----- STUPID -----STUPID'
        PRINT *, NUMB
C  2 :  transformation from Z2( ) and Z3( ) to final strength, XF1( )
C       XF2(  ) , respectively.
C       Sorting of retained fracture strength
        DO 46 N = 1 , 1000
         DD = KC/Y/(3.14159*X(N))**0.5/1E+6
          J = DD/4
         II(J) = II(J) + 1
 46     CONTINUE
        IF (K .EQ. 0) GO TO 155
        DO 50 N = 1 , K
          XF1(N) = Kc/Y/(3.14159*Z2(N))**0.5/1E+6
          J = XF1(N)/4
          I1(J) = I1(J) +1
 50     CONTINUE
 155     IF (KK .EQ. 0) GO TO 157
        DO 60 N = 1 , KK
          XF2(N) = Kc/Y/(3.14159*Z3(N))**0.5/1E+6
          J = XF2(N)/4
         I2(J) = I2(J) +1
 60     CONTINUE
 157    DO 49 WN = 0, 50
         WRITE (2,*) WN*4+2 , II(WN) , I1(WN) , I2(WN)
 49     CONTINUE
         WRITE (2 , *)
         WRITE (2, *)
 888    CONTINUE
        STOP
        END


        SUBROUTINE CHIUCH(A, B, C, Z1 , ZT , ZTRIAL)
        DOUBLE PRECISION A , B, C, Z1, ZT, ZTRIAL
        ZTRIAL = A*(1/(1+C*Z1**3)-1/(1+C*ZT**3))-B*(ZT**2-Z1**2)
        RETURN
        END


        SUBROUTINE HRONG(CRACK, A,B,C,D,  DELTAT, FINAL, NUMB)
C       To consider the subcritical crack growth, we first calculate
C       transient thermal stresses using thermoelastic theory.  If K
C       exceeds Ko, the pre-existing cracks Z( ) has subcritical crack
C       growth.  Once the crack length satisfies the Griffith's criterion,
C       the crack grows.  The temperature considered is the instaneneous
C       surface temperature.  If the crack length does not, the crack
C       still grows according to subcritical crack growth.

        DOUBLE PRECISION X(0:7),CRACK, A, B, C, D,DELTAT, FINAL
        DOUBLE PRECISION XP,XQ,PP,QQ,RR,XP7,RR7,TEMP7, XM1,XM2,XM3
        DOUBLE PRECISION ZT1, ZT2, ZT3, W1, W2, W3, TC
        REAL TEMP, STRESS1, STRESS2
        INTEGER M

C       INPUT some parameters
        BIOT = 150
        H = 0.6E-3
        Z = 0.6E-3
        DI = 4.8E-7
        EX = 6.5E-6
        E = 70.0E+9
        V = 0.25

C     TO calculate the eignvalue X( ), for X( )*TAN(X()) = Biot
C     by neans of interval-half method
```

```
      DO 310 , M = 0 , 5
        XM1 = 0 + 3.14159 * M
        XM2 = 1.570795 + M * 3.14159
       DO 320 , N = 1 , 60
          XM3 = (XM1 + XM2)/2
          XXM1 = XM1 * TAN(XM1) - BIOT
          XXM2 = XM2 * TAN(XM2) - BIOT
          XXM3 = XM3 * TAN(XM3) - BIOT
          IF (ABS(XM1 - XM2) .LT. 0.00000001) THEN
             GO TO 315
          ELSE
             IF (XXM1*XXM3 .GT. 0.0) THEN
                XM1 = XM3
                XM2 = XM2
             ELSE
                XM1 = XM1
                XM2 = XM3
             END IF
          END IF
320       CONTINUE
315        X(M) = XM3
310       CONTINUE

C     TO calculate the thermal stress and Ko
          TIME1 = 0.0
          STRESS2 = 0.0
        DO 10 , AN = 1 , 500
          TIME = 0.00001 * AN**2.4
          STRESS1 = 0.0
          TEMP = 0.0
          TEMP9 = 0.0
         DO 20, M = 0 ,5
           XP = SIN(X(M)) * COS(X(M)*Z/H)
           XQ = X(M) + SIN(X(M)) *COS(X(M))
           PP = EXP(-DI*(X(M)/H)**2 * TIME)
           QQ = SIN(X(M))/(X(M) + SIN(X(M))*COS(X(M)))
           RR = SIN(X(M))/X(M) - COS(X(M) * Z /H)
           STRESS1 = STRESS1+ PP*QQ*RR*(2*EX*E*DELTAT/(1- V))
           TEMP = TEMP + 2* DELTAT * XP /XQ * PP
           TEMP7 = 0.0
         DO 12, L = 1 , 11
           ZZ = H/10 * (L-1)
           XP7 = SIN(X(M)) * COS(X(M) * ZZ/H)
           RR7 = SIN(X(M))/X(M) - COS(X(M) * ZZ/H)
           TEMP7 = TEMP7 + 2*DELTAT *XP7 /XQ *PP
C     The purpose of LOOP 12 is to find the average temperature, temp9,
C     at instaneneous time of thermal shock
  12       CONTINUE
           TEMP9 = TEMP9 + TEMP7 / 11

  20       CONTINUE


            KI = 1.1214 * STRESS1 * (3.14159 * CRACK)**0.5

C          PRINT *,  STRESS1 , TEMP, TEMP9, KI
           IF((KI .LT. 0.248E+6).AND. (STRESS1 .GT. STRESS2)) THEN
              STRESS2 = STRESS1
              TIME1 = TIME
              GO TO 10
           END IF
C     It means that no subcritical crack growth occurs, but the crack
C     still has potential to grow in the near further.

        IF((KI .LT. 0.248E+6).AND.(STRESS1 .LT. STRESS2)) GO TO 70
C     It means that subcritical crack growth CAN NOT occur any more.
```

```
            IF (KI .GT. 0.248E+6) THEN
                CRACK1 = CRACK
               VELOCITY = EXP(10.3) * EXP((-1.088E+5 +0.11* KI)/
     C                     (TEMP + 273)/8.3)
C          PRINT *, VELOCITY
               CRACK = VELOCITY * (TIME - TIME1) + CRACK
               TIME1 = TIME
               STRESS2 = STRESS1
C             PRINT *, CRACK
C     It means that subcritical crack growth occurs.
            END IF

            IF(CRACK .GT. 0.1E-3 ) THEN
               CRACK = CRACK1
               NUMB = NUMB + 1
               GO TO 70
            END IF

               TC = D**0.5 * (1+C*CRACK**3)/CRACK**0.5
            IF (TC .LT. TEMP9) GO TO 80

C     It means that the crack length satisfies the Griffith failure
C     criterion.  The program will go into the "pop-in" crack growth
C     loop again.

 10       CONTINUE

C  The purpose of DO LOOP 80 is to find the final crack length due to
C  the 'pop-in crack growth length' after the activation of the
C  subcritical crack growth.

         GO TO 70

C 80     PRINT *, VELOCITY , CRACK
C        PRINT *, TC , TEMP9
 80     ZT1 = CRACK * 1.0000000001
        DO 30 N = 1 ,20
          W1 = A*(1/(1+C*CRACK**3) - 1/(1+C*ZT1**3)) -B*(ZT1**2-
     C           CRACK**2)
           IF (N .EQ. 1) THEN
             W3 = W1
             ZT3 = ZT1
             GO TO 30
           ELSE
             IF (W1*W3 .GT. 0.0) THEN
               W3 = W1
               ZT3 = ZT1
               ZT1 = CRACK * 1.5**N
               GO TO 30
             ELSE
               GO TO 35
             END IF
           END IF
 30     CONTINUE
         GO TO 70
C        IT means that the crack is long enough that no 'pop-in'
C        crack growth can occur in such a situation.

 35     DO 38 NM = 1, 20
          ZT2 = (ZT1 + ZT3) /2
          W2 = A*(1/(1+ C* CRACK**3) - 1/(1+ C*ZT2**3)) -
     C         B*(ZT2**2 - CRACK**2)
            IF (W3*W2 .GT. 0.0) THEN
                W3 = W2
                ZT3 = ZT2
```

```
            ZT2 = (ZT1 + ZT3)/2
         ELSE
            W1 = W2
            ZT1 = ZT2
            ZT2 = (ZT1 + ZT3)/2
         END IF
         IF (ABS(ZT1 - ZT3) .LT. 0.0000001) GO TO 29
38     CONTINUE
29     FINAL =  ZT2
       GO TO 100

70     FINAL = CRACK

100     RETURN
        END
```